THE RECRUITMENT AND FUNCTION OF INHIBITIORY INTERNEURONS IN OLFACTORY BULB PROCESSING

by

Sonya B. P. Giridhar

B.S. Neuroscience, University of Minnesota, 2007

Submitted to the Graduate Faculty of

the Kenneth P. Dietrich School of Arts and Sciences in partial fulfillment

of the requirements for the degree of

Doctor of Philosophy

University of Pittsburgh

2012

UNIVERSITY OF PITTSBURGH

DIETRICH SCHOOL OF ARTS AND SCIENCES

This dissertation was presented

by

Sonya B. P. Giridhar

It was defended on

April 9, 2012

and approved by

Stephen D. Meriney, PhD, Associate Professor, Department of Neuroscience

Brent Doiron, PhD, Assistant Professor, Department of Mathematics

Erika Fanselow, PhD, Assistant Professor, Department of Neurobiology

Charles C. Horn, PhD, Associate Professor, Department of Medicine

Mark Stopfer, PhD, Investigator, National Institutes of Health

Dissertation Advisor: Nathan N. Urban, PhD, Professor, Department of Biological Sciences

THE RECRUITMENT AND FUNCTION OF INHIBITIORY INTERNEURONS IN OLFACTORY BULB PROCESSING

Sonya B. P. Giridhar, PhD

University of Pittsburgh, 2012

Inhibitory interneurons are the "shush"-ers of the brain—their output causes a reduction in the output of other neurons. Inhibitory interactions play a critical role in the olfactory bulb, where they shape olfactory representations that guide behavior. However, the mechanisms by which interneuron activation improves olfactory function remain debated. In particular, the relative importance neural activity over short periods of time (~tens of milliseconds) versus long periods of time (hundreds to thousands of milliseconds) has provoked significant debate.

Granule cells are inhibitory interneurons in the olfactory bulb that can respond and influence olfactory bulb activity across a wide range of timescales. The first part of this dissertation investigates the physiological mechanisms driving the timing of granule cell recruitment. We found that the specific timing of recruitment depends on the timing of synaptic excitation delivered from tufted cells. Tufted cells (unlike the more commonly studied mitral cells) are able to fire at long latencies due to intrinsic membrane properties that allow them to integrate weak inputs slowly while responding rapidly to strong inputs. Computational modeling revealed that the long-latency inhibition generated by this mechanism can improve performance on stimulus discrimination tasks.

The second portion of this dissertation focuses on the downstream effects of granule cell recruitment. Highly correlated spiking can be advantageous for propagating information. However, these same correlations limit encoding by introducing redundancy. We investigated how granule cell recruitment altered correlations between mitral cell pairs across timescales. We found that granule cell recruitment increased fast timescale correlations (i.e. synchronous spiking) while simultaneously decreasing slow timescale correlations (i.e. firing rate similarity). Using computational modeling, we show that timescale-dependent correlation changes are functionally advantageous because they can circumvent the tradeoff between propagation and encoding.

Taken together, these studies extend our understanding of olfactory bulb physiology by providing a mechanistic description of how inhibitory circuits shape activity across timescales. Our results indicate that granule cell recruitment requires dynamic and stimulus-dependent interactions between mitral, tufted, and granule cells, and that the inhibition recruited by this mechanism works at multiple timescales to effectively encode and propagate stimulus information.

TABLE OF CONTENTS

LIST OF TABLES

LIST OF FIGURES

LIST OF ABBREVIATIONS

4-AP:	4-aminopyriadine
AMPA:	α-amino-3-hydroxy-5-methyl-4-isoxazolepropionic acid
EPSC:	Excitatory post-synaptic current
Fura-2 AM:	Fura-2-acetoxymethyl ester
GABA:	gamma aminobutyric acid
IPSC:	Inhibitory post-synaptic current
LFP:	Local field potential
LLD:	Long-lasting depolarization
NMDA:	N-methyl-D-aspartate
PSTH:	Peri-stimulus time histogram

ACKNOWLEDGEMENTS

Attending graduate school is an absolute privilege. It is time when you can select your favorite ideas and pursue them wholeheartedly. You can follow your passion, study what excites you most, and have the support of a terrific scientific community. I feel immensely grateful to have had this opportunity.

Moreover, I feel very privileged to have been trained by Dr. Nathan Urban. His enthusiasm for research is truly contagious. In addition to his vast breadth of knowledge and ideas, I have been particularly impressed by his unique ability to identify and foster strengths in young students. I have undergone immense intellectual growth during my time in the lab and I owe much of that to his support. From day one in the lab, he has encouraged me to learn new things, and to think of old things in a new way.

Much of the work contained within this dissertation involves computational modeling and analysis of neural networks. If you have never written a line of computer code in your life, then you know *exactly* as much about this as I did when I entered graduate school. I was exceptionally fortunate to have Dr. Brent Doiron take me on as a rotation student to teach me techniques in computational neuroscience. Since then, computational ideas about coding and how networks function have become an enormous influence on how I think about science. My rotation in his lab was a critical point in my graduate career that significantly shaped the direction of my PhD, and I am grateful for his influence.

I would also like to thank the other members of my dissertation committee, Dr. Stephen Meriney, Dr. Erika Fanselow, Dr. Charles Horn, and Dr. Mark Stopfer. Their ideas, support, and encouragement have challenged me to reach beyond my comfort zone. They have counseled me on everything from experimental design to career planning and I am very thankful to have the support of such wonderful scientists.

Lastly, I would like to thank my husband. He is a constant source of love, companionship, and joy in my life. Karthik: you are my favorite person and I love you to pieces.

This work was supported by grants from the National Institute of Deafness and Other Communication Disorders R01 DC0005798 (N.U.), the National Institute on Drug Abuse T90DA022762 (S.G.), an NSF IGERT Fellowship DGE-0549352 (S.G.) and an Andrew Mellon Predoctoral Fellowship (S.G.)

PREFACE

Imagine that you are a neuron. The only way that you can communicate is by emitting short blips, much like the "dits" that make up Morse code. Armed only with these blips, you are charged with the responsibility of representing the smell of a lemon. How would you do it? Moreover, how would your strategy change if you had one or more additional neurons to help you represent this information?

This scenario encompasses a fundamental question about neural coding: how do neurons effectively represent information about stimuli. This is an idea that continues to fascinate me, and in this dissertation I will describe a series of experiments and models aimed at addressing this question in the mammalian olfactory system.

The work presented in this dissertation is based on two manuscripts.

Chapter 3 is based on:

Giridhar, S. and Urban, N.N. Mechanisms and benefits of granule cell latency coding in the mouse olfactory bulb. (in review)

Chapter 4 is based on:

Giridhar, S., Doiron, B., and Urban, N.N. (2011) Timescale-dependent shaping of correlation by olfactory bulb lateral inhibition. PNAS 108(14): 5843-5848.

1.0 INTRODUCTION

1.1 THE OLFACTORY BULB AS A MODEL SYSTEM

The inner workings of the brain represent one of biology's greatest puzzles. However, solving this puzzle is difficult given the brain's anatomical and functional complexity. How should we go about understanding the billions of neurons, trillions of synapses, and countless functions of the brain? Because of this overwhelming complexity, our approach to understanding brain function relies heavily on the use of model systems. Model systems refer to experimental preparations (often isolated regions of the brain) that can be carefully controlled, manipulated, and studied to elucidate how neurons confer function. The selection of a model system, of course, depends on the question one wishes to answer about brain function.

One of the most critical roles of the nervous system is to represent the external environment. Not only is this crucial for survival, it is a fascinating problem from a neural coding standpoint. Neural coding aims to understand how information is represented by the firing patterns of neurons. Neurons in different brain regions can represent a wide variety of environmental features including light, sound, touch, and chemical information. In particular, the olfactory system has emerged as a powerful model system for understanding how neurons

represent environmental information. While we (and other primates) rely mostly on vision to sense our environments, many animals rely primarily on odor inputs. Understanding how binary spike trains can be used to represent information such as odors has been a key goal in neuroscience.

What advantages does the olfactory bulb have as a model system? In this thesis, I have set out to better understand how 1) single neurons respond to stimuli, 2) how local circuit processing improves sensory representations, and 3) how populations of neurons can represent multidimensional stimuli. The olfactory bulb is particularly well-suited to address these questions because it uses population activity to represent multidimensional stimuli, and relies heavily on local processing to shape and improve these representations. As the following sections outline, the olfactory bulb is a useful model for answering these questions about brain function because it is behaviorally important, has a simple organization, yet it mediates many complex computations.

1.1.1 Behavioral importance of the olfactory bulb

In order to elucidate the coding strategies in a particular system, one must first understand its function. Simply stated, what is the job of the olfactory bulb? Olfaction informs a wide array of natural behaviors owing to the fact that most features of the environment contain or excrete chemical compounds that can be detected by a sensitive enough olfactory system. Rodents (Vander Wall, 1998; Johnson and Jorgensen, 1981) and insects (Asahina et al., 2008) use their sense of smell to localize hidden food sources (an ability that confers a survival advantage in competitive environments). Olfaction is also used for kin recognition. Infant

rats—despite the fact that their eyes and ears have not yet opened—can locate their mother (Gregory and Pfaff, 1971), even when they must navigate through a maze to find her (Nyakas and Endroczi, 1970). Likewise, olfaction mediates behaviors on the behalf of the mother, and is thought to dictate the timing of onset of maternal behaviors (Fleming and Rosenblatt, 1974a; Fleming and Rosenblatt, 1974b). Olfaction-mediated social behaviors also include mating preference and increased investigation of high-quality sexual partners (Da Yu Lin et al., 2005). Lastly, olfactory cues from predators are also used to modify behavior (Blumstein et al., 2002). Thus olfactory cues drive a wide range of behaviors that help to acquire food, mate successfully, raise young, and avoid predation.

However, to understand the specific role of the *olfactory bulb* in these odor-guided behaviors, we must examine which aspects of these behaviors rely critically on activity in the olfactory bulb. Targeted manipulations of the olfactory bulb have been performed to assess its behavioral importance. One such manipulation is to remove the olfactory bulb completely—a procedure known as olfactory bulbectomy. Bulbectomized rodents demonstrate a variety of behavioral deficits. Bulbectomy in neonates results in high mortality and failure to gain weight because of reduced feeding (Hill and Almli, 1981; Tobach et al., 1967; Singh and Tobach, 1975). Surviving animals remain smaller than control animals, even as adults (Hill and Almli, 1981). Rodents bulbectomized in adulthood exhibit hyperactivity and impaired habituation during exploratory behaviors (Zueger et al., 2005), as well as impaired performance on spatial learning and memory tasks (Hozumi et al., 2003). This line of data suggests that olfactory bulb plays a critical role in rodents' ability to sense their environments and thus interact with it appropriately.

More recently, genetic tools have become available to facilitate more targeted (and less drastic) manipulations of the olfactory bulb and its inputs. Some of these approaches have

focused on reducing or eliminating odor responsiveness by deleting genes in the sensory inputs to the olfactory bulb, such as olfactory marker protein (Buiakova et al., 1996), cyclic nucleotide gated channel subunits (Zhao and Reed, 2001; Lin et al., 2004), and adenylyl cyclace III (Wong et al., 2000). Based on the magnitude of olfactory receptor activity reduction, deficits induced by these manipulations range from complete anosmia to impaired ability to detect and discriminate subsets of odors (Wong et al., 2000; Zhao and Reed, 2001; Youngentob and Margolis, 1999; Youngentob et al., 2001).

Genetic approaches have also applied to cells housed within the olfactory bulb. These manipulations are of particular interest because they leave the peripheral inputs to the olfactory bulb intact, as well as the olfactory bulb's outputs to cortex. Because of this, these manipulations are a particularly useful tool for understanding how olfactory bulb cells contribute to behavior. The olfactory bulb contains many inhibitory interneurons that participate in odor-evoked responses (Cang and Isaacson, 2003). Olfactory bulb inhibition mediated by gamma amino butyric acid (GABA) has been manipulated genetically by increasing or decreasing the responsiveness of olfactory bulb interneurons. For example, β3(-/-) mice have been genetically engineered to have increased GABA-mediated oscillatory synchrony (Nusser et al., 2001). These mice demonstrate an *enhanced* ability to make fine discriminations between closely related odor stimuli. Other genetic enhancements of olfactory bulb inhibition have also been shown to improve discrimination performance, while performance is degraded in inhibition-suppressed animals (Abraham et al., 2010). These findings are of particular interest here because they suggest that not only is the olfactory bulb necessary for tasks like discrimination, but that local processing within the bulb is *required* for successful coding of some stimuli.

The ubiquity of olfactory cues in driving behavior and the reliance of these behaviors on olfactory bulb activity suggests that the olfactory bulb does not have a single job (for example, finding food), but rather acts to provide a complete view of the external environment. The olfactory bulb must encode a wide diversity of chemical signals in a format that can be decoded to inform behavior. As such, the olfactory bulb represents a very useful model in advancing our understanding of how populations of neurons encode information.

1.1.2 Stimulus processing in the olfactory bulb

Generally speaking, sensory coding involves two steps. First, stimulus information must be encoded. This means that relevant features of olfactory stimuli (such as chemical composition and concentration) must be represented by the spiking patterns of neurons. These spike patterns can be shaped by several factors, including the integration properties of neurons as well as interactions with local circuits. Secondly, these spike patterns must be decoded by postsynaptic neurons so that downstream neurons have access to stimulus information.

From this view, each neuron can be considered as a site of encoding and decoding. An individual neuron must decode the relevant features of its inputs and in turn encode that information by generating informative spiking for the next neuron. At a larger scale, the encoding/decoding process can be described across brain regions. In the context of the olfactory processing, primary sensory information must be encoded and processed by the olfactory bulb, and then sent to piriform cortex. There, it will be decoded for perception of the olfactory environment and used to guide behavior.

1.1.2.1. Encoding chemical information

Olfactory coding presents an intriguing problem because odor stimuli are multidimensional and qualitative. Consider the smell of a lemon. We can describe its smell as being "citrusy", yet many other stimuli also fall into this group. How does the smell of a lemon differ from that of an orange, grapefruit, or lime? Even though these perceptions are easily identifiable and distinct, describing the nature of these stimuli is quite difficult. Representing these differences systematically from binary spike trains is an even more difficult problem.

By comparison, other sensory modalities have more easily quantifiable stimulus features: the spatial arrangement of lightness and darkness easily describes simple visual images, as does wavelength and amplitude for auditory stimuli. Features of odor stimuli vary along many unrelated axes of chemical features such as volatility, carbon chain length, and presence of various chemical groups, which can influence odorant binding to primary sensory neurons. However, modifying chemical groups does not alter olfactory perception in a systematic, linear, or predictable way (Keller et al., 2007). Psychometric studies have made great progress in characterizing the relationship between chemical structure and olfactory perception (Keller and Vosshall, 2007; Amoore, 1969; Wise et al., 2000), but the fact remains that many descriptors (dimensions) are required to characterize even simple, monomolecular odorants. This "elusive" nature of olfactory stimuli is one reason it makes an interesting model for studying coding, as there is not a clear continuum of odor space. For example, olfactory bulb neurons cannot simply encode odorants by emitting high firing rates for lemon, and low firing rates for non-lemon

stimuli. Instead, they must use other strategies to recognize and encode many stimulus-specific features.

1.1.2.2. Transforming stimulus-evoked activity patterns

The complex nature of the olfactory environment puts additional demands on the (already formidable) task of encoding chemical information with spike trains. Animals are adept at functioning in natural environments containing complex mixtures of many different odorants. From these mixtures, animals must be able to recognize odors, extract relevant odors from a complex background, and discriminate between mixtures with very small differences (Hopfield, 1999). The olfactory bulb is thought to facilitate these computations by a variety of mechanisms, including adaptation (Hopfield, 1999) and interactions with inhibitory interneurons. As mentioned above, animals cannot complete certain olfactory discrimination tasks when local inhibitory transformations in the olfactory bulb/antennal lobe are disrupted (Stopfer et al., 1997; Abraham et al., 2010; Gheusi et al., 2000; Mwilaria et al., 2008). This indicates that the olfactory bulb cannot act simply as a relay station, propagating primary sensory inputs to cortex. Rather, the olfactory bulb acts as a site of processing that is required for certain olfactory behaviors.

1.1.2.3. Downstream decoding olfactory bulb activity

In addition to shaping odor representations, local olfactory bulb transformations may act to optimize excitatory output to cortex. Olfactory bulb spike patterns need to be in a format that can be successfully propagated to downstream neurons. Further, these patterns must be

interpreted within cortical areas in the presence of noise. The majority of olfactory bulb outputs project to piriform cortex, with a smaller subset projecting to more anterior areas such as the olfactory tubercle and accessory olfactory nucleus (Shepherd, 2004). Responses of these cortical neurons to olfactory stimuli are both qualitatively and quantitatively different from the patterns evoked in the olfactory bulb. Spiking in piriform cortex is much sparser and exhibits certain stimulus-evoked features that are not observed in the olfactory bulb, such as concentration invariance and mixture facilitation and suppression (Zou and Buck, 2006; Yoshida and Mori, 2007). In addition to being shaped by odor stimuli, activity in piriform cortex is significantly shaped by learning and reward (Chapuis and Wilson, 2011). These findings suggest that piriform cortex can both read out accurate information about stimuli from the maps established in the olfactory bulb, and also integrate this information with motivated behavior and other salient features of the environment.

In summary, our understanding of how the brain encodes information is far from complete. As a model system, the olfactory bulb has many advantages in improving our knowledge of how the brain encodes qualitatively complex stimuli in the face of competing computational demands. These features, along with the fact that the olfactory bulb is accessible and easy to isolate from other circuits make it an excellent system to study neural coding from both a physiological and a computational perspective.

1.2 OLFACTORY BULB ANATOMY

1.2.1 Olfactory receptor neurons

Understanding how the olfactory bulb mediates the encoding, transformations, and olfactory-guided behaviors described in the previous section requires an understanding of its anatomical organization. The first cells involved in odor processing are olfactory receptor neurons, which form the link between the peripheral environment and the brain (**Figure 1.1**). Olfactory receptor neuron dendrites terminate in the olfactory epithelium of the nose. These dendrites express odorant receptors which bind odorant molecules and depolarize the olfactory receptor neurons via seven-transmembrane G-protein coupled receptor signaling cascades (Buck and Axel, 1991). Since odorants are present in the air, inhalation brings these airborne molecules in contact with olfactory receptor neurons, which in turn become depolarized. These primary sensory responses constitute the inputs to the olfactory bulb.

Mice express approximately 1300 different functional odorant receptors (Young et al., 2002; Zhang and Firestein, 2002). Each olfactory receptor neuron expresses only one type of receptor (Ngai et al., 1993; Vassar et al., 1993; Ressler et al., 1993). Because of this one-to-one organization, the response of individual olfactory receptor neurons is dictated by the odorant binding properties of its expressed receptor. Sensory neurons (and neurons in general) are often characterized by their receptive field—a description of what range of stimulus features elicit activity. For example, individual neurons can be selective for features such as spatial location,

orientation, movement direction or frequency. The analogous description for olfactory receptor neurons is the molecular receptive range—a measurement that indicates whether responses are selective (responding to only one specific odorant molecule) or promiscuous (responsive to many different compounds). Different olfactory receptors vary significantly in their selectivity with some responding to a very small subset of odors and others responding more generally (Araneda et al., 2000). Because of this variability in stimulus selectivity, individual odors do not elicit activity in only one type of olfactory receptor neuron. Instead, odors evoke patterns of population activity across the olfactory epithelium.

Olfactory receptor neurons provide sensory input to the olfactory bulb. The olfactory bulb is a radially organized laminar structure that processes primary olfactory inputs. It consists of a glomerular, plexiform, mitral cell, and granule cell layers (**Figure 1.1**).

1.2.2 Glomeruli

The glomerular layer is the site of sensory input to the olfactory bulb. Olfactory bulb glomeruli are spherical neuropils that receive inputs from the axons of olfactory receptor neurons (Shepherd, 2004). Olfactory receptor neurons expressing the same receptor converge onto the same glomeruli (Mombaerts et al., 1996). Thus the spatially distributed activity present in the olfactory epithelium gives rise to functionally organized activity patterns across the glomerular layer (Grossman et al., 2008; Lin et al., 2006; Spors and Grinvald, 2002; Spors et al., 2006).

The glomerular layer also contains inhibitory interneurons called periglomerular cells. As their name suggests, periglomerular cells are located around the periphery of glomeruli. They provide local inhibition within and between neighboring glomeruli. Periglomerular cells are

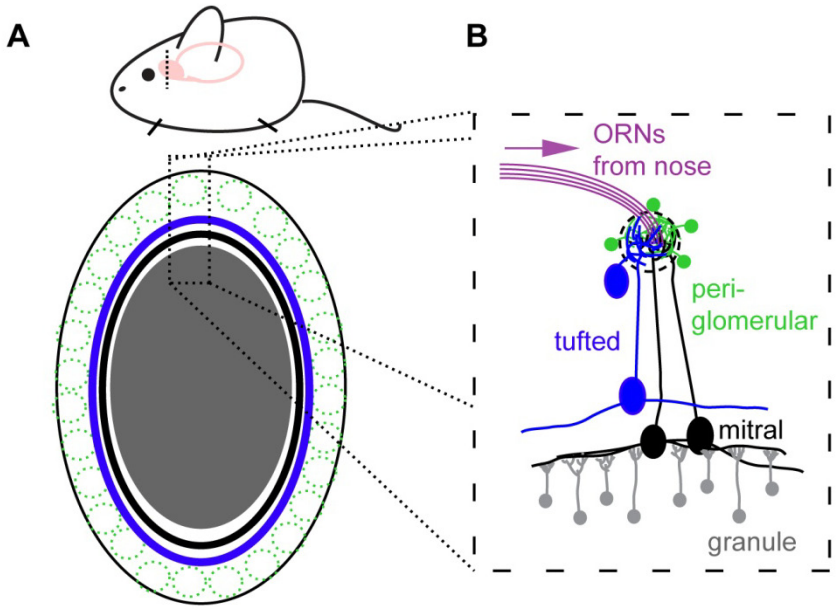

Figure 1.1: Olfactory bulb anatomy. (A) The olfactory bulb is located at the most rostral portion of the rodent brain (shown in solid pink). Coronal sectioning (as shown by the dashed line) reveals a radially symmetric laminar organization (oval; below). This includes the glomerular, external plexiform, mitral, and granule cell layers. **(B)** Synaptic organization of the olfactory bulb. Olfactory receptor neuron inputs from the olfactory epithelium converge into spherical glomeruli, where they synapse onto mitral, tufted, and periglomerular cells. Mitral and tufted cells interact laterally with inhibitory granule cells and send their axons to piriform cortex.

thought to be an important source of gain control for sensory inputs, as they scale their output with stimulus strength to boost weak inputs and attenuate responses to very strong stimuli (Olsen and Wilson, 2008). In this way, periglomerular cells may be important for keeping olfactory bulb responses within an appropriate dynamic range. Further, periglomerular cells provide lateral inhibition between neighboring glomeruli (Leonard, 1980). This motif is akin to the traditional "center surround" inhibitory circuitry of the retina, whereby local inhibition amplifies firing rate differences between nearby cells.

1.2.3 Mitral and tufted cells

Within glomeruli, the axons of olfactory receptor neurons also terminate onto the principal coding cells of the olfactory bulb: mitral and tufted cells. Both mitral and tufted cells extend a single apical dendrite into one glomerulus from which they receive glutamatergic primary sensory inputs. Mitral and tufted cells are the only olfactory bulb neurons projecting to cortex. Thus their activity is solely responsible for informing the rest of the brain about the olfactory periphery.

Mitral and tufted cells can be identified and categorized based on their morphological characteristics (Mori et al., 1983; Orona et al., 1984). Mitral cell somata are located in the mitral cell layer—an easily identifiable band that stretches across the entire bulb (although a few—termed displaced mitral cells—are located slightly outside of this layer). Mitral cells have multiple, far-reaching lateral dendrites that span up to 1000 μm away from the cell body (Pinching and Powell, 1971). These lateral dendrites make synaptic contacts with inhibitory interneurons called granule cells.

Tufted cells come in a variety of subtypes which are classified based on somatic location as well as dendritic morphology. External tufted cell somata are located in the glomerular layer, adjacent to the glomerulus into which the highly arborized tuft projects. The cell bodies of middle tufted cells are located in the plexiform layer, while inner tufted cells are located slightly superficially to the mitral cell layer (overlapping the somatic location of displaced mitral cells). Like mitral cells, middle and inner tufted cells have far-reaching lateral dendrites.

Mitral and tufted cells are often grouped together and considered to be functionally equivalent (or at least nearly functionally equivalent). Part of this grouping of is due to the fact that isolating mitral versus tufted cell responses from *in vivo* recordings can be difficult. Because of this ambiguity, many reports of olfactory bulb activity refer to "mitral/tufted" or MT activity rather than specifying the exact identity of each neuron. Similarities between mitral and tufted cell spiking also contribute to this lumping of cell types. Mitral and tufted cells terminating within the same glomerulus are coupled both by their inputs and also potentially by glutamate spillover, gap junction coupling (Hayar et al., 2005), and the synchronizing influence of inhibitory periglomerular cells (Karnup et al., 2006). Because of these factors, the response properties of mitral and tufted cells can be similar under some conditions.

Despite the tendency to group mitral and tufted cells together, significant differences have emerged that distinguish the connectivity and physiology of mitral and tufted cells. Tufted cells form synapses with more superficial portions of the granule cell layer whereas mitral cells are more likely to synapse with deep granule cells (Orona et al., 1983; Orona et al., 1984; Mori et al., 1983). Mitral and tufted cells project their axons out of the olfactory bulb via the olfactory nerve. This fiber bundle carries the axons to areas of the brain that use olfactory information to drive behavior, notably piriform cortex and the olfactory tubercle. Mitral and tufted cells vary in

their areas of axonal termination. Mitral cells preferentially target piriform cortex while tufted cells target the olfactory tubercle with higher probability (Shin Nagayama et al., 2010). Within the olfactory cortex, mitral cells preferentially target rostrolateral areas whereas tufted cells target more rostromedial areas (Haberly and Price, 1977; Schoenfeld and Macrides, 1984).

Physiological differences have also been observed between mitral and tufted cells. Tufted cells tend to exhibit higher excitability than mitral cells. External tufted cells have intrinsic properties that predispose them to bursting (Hayar et al., 2004). These same cells also have higher stimulus-evoked firing rates than mitral cells (Nagayama et al., 2004). Mitral cell responses are more strongly modulated by respiration (Phillips et al., 2012) and lateral inhibitory inputs (Nagayama et al., 2004; Ezeh et al., 1993), whereas tufted cell responses depend more heavily on intrinsic properties (Hayar et al., 2004). These observed differences in connectivity and physiology raise important questions about the function of mitral and tufted cells and their collective (and perhaps separate) roles in odor coding. This idea is examined in greater detail in chapter 3.

1.2.4 Granule cells

There are two main subtypes of inhibitory interneurons in the olfactory bulb: periglomerular cells (as discussed in 1.2.2), and granule cells. Granule cells are highly unusual in their abundance, morphology, and synaptic structure. They have been an enigmatic cell for researchers since their first description by Golgi in 1875.

Granule cells are located in the expansive medial portion of the olfactory bulb known as the granule cell layer. In the cortex, the ratio of inhibitory to excitatory cell types is typically between 1:10 to 2:10 (Meinecke and Peters, 1987). By contrast, granule cells *outnumber* mitral and tufted cells by a factor of 50:1-100:1 (Shepherd, 2004). In addition to their sheer abundance, granule cells are also unusual in their morphology because they have exclusively dendrites and no axon. In this way, they defy the "law of dynamic polarization", which states that neurons receive inputs via dendrites and send outputs via axons (Cajal, 1911). For many years, it was unknown how or why granule cells defied this law. Later, it was discovered that granule cells circumvent the law of dynamic polarization by communicating through highly unusual reciprocal, dendrodendritic synapses (Rall et al., 1966). Granule cells are excited by glutamate release onto their dendritic spines, and they in turn release GABA from their dendrites back onto mitral cell dendrites (Jahr and Nicoll, 1980; Phillips et al., 1963; Nicoll, 1969; Price and Powell, 1970a; Price and Powell, 1970b). Outside of the olfactory bulb, dendrodendritic signaling is extremely rare, although examples have been observed in certain thalamic regions of cats (Morest, 1971) and rats (Pinault et al., 1997).

Their unusual synaptic organization allows granule cells to mediate both feedforward (lateral inhibition (Isaacson and Strowbridge, 1998)) as well as feedback (reciprocal) inhibition of mitral and tufted cells along their lateral dendrites. These interactions are extremely important for temporal patterning of mitral and tufted cell activity. GABAergic transmission from granule cells can generate oscillations (Lagier et al., 2004; Lagier et al., 2007) as well as non-oscillatory changes in correlation (Galan et al., 2006; Christensen et al., 2003) and firing rate (Arevian et al., 2008; Urban and Sakmann, 2002). Granule cells' ability to generate particular spike patterns is thought to rely in part on their ability to generate and sustain activity across long timescales.

Long timescale activity in granule cells may be shaped by their inputs, as well as their unusual calcium buffering mechanisms. Calcium influx is a critical step in action potential generation. These calcium transients typically decay rapidly following spiking activity. However, granule cell calcium signals decay slowly due to slow calcium extrusion (Egger and Stroh, 2009). The long lasting calcium transients in granule cell dendrites and individual spines may foster long timescale activation of granule cells. This may be important for granule cell physiology by giving rise to asynchronous recruitment of large populations of granule cells or even asynchronous release from individual spines within a granule cell (Egger and Stroh, 2009).

1.3 OLFACTORY BULB PHYSIOLOGY

As is described anatomically in the previous section, the general flow of information through the olfactory bulb is the following:

1) Olfactory receptor neurons are excited by odorant molecules
↓
2) Excitation of mitral and tufted cells ↔ granule cell interactions
↓
3) Activity propagated to piriform cortex.

Given the one-to-one organization of receptors to olfactory receptor neurons, one could imagine that the number of distinct receptor types could set an upper bound for the number of encodable odorants (i.e. 1000 olfactory receptor neuron types could enable animals to discriminate between 1000 different odorants). This so-called labeled line hypothesis suggests

that activity at the level of receptor activation simply need to be propagated through the olfactory bulb to cortex to enable identification and discrimination. However, contrary to the labeled-line hypothesis, rodents can encode thousands more odorants than would be predicted by the number of olfactory receptor types. This expansion relies on the rich dynamics of odor-evoked activity. The following section reviews the characteristics of odor-evoked activity in the olfactory bulb and how these activity patterns have shaped hypotheses on how mitral and tufted cells represent odor information.

1.3.1 Odor-evoked activity

Odor-evoked activity in the olfactory bulb (and antennal lobe) is characterized by complex and spatially distributed spiking. Typical responses are temporally variable and consist of epochs of high and low firing (Cang and Isaacson, 2003; Bathellier et al., 2008; Nagayama et al., 2004). Interestingly, the duration of odor-evoked activity patterns is long-lasting, often persisting for hundreds to thousands of milliseconds beyond stimulus presentation. These aspects of odor-evoked activity remain conserved across a wide range of species, including insects (Laurent and Davidowitz, 1994; Stopfer et al., 1997; Wilson et al., 2004), zebrafish (Friedrich and Laurent, 2001; Friedrich et al., 2004), and rodents. The conservation of these stimulus-evoked patterns suggests that they may contain general principles for representing chemical information. The following sections describe different aspects of mitral and tufted cell activity patterns and how these features may relate to odor stimuli.

1.3.2 Putative olfactory coding mechanisms

1.3.2.1. Spatial coding

Odors evoke activity patterns across glomeruli that can be characterized in terms of their spatial arrangement (Sharp et al., 1975; Mori et al., 1992; Cinelli et al., 1995; Friedrich and Korsching, 1997; Rubin and Katz, 1999). In some cases, a simple decoder can reliably distinguish between these spatial patterns even though they lack any detailed information about firing rate (Johnson and Leon, 2000). This observation has led to the hypothesis that spatial information alone may be sufficient to represent odorant information (**Figure 1.2 A**). Spatial coding across the surface of the olfactory bulb (glomeruli) is conceptually akin to spatial coding in the retina, where the spatial distribution of activity directly reflects the spatial distribution of light in the environment. However, since odor information cannot be mirrored spatially in the same way, spatial coding in the olfactory bulb requires that chemical information be translated such that evoked patterns are related to stimulus features and/or perception.

Indeed, the spatial organization of glomeruli reveals a coarse odotopy (spatial arrangement of odorant features) related to chemical features (Nikonov et al., 2005; Uchida et al., 2000; Mori et al., 1999). In zebrafish (Friedrich and Korsching, 1997; Friedrich and Korsching, 1998) as well as mammals (Belluscio and Katz, 2001) the arrangement of glomeruli is loosely arranged along a gradient in molecular selectivity. Subregions of the bulb (groups of neighboring glomeruli) are selective for particular chemical functional groups (for example: fatty acids, alcohols, or aliphatic aldehydes). Chemotopic organization is also observed at a smaller spatial scale. Within these subregions, different combinatorial patterns represent secondary

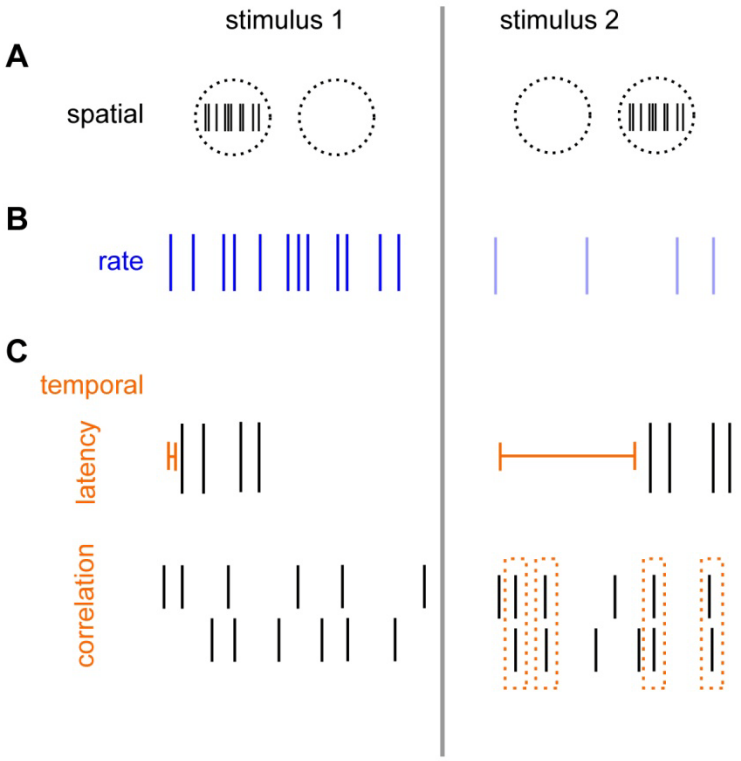

Figure 1.2: Putative coding schemes. Neurons may represent stimulus-specific information in several different ways. For example, **(A)** the spatial arrangement of activated cells, **(B)** the frequency of emitted action potentials and/or **(C)** the specific timing of action potential emission could be used to represent information. Spike timing can be measured and quantified in several different ways including delays before spiking (latency) or the similarity of spike timing across groups of neurons (correlation).

features (such as chemical group location or carbon chain length) (Uchida et al., 2000). Individual mitral cell activation has can be highly specific to particular odorants—even enantiomers (Rubin and Katz, 2001)—and minimally influenced by the presence of additional components in stimulus mixtures (Lin et al., 2006). The conserved spatial relationship between chemical features across animals (Soucy et al., 2009), suggests that spatial organization may represent a useful feature of olfactory coding.

Further evidence for spatial coding comes from an observed correlation between spatial activity patterns and perception. In behavioral discrimination tasks, animals confuse odorants with similar evoked spatial patterns with higher frequency than odors with non-overlapping spatial patterns (Linster et al., 2001; Youngentob et al., 2006). Interestingly, this holds true even if the two stimuli evoking similar patterns are chemically very dissimilar. Thus both chemical and perceptual features can be (at least in part) predicted by the spatial distribution of activated glomeruli.

However, the spatial coding hypothesis has several limitations. For one, while evoked spatial patterns can be clearly distinguished in the case of some simple monomolecular odorants, the olfactory bulb more often processes stimuli in a complex environment in which complex mixtures are prevalent. In these instances, the evoked spatial patterns are much more similar and may require additional processing to disambiguate (Abraham et al., 2004). Further, chemical stimuli are multidimensional in nature while glomerular location is restricted to a two-dimensional plane along the surface of the bulb. Given this reduction in dimensionality, olfactory bulb odotopy describes a general organization and relationship between stimulus evoked patterns rather than an exact organization of chemical features in space. Lastly, spatial patterns refer to a static "image" of activation across the olfactory bulb surface(Ma et al., 2012).

Because these images are composites of activity patterns occurring over time, it is possible that their efficacy derives (at least in part) by processing at a finer timescale. While this type of processing might be reflected in these composite images, it is possible that they are simply the byproduct of some other coding scheme.

1.3.2.2. Rate coding

Most approaches to investigating neural coding involve electrical recordings from neurons because action potentials are the currency of neuronal communication. A central question in linking neural activity to perception is elucidating which aspects of spike trains are informative. Since spikes are discrete, all-or-nothing events, firing patterns can be described in terms of when or how many spikes occur across time. Rate-based quantification relies on counting the number of spikes emitted by neurons across long (>100 ms) periods of time.

As a coding strategy, rate coding operates by neurons emitting more action potentials to some stimuli and fewer action potentials in response to other stimuli (**Figure 1.2 B**). Rate coding has been observed ubiquitously in sensory systems, deriving from the observation that neural firing rates increase with increased sensory stimulation (Adrian, 1928). Rate coding is related to spatial coding in that the intensity of a spatial activation pattern is presumed to rely on firing rate intensity. However, rate coding offers several advantages over spatial coding because it allows for coding in the temporal domain. Rate coding can be computationally effective for reducing the impact of trial-to-trial noise and preventing noise from amplifying as activity is propagated across populations (Shadlen and Newsome, 1998). In the olfactory bulb, rate coding

is believed to be a plausible coding scheme because mitral and tufted cell responses are sparse and stimulus-specific (Davison and Katz, 2007; Da Yu Lin et al., 2005; Rubin and Katz, 1999). That is, since individual mitral cells respond to only a small subset of odors, the firing rate and identity of active neurons may be sufficient to represent odors.

1.3.2.3. Temporal coding

While the exact time window describing rate coding is variable, it typically refers to spike counts over medium-to-long chunks of time (~100 to 1000 ms). One intrinsic limitation of rate coding is that it ignores any stimulus-specific activity patterns occurring at shorter timescales (0-100 ms; **Figure 1.2 C**). Patterns of activity at these shorter timescales are typically categorized as temporal coding strategies. Importantly, temporally complex spiking at these short timescales is highly characteristic of odor-evoked responses. These short timescale patterns may be informative about stimuli, or important for driving downstream neurons. Using short timescale information to encode stimuli can increase the information content of spike trains and improve performance on pattern recognition tasks (Hopfield, 1995).

However, the utility of temporal coding schemes in olfaction has been debated in part because of the "slowness" of olfactory sensation. Short timescale spike train statistics can be useful for tracking fast changes in stimulus content (for example, "flickering" of light). However, the olfactory environment does not fluctuate rapidly across time because diffusion of odor molecules through air is slow. Further, even if olfactory stimuli did have rapidly

fluctuating statistics, they would not necessarily be sampled because odor sampling is limited by the respiratory cycle and animals cannot sniff at extremely high frequencies.

Despite these conceptual limitations regarding temporal coding in olfaction, evidence for temporal coding in the olfactory bulb has been observed in both insects and rodents. Seminal studies in honeybees examined behavior in the presence of the $GABA_A$ antagonist, picrotoxin (Stopfer et al., 1997). Importantly, this drug disrupts short timescale temporal patterning while leaving overall firing rates unchanged. Application of picrotoxin significantly impaired performance in fine discrimination tasks, suggesting that relevant information is contained at fine timescales. Optogenetic manipulations reveal that mice are sensitive to discriminating differences in spike timing on the order of ~10 ms—much short than would be accounted for by any rate-based strategy (Smear et al., 2011). These examples suggest that at least in some cases, rate information provides an incomplete picture of the information encoded by the olfactory bulb. Latency and correlation coding are two forms of temporal coding that have been posited to play a role in olfactory bulb coding.

1.3.2.3.1. Latency

In latency coding, the delay (latency) of action potential onset across neurons is used to encode stimulus information (**Figure 1.2 C**). Latency responses are sometimes referred to as cascades or "tiled responses" because each stimulus evokes a unique sequence of activation across a population of neurons. Evidence for this type of coding has been obtained in many primary sensory areas including visual (Gollisch and Meister, 2008; Gawne et al., 1996),

auditory (Furukawa and Middlebrooks, 2002; Heil and Irvine, 1997; Heil and Irvine, 1996; Chechik et al., 2006; Chase and Young, 2007), somatosensory (Johansson and Birznieks, 2004; Panzeri et al., 2001; Petersen et al., 2002), and olfactory areas (Kapoor and Urban, 2006; Spors et al., 2006; Balu et al., 2004; Schaefer and Margrie, 2007; Brody and Hopfield, 2003; Chen et al., 2009; Shusterman et al., 2011). Latency coding is computationally effective (Margrie and Schaefer, 2003), enabling rapid stimulus identification (Thorpe and Gautrais, 1997), intensity invariance (Margrie and Schaefer, 2003), and processing of complex stimuli (Van Rullen et al., 1998). Most examples of latency coding involve small (<50 ms) differences between action potential timing in different cells. A notable exception is long timescale activity in the olfactory bulb, where odors evoke distinct spatiotemporal activity patterns persisting for many seconds, including long latency spiking (Chen et al., 2009; Luo and Katz, 2001).

Stimulus-evoked latency patterns are observed in many cell types in the olfactory bulb, spanning all layers of this circuit. In the glomerular layer on the surface of the olfactory bulb/antennal lobe, a latency structure is already established by the olfactory receptor neuron inputs, whereby different glomeruli are activated at different, stimulus-specific latencies established both within and across sniff cycles (Spors et al., 2006; Raman et al., 2010). Similarly, latency patterns of activity have been observed in mitral and tufted cells, whose first action potentials are tiled across the sniff cycle, giving rise to stimulus-specific sequences of neural activity (Margrie and Schaefer, 2003; Shusterman et al., 2011). Lastly, stimulus-specific latency patterns are also observed in inhibitory granule cells, whose glomerulus-specific latencies can be extremely long—up to 1000 ms (Kapoor and Urban, 2006). The observation of stimulus-specific latency patterns in inhibitory interneurons is especially intriguing because the impact of distributed latency inhibition on excitatory spike trains has not been investigated. Our

investigation of the generation and consequences of these latency patterns in the olfactory bulb is described in chapter 3.

1.3.2.3.2. Correlation

The approach of counting spikes—either over short or long periods of time—is very useful for describing the response properties of individual neurons. However, these quantifications lack a detailed description of the relationship of firing across cells. Sensory coding (particularly in primary sensory areas) relies on the recruitment of many cells. This is especially true in the olfactory bulb, where even simple monomolecular odorants can evoke large populations of neurons that are distributed throughout the olfactory bulb. In order to capture the relationship of firing patterns across cells, a variety of metrics have been developed. One commonly used metric is correlation, which measures how similar (or different) spike trains are.

For pairs of spike trains, a correlation coefficient measures the covariability of spiking between the two cells. That is, spiking is correlated when an increase or decrease in firing in one cell can be predicted by activity in the other cell. This calculation is normalized by the variance of firing in each cell in order to measure spiking that is correlated above chance.

Some of the first descriptions of pairwise spiking correlation came from paired recordings of primate cortical areas (Gawne and Richmond, 1993; Zohary et al., 1994; Lee et al., 1998) where it was noted that the number of spikes emitted by individual neurons varied across repeated presentations of the same stimulus. Further, this variability was not independent across neurons—they tended to increase or decrease their firing together. The strengths of these

correlations observed in cortex were typically in the range of 0.1-0.2 (Zohary et al., 1994; Gawne and Richmond, 1993).

In the olfactory bulb, correlated activity has mostly been studied in the context of fast oscillatory correlations (Laurent and Davidowitz, 1994) and pattern correlations (Friedrich and Laurent, 2001; Wiechert et al., 2010). Correlated activity was observed in the form of oscillations even in the first recordings of the mammalian olfactory bulb (Adrian, 1942). These fast oscillations reflect spike synchrony at a fast timescale and are believed to arise from rhythmic interactions between excitatory and inhibitory cells (which can be either periodic (Lagier et al., 2004; Kay et al., 2009) or non-periodic (Galan et al., 2006; Aylwin et al., 2005)). This type of fast correlation is believed to be functionally relevant because its magnitude changes dynamically with discrimination task difficulty (Beshel et al., 2007) and is correlated with correct behavioral performance (Nusser et al., 2001; Stopfer et al., 1997). While granule cells appear to exert a correlating effect on mitral cell spike train statistics, these same interneurons are believed to shape population activity in additional ways, including pattern decorrelation (Friedrich and Laurent, 2001; Wiechert et al., 2010), leading to debate over whether local olfactory bulb circuitry actively correlates or actively decorrelates activity patterns. Thus the precise structure of spike train correlations in the bulb remains unclear.

Even if the structure of olfactory bulb correlations were fully understood, the utility and impact of spike train correlations is an issue of ongoing debate and discussion (Averbeck et al., 2006). On the one hand, correlations can impact coding negatively because they introduce redundancy. Imagine two spike trains that are identical copies of one another. In this scenario, the population of two neurons is redundant because it only contains one signal, while it has the capacity to send two different signals. Correlations can also prevent noise from being eliminated

through population averaging (Zohary et al., 1994). Conversely, correlations can have many benefits, such as increasing a population's coding accuracy (Abbott and Dayan, 1999; Romo et al., 2003), facilitating propagation (Kumar et al., 2010), mediating binding (Milner, 1974; Singer and Gray, 1995), regulating gain control, and shaping variability (Salinas and Sejnowski, 2000). In short, the generation (de la Rocha et al., 2007) and impact of spike train correlations is highly complex and can vary based on the response properties of neurons, the dynamics of local interactions, and the role of the population in coding information. Because of this diversity, we lack a complete understanding of how correlated variability impacts coding in different circuits.

Colloquially, the term correlation has been used rather non-specifically to describe spike train similarities. However, a rigorous description of spike train correlation requires specifying the temporal window over which correlations are measured. Consider the schematic example in **Figure 1.3**. If one were to quantify whether the two spike trains were similar or different, one might count the number of spikes occurring over a period of time. As the time window varies, so too does this simple measure of spike similarity. Fast correlations (commonly referred to a spike synchrony) are measured over small time bins, whereas slow correlations (such as correlation of firing rates) are measured over large bins. The relationship of correlations at short and long timescales in the olfactory bulb remains poorly understood. This ambiguity was a major motivation for the studies presented in chapter 4.

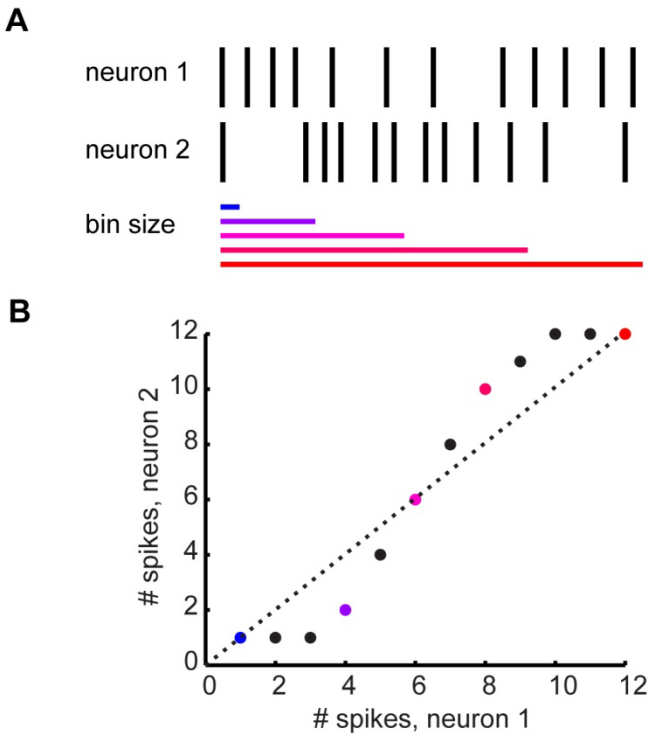

Figure 1.3: **Examining spiking characteristics across bin sizes.** **(A)** Given two spike trains—neuron 1 and neuron 2—we can quantify and compare their spikes at different bin sizes (colored bars below). **(B)** For each bin size, one can compare the number of spikes in neuron 1 and neuron 2. Picking any particular bin size ignores some of this relationship while reporting spiking activity across timescales yields a more complete description of the neural activity.

1.3.2.4. Multiplexed coding

As the previous sections highlight, patterns of stimulus-evoked activity in the olfactory bulb are complex and can be described by a wide variety of metrics. Encoding information via any one of these metrics has its own set of advantages and disadvantages. The strong evidence for the existence and utility of each of these coding schemes has led many to think about olfactory coding in a multiplexed framework (Panzeri et al., 2010). This view states that information can be encoded in a variety of ways by spiking neurons simultaneously; for example, using spatial, rate, and temporal patterns. Then, the relevant features of these spike trains (which may vary with different stimuli or task demands) can be accessed by downstream neurons.

The existence of multiplexed codes has been particularly well-studied in the visual system, where different timescales can encode complimentary information about stimuli, such as fast stimulus fluctuations versus stimulus history (Fairhall et al., 2001). Complimentary information at different timescales has proven feasible in modeling and experimental frameworks (Masuda, 2006; Kumar et al., 2010) and has been observed in vitro (Reyes, 2003), in the visual (Montemurro et al., 2008; Belitski et al., 2008; Mazzoni et al., 2008) and auditory (Kayser et al., 2009) cortices, as well as in the olfactory bulb (Friedrich et al., 2004; Bathellier et al., 2008). This perspective suggests that the putative coding strategies described in the previous sections need not be considered as competing and mutually exclusive hypotheses, but rather as complimentary views that can be used in concert to better understand neural activity.

1.4 STATEMENT OF THESIS GOALS

In summary, mitral and tufted cells are charged with the responsibility of representing all information about odors in the environment and they may accomplish this with a variety of different coding strategies. While many studies have documented the importance of granule cell circuits in shaping odor-evoked activity and behavior, the specific mechanisms by which this is accomplished are not fully understood. My specific interest is in understanding what strategies are used by granule cell circuits to improve olfactory coding. I am particularly intrigued by a timescales problem within these circuits: understanding what lengths of time are relevant for coding, and how the olfactory bulb shapes its output to operate effectively in these time windows. With this thesis, I will provide experimental and computational evidence to address these questions within the context of olfactory processing.

Chapter 3 of my thesis was motivated by the report that olfactory bulb granule cells are recruited at extremely long yet reliable latencies. Long-timescale granule cell activity is known to participate in this activity, but two large questions remain: HOW is long-latency inhibition generated by olfactory bulb circuits, and WHY is it generated? Chapter 3 first describes experiments that aim to discover the source of long-latency activity in the olfactory bulb. Later in this chapter, I use computational models to argue that long-latency inhibition is an effective strategy for disambiguating similar or overlapping stimulus representations.

While Chapter 3 focuses on these timescales issues from the perspective of granule cell physiology and output, Chapter 4 examines a related issue of olfactory bulb timescales by investigating the output of olfactory bulb coding cells (mitral cells) directly. This chapter focuses on a tradeoff between propagation and encoding. Correlated spike trains are effective at propagating information to other brain areas (because they can "double" the strength of a signal). However, correlations pose a problem for encoding because they introduce redundancy and limit the amount of information that can be sent at one time. In Chapter 4, I describe a new way to think about this problem by investigating correlations at different timescales. I present paired recordings showing that recruitment of olfactory bulb inhibition acts to simultaneously increase fast correlations and decrease slow correlations. I then use computational modeling techniques to demonstrate the utility of timescale-dependent correlation changes for enhancing stimulus discriminability.

Together, these chapters emphasize that understanding the timescales of evoked activity are not only useful for advancing our understanding of the demands on a circuit, but being mindful of activity across timescales can answer basic questions about sensory coding as well as provide a constructive framework for some old debates about the nature of temporal coding, relevant timescales, and correlations.

2.0 MATERIALS AND METHODS

2.1 SLICE PREPARATION

All procedures were done in accordance with the guidelines for the care and use of animals at Carnegie Mellon University and as previously described (Arevian et al., 2008; Galan et al., 2006; Castro et al., 2007). C57BL/6 mice (age P11–P20) were anesthetized using isofluorane. Anesthesia was monitored by responsiveness to tail pinch and animals were decapitated. Dissection and slicing were both performed in ice-cold Ringer's Solution (in mM: 125 NaCl, 25 glucose, 2.5 KCl, 25 $NaHCO_3$, 1.25 NaH_2PO_4, 1 $MgCl_2$, and 2.5 $CaCl_2$.) Coronal slices (300–350 μm) were obtained from the olfactory bulb using a vibratome (VT1200S; Leica). Slices were placed in oxygenated Ringer solution at 37° C for 15 minutes and then allowed to recover for 30 minutes before being used for electrophysiology or imaging.

2.2 ELECTROPHYSIOLOGY

Data were recorded using software written in Igor Pro (WaveMetrics) with a 700B amplifier (Molecular Devices) and ITC-18 data acquisition board (InstruTech). Whole-cell patch pipettes (1–3 MΩ) with internal solution (in mM: 130 potassium gluconate, 10 HEPES, 2 $MgCl_2$, 2 MgATP, 2 Na_2ATP, 0.3 GTP and 4 NaCl) were used to make recordings. Whole-cell current-clamp and voltage-clamp recordings were performed, as well as cell attached recordings. For

experiments shown in Figure 3.3, 50 uL of the fluorescent tracer AlexaFluor 594 (Invitrogen) was added to the internal solution to allow visualization of cell morphology and apical tuft location. Recordings were performed in the same Ringer's solution used for dissection. For Figure 3.6, tufted cells were recorded in the presence of drugs to block synaptic transmission: 25 μM APV, 10 μM CNQX, and 10 μM bicuculline to block NMDA, AMPA, and $GABA_A$ receptors, respectively). Where noted, 20 μM 4-aminopyridine (4-AP; a voltage-gated potassium channel blocker) was added.

Chapter 3 electrophysiology: Glomerular stimulation was applied using a coiled formvar-insulated nichrome microwire or monopolar glass stimulating electrode inserted into a glomerulus. Glomeruli were identified as spherical neuropils surrounded by small cell bodies, located near the edge of the slice. A brief (0.3-3 ms) pulse was applied by connecting the stimulating electrode to an SIU (stimulus isolation unit) controlled by TTL (transistor-transistor logic) pulses from an ITC-18 data acquisition board. Stimulation amplitude was selected to be the minimum amplitude that elicited low probability spiking or long lasting depolarizations s in granule cells.

The rise time of prolonged depolarizations (Figure 3.1 B) was calculated as the time at which the depolarization reached 50% of its maximum value. Decay time was identified as the time point at which the depolarization decayed to within 5% of baseline. For the spike latency data, trials were excluded if they had spikes preceding glomerular stimulation or latencies longer than 1000 ms, as these are likely spontaneous and not stimulus evoked events. To identify EPSC onset, we subtracted the mean from current traces and identified EPSCs from threshold crossings of both the voltage clamp data and the derivative of the current trace. Since noisy fluctuations occurring in the first 100 ms following glomerular stimulation were insufficient to drive spiking,

we selected conservative thresholds so that very noisy or very small events were excluded. EPSC onset was defined as the mean of the first two identifiable EPSC times. For comparisons of means, significance was determined using a t-test (Figure 3.4). For comparisons of distributions, a Kolmogorov-Smirnov test was used. A 0.05 significance level was used for all.

Chapter 4 Electrophysiology: Since granule cells are typically quiescent in slice preparations (due to fewer active mitral cell inputs), we increased granule cell excitability either by reducing magnesium concentration in the extracellular solution to 0.2 mM (Kapoor and Urban, 2006), or by using standard ringer solution with 10 μM DHPG ((*S*)-3,5-dihydroxyphenylglycine, an mGluR agonist that increases granule cell excitability (Castro et al., 2007; Dong et al., 2007)). DHPG has previously been shown to increase the rate of spontaneous inhibitory events without changing the waveforms of IPSCs (Castro et al., 2007). Experiments were performed at 37°C.

Stimulus currents were defined by a direct current offset (50–1000 pA) applied for 2000 ms to evoke mitral cell firing. This elicited a range of firing rates across pairs (6–55 Hz). The amplitude of the injected current was set so that firing rates in the two cells were roughly equal. We discarded sweeps in which firing rate was greater than two standard deviations from average, as these changes are likely due to random spontaneous activity rather than evoked inhibition. Since we wanted to include pairs in which the effects of inhibition were observable, we included mitral cell pairs displaying at least some slow decorrelation as this effect has already been shown to be inhibition mediated in this preparation (Arevian et al., 2008). As mentioned above, we used two methods to increase granule cell excitability: reduced Mg^{2+} concentration or DHPG. We found that the spontaneous rate of IPSCs in the DHPG experiments was consistent over time whereas low magnesium often caused the spontaneous rate of inhibition to fluctuate at very slow

timescales (observed as 0.2–1 Hz bursts in IPSC frequency; data not shown). For this reason, more low Mg^{2+} pairs (10/13) than DHPG pairs (4/11) were excluded from analysis.

Firing rates were measured over 2-second periods across repeated trials (20–80). Cross-timescale correlation was calculated by binning spike trains at bin sizes ranging from 1 to 1000 ms and calculating correlation using the following equation. Synchrony was defined as correlation measured at a bin size of 10 ms.

$$\rho_T = \frac{\langle n_1 n_2 \rangle - \langle n_1 \rangle \langle n_2 \rangle}{\sqrt{\langle n_1^{\,2} \rangle - \langle n_1 \rangle^2} \sqrt{\langle n_2^{\,2} \rangle - \langle n_2 \rangle^2}}$$

Coincidence was calculated by eliminating chance correction in the correlation formula:

$$c_T = \frac{\langle n_1 n_2 \rangle}{\sqrt{\langle n_1^{\,2} \rangle} \sqrt{\langle n_2^{\,2} \rangle}}$$

All p-values noted were calculated using a t-test.

2.3 IMAGING

Olfactory bulb slices were loaded with a fluorescent calcium indicator dye by being transferred to a chamber containing 500 µl of Ringer's solution with 3 µl of 0.01% pluronic (Invitrogen) and 5 µl of a 1 mM solution of fura-2 AM (Invitrogen) in 100% DMSO solution. Slices were incubated in this solution at 37°C for 90 min while humidified air was passed above the liquid in the chamber to keep the solution oxygenated.

After fura-loading, slices were placed in a submersion recording chamber under an upright microscope using 40 or 60x water immersion objectives. Images and movies were recorded at 75 ms per frame using a cooled back-illuminated frame transfer CCD camera (Cascade 512B; Princeton Instruments). Images were acquired and stored using software written in Igor Pro (WaveMetrics) with drivers (SIDX, Bruxton Scientific). We recorded 1500-ms-long movies of the granule cell layer during glomerular stimulation ± somatic stimulation of a single tufted cell.

2.4 NEURAL MODELS

2.4.1 Granule cell latency model

All simulations were performed in Matlab using mex files to interface with C. The granule cell latency model described in chapter 3 consisted of 100 leaky integrate-and-fire neurons (simulated mitral cells) described by the following equation:

$$\tau_m \frac{dV}{dt} = -I_{stim} - I_{noise}(t) - I_{leak}(t) - I_{inhib}(t)$$

Where τ_m is the membrane time constant. The time step Δt=0.01 ms and a standard Euler integration scheme were used. The excitation delivered to model mitral cells (I_{stim}) was set at a constant for each cell on each trial. Noise currents (I_{noise}) were uncorrelated across cells and were generated as the sum of two 100-Hz Poisson trains convolved with a decay constant (τ_{noise}=3 ms) and scaled by 1 for excitatory trains and -1 for inhibitory trains. A direct current offset between 0

and 1 was then added to this noise. Leak current (I_{leak})= $g_L(V_i(t)-V_L)$, where g_L is the unitary leak current and V_L is the reversal potential of the leak term. When an excitatory cell was depolarized to threshold (V_{thresh}), a spike was identified and the membrane potential was reset to V_{reset} for a refractory period of τ_{ref}. The full list of parameters used in the model can be found in **Table 2.1.**

Inhibitory synaptic currents (I_{inhib}) were generated by a population of 50 interneurons (simulated granule cells). We generated a template of population spiking using a 10-Hz Poisson rate for each interneuron to generate a population peri-stimulus time histogram. We then used this template to generate interneuron spikes based on the specified range of interneuron latencies. We assigned each cell a stimulus-specific latency ranging from 0 to 100 ms (in the most narrowly distributed model) to 0 to 1000 ms (in the most widely distributed model). Each cell was prohibited from spiking prior to its assigned latency, but was free to spike anytime thereafter. To generate spike times for all model variants, we counted the number of spikes (k) occurring at each millisecond (i) in the template data (k_i). Then, for each time bin, we randomly selected k_i cells that were available to spike (i.e. time had exceeded cell's assigned latency and cell was not in a refractory period (40 ms)) and assigned spikes to those cells for time bin i. Drawing from the template spiking data in this way ensured that the number of interneuron spikes per millisecond was identical in all model variants. Each excitatory cell in the model received input from 10% of the 50 interneurons. The same connectivity matrix was used for all model variants.

Symbol	Parameter	Value
τ_m	membrane time constant	9.5 ± 0.5 ms
Δt	Simulation time step	0.01 ms
I_{stim}	Mitral cell current injection amplitude	17 ± 1
r_noiseE	Rate of excitatory noise, poisson rate	100 Hz
r_noiseI	Rate of inhibitory noise inputs, poisson rate	100 Hz
τ_{noise}	Decay of noise pulses	3 ms
a_noise	Noise DC offset	0.5 ± 0.5
g_L	Unitary leak current	1
V_L	Leak reversal	-55 mV
V_{thresh}	Spike threshold	-44.5±0.5 mV
V_{reset}	Spike reset voltage	-53.5 ± 0.5 mV
τ_{ref}	Refractory period	6 ms
rI	Firing rate of granule cells	10 Hz
$\tau_{ref,I}$	Interneuron refractory period	40 ms
p_con	Connection probability between E-I pairs	0.1

Table 2.1: Parameters of latency network model.

For the stimulus discrimination analyses, we used spike count data occurring during the first 500 ms of stimulus presentation for analysis. This time frame was selected because it represents a behaviorally relevant timescale for olfactory discriminations (Rinberg et al., 2006; Abraham et al., 2004; Abraham et al., 2010). Classification accuracy was calculated by training a linear classifier on data from 50% of trials and using the other 50% of trials as a test set. Accuracy was defined as the portion of correct classifications for each stimulus.

2.4.2 Two-cell model

The two-cell model consists of two excitatory LIF neurons described by the following equation:

$$\tau_m \frac{dV_i}{dt} = -I_{stim} - I_{syn,I,i}(t) - I_{noise,i}(t) - I_{leak,i}(t)$$

where τ_m is the membrane time constant. The full list of parameters used in the model can be found in **Table 2.2.** The time step Δt=0.01 ms and a standard Euler integration scheme was used. The stimulus (I_{stim}) was set at a constant for each cell. Noise currents (I_{noise}) were uncorrelated across cells and were generated as the sum of two 100 Hz Poisson trains convolved with a time constant describing decay (τ_{noise}) and scaled by 0.3 for excitatory trains, and -0.3 for inhibitory trains. Inhibition ($I_{syn,I}$) was modeled as pools of Poisson-rate inhibitory current delivered to the two excitatory cells. The correlation of inhibitory input was set by the parameter *c*, which set the portion of the inhibitory pool that was shared by the pair (while the unshared portion is described by 1-*c*). Leak current (I_{leak}) = $g_L(V_i(t)-V_L)$, where *gL* is the unitary leak current and V_L is the reversal potential of the leak term.

Symbol	Parameter	Value
τ_m	Membrane time constant	10 ms
Δt	Simulation time step	0.01 ms
I_{stim}	Stimulation intensity	1.5 units
f_{noise}	Frequency of (+) and (-) noise inputs	100 Hz
τ_{noise}	Time constant of noise input decay	3 ms
a_{noise}	Scaled amplitude of noise inputs	0.3
c	Correlation of inhibitory inputs	0-1.0
gL	Unitary leak current	1
V_L	Reversal potential of leak	0
V_{thresh}	Spike threshold	1
V_{reset}	Spike reset potential	0
$t_{refract}$	Absolute refractory period	5 ms
$\tau_{\alpha,\ rate}$	Time constant of alpha function kick to Poisson rate	2.5
$a,\ b,\ d$	Constants describing hyperbolic tangent function	0.4; 30; -3.5 (unshared -) 0.75; 65; -5 (shared -)
$\tau_{\alpha,\ current}$	Time constant of synaptic current (alpha function)	1.1
$k_{current}$	Amplitude scalar for synaptic inhibition current	-6.0

Table 2.2: Parameters of two-cell model.

When either of the excitatory cells was depolarized to threshold (V_{thresh}) a spike was identified and the membrane potential was reset to V_{reset} for the duration of the refactory period ($t_{refract}$). Spikes from either excitatory cell resulted in an 'alpha' function determining the time-varying Poisson rate, $P_{(-)}$ at which inhibitory pools were activated.

$$P_{(-)} = k\sum_{i=1}^{2}\sum_{j}\frac{t-t_{ij}}{\tau_\alpha^{\,2}}e^{\left(\frac{-(t-t_{ij})}{\tau_\alpha}\right)}$$

where t_{ij} is the j^{th} spike time from the i^{th} excitatory cell. Since inhibition should be bounded in any real neural circuit, we convolved this activity-evoked probability by a hyperbolic tangent function to induce a saturation in the amout of available inhibition. This saturation was described by the following equation:

$$P_{(-),conv} = \frac{a}{2}\left(\tanh\left(2bP_{(-)} + d\right)+1\right)$$

Where a, b, and d are constants specific to shared and individual pools of inhibition (for unshared inhibitory pools, a = 0.4, b=30, d=-3.5, for shared inhibitory pool, a=0.75, b=65, d=-5). The resultant Poisson rate for each inhibitory pool is scaled by the proportion of shared inhibition such that

$$P_{(-),indiv} = (1-c)P_{(-),conv}$$

and

$$P_{(-),shared} = cP_{(-),conv}$$

Inhibitory current delivered to mitral cells is also described by the alpha function equation where τ_α=1.1 and k=-6.0.

2.4.3 Timescale-dependent correlations model

All parameters used in the timescale-dependent correlations model can be found in **Table 2.3.** Stimuli applied to the network model were generated by randomly dividing the excitatory cells into two groups: group A and group B. For stimulus 1, group A was stimulated at a higher intensity 1 (I_A) while group B was stimulated at a slightly lower intensity 2 (I_B). For stimulus 2, group B was stimulated at the higher intensity and group A was stimulated at the lower intensity. For all cells, the initial value of stimulation current was given a slight slope across time (0.0002t) to attain physiologically realistic values of pairwise correlation in the no coupling scenario. Whether this source of slow correlation was a ramp or sinusoid did not impact results over our range of analyzed timescales.

Since we wanted to know how well an unbiased observer of the network could discriminate between stimuli, we again divide the network into two observation groups (unrelated to stimulus-defined groups A and B). Cells were assigned to observation groups 1 or 2 with 50% probability and output patterns were quantified as the average firing rate in each group measured over 500 ms epochs. Pattern representations (Figure 4.6 E-F, Figure 4.7 C-D) were plotted using group 1/group 2 firing rate data collected over 150 trials.

In order to quantify the degree to which stimuli 1 and 2 were discriminable via observation of groups 1 and 2, we employed a linear discriminant and receiver-operator characteristic (ROC) analysis. For each model variant, we identified the plane along which stimulus 1 and stimulus 2 were most discriminable given the observed stimulus-evoked patterns (Figure 4.6 E-F, Figure 4.7 C-D). Briefly, we calculated the center of the stimulus 1 and stimulus 2 distributions in (x,y) coordinates and a line perpendicular to the line connecting the

centers of stimulus 1 and stimulus 2 distributions was used as the plane of maximum discriminability. As this line was translated along the y-axis, the number of true positive trials (α, correct identification of applied stimulus) and false positive (β) trials were counted. The discriminability metric (d) was calculated by integrating the area under each curve and subtracting 0.5 (since 0.5 corresponds to chance levels of identification) and multiplying by 2. Thus, d describes on a scale of 0-1 how well above chance the network's evoked responses are discriminable above chance.

Based on the architecture of the mammalian olfactory bulb, our model consists of 900 current-based LIF neurons, 11% of which are excitatory and 89% of which are inhibitory. Excitatory and inhibitory cells are connected via reciprocal dendrodendritic synapses with a pairwise connection probability of 20%. The model lacks excitatory-excitatory and inhibitory-inhibitory connections. Each cell in the model obeyed the following:

$$\tau_m \frac{dV_i}{dt} = -g_L\left(V_i(t) - V_L\right) - I_{syn,E,i}(t) - I_{syn,I,i}(t) - I_{noise,i}(t) - I_{stim}$$

Where V_i is the membrane voltage of the i^{th} neuron, τ_m is the membrane time constant, gL is the unitary leak current and V_L is the reversal potential of the leak term. I_{synE} and I_{synI} describe excitatory and inhibitory synaptic activity, respectively, arising from activation of synapses in the network. All synaptic currents were described by the following:

$$\tau_x \frac{dI_x}{dt} = -I_{x,i}$$

where τ_x is the time constant describing the decay of synaptic excitatory or inhibitory input currents. When a cell's membrane potential reaches threshold (V_{thresh}), the neuron fires an action potential, a spike time is identified, and that neuron's membrane potential is reset to (V_{reset}).

Symbol	Parameter	Value
P_A	Probability of a cell being assigned to group A	0.5
I_A	Stimulation intensity of group A	11.5 ± 0.5
I_B	Stimulation intensity of group B	10.7 ± 0.5
P_{ObsA}	Probability of a cell being in observation group A	0.5
N_E	# of excitatory neurons (model mitral cells)	100
N_I	# of inhibitory neurons (model granule cells)	800
$P_{connect}$	Connection probability between pairs of mitral and granule cells	0.2
τ_m	Membrane time constant	9.5 ± 0.5 ms
gL	Unitary leak current	0.5
V_L	Reversal potential of leak term	-55 mV
τ_E	Time constant of EPSCs	3 ms
τ_I	Time constant of IPSCs	3 ms
Δi_E	EPSC amplitude	$OB_{(-)}$=0.55; $sync_{(\pm)}$=0.35, $async_{(-)}$=0.65
Δi_I	IPSC amplitude	$OB_{(-)}$,-0.82; $sync_{(\pm)}$=-2.2; $async_{(-)}$=-1.2
V_{thresh}	Membrane threshold	-45.5±0.5 mV
V_{reset}	Membrane resent potential	-54.5±0.5 mV
$t_{refract}$	Absolute refractory period	5 ms
F_{noise}	Firing rate of noise inputs	100 Hz
τ_{noise}	Time constant of noisy IPSC/EPSC decay	3 ms
ΔI_{noise}	Amplitude of noise inputs	±2.2
Δt	Simulation time step	0.01 ms

Table 2.3: Parameters of olfactory bulb propagation/encoding model.

After being reset, the neuron remains refractory for a fixed amount of time, $t_{refract}$. The synaptic current received by the cell's postsynaptic targets is augmented by the following equation:

$$I_{x,i}(t) = I_{x,i}(t) + \Delta I_x$$

Where Δi_x is the unitary augmentation in synaptic current evoked by presynaptic activity. Unitary currents were adjusted slightly for each model variant to normalize amplitudes of correlation changes. ($OB_{(-)}$:Δi_E=0.55 , Δi_E=-0.82; $sync_{(\pm)}$:Δi_E=0.35, Δi_E=-2.2, $async_{(-)}$, Δi_E=0.65 , Δi_E=-1.2). Noise currents were uncorrelated across cells and were generated as the sum of two 100 Hz Poisson trains convolved with a time constant describing decay (τ_{noise}) and scaled by 2.2 for excitatory trains, -2.2 for inhibitory trains. The sum of these trains is thought of as a barrage of uncorrelated excitatory and inhibitory synaptic input from sources external to our network (for example, inputs from olfactory receptor neurons, periglomerular cells, or centrifugal inputs from cortex). Lastly, I_{stim} is a constant DC offset current delivered to neurons as described in the stimulus generation section above (I_{stim} = 10.7 ± 0.5 for group A, 11.5 ± 0.5 for group B). Spike trains generated by these models were analyzed using the same methods described above.

3.0 GRANULE CELL LATENCY CODING

3.1 ABSTRACT

Inhibitory circuits are critical for shaping odor representations in the olfactory bulb. There, individual granule cells can respond to brief stimulation with extremely long (up to 1000 ms), input-specific latencies that are highly reliable. However, the mechanism and function of this long timescale activity remain unknown. We sought to elucidate the mechanism responsible for long-latency activity, and to understand the impact of widely distributed interneuron latencies on olfactory coding. We used a combination of electrophysiological, optical, and pharmacological techniques to show that long-latency inhibition is driven by late onset synaptic excitation to granule cells. This late excitation originates from tufted cells, which have intrinsic properties that favor longer latency spiking than mitral cells. Using computational modeling, we show that widely distributed interneuron latency increases the discriminability of similar stimuli. Thus, long-latency inhibition in the olfactory bulb requires a combination of circuit- and cellular-level mechanisms that function to improve stimulus representations.

3.2 INTRODUCTION

Temporal coding strategies are those in which the timing of action potentials (instead of, or in addition to mean firing rate) encodes information (Theunissen and Miller, 1995). Information content at short timescales has been traditionally considered in the visual (McClurkin et al., 1991; Bair and Koch, 1996; Gawne et al., 1996) and auditory systems (Knudsen and Konishi, 1979; Simmons, 1979), where stimulus statistics can change rapidly across time. However, temporally precise activity patterns have also been observed in the olfactory bulb. The importance of temporal codes is a topic of intense interest and debate, yet only a few mechanisms for generating such codes have been proposed (Buonomano, 2000), and even fewer have been identified physiologically (Margrie and Schaefer, 2003). Latency coding is a specific temporal coding scheme in which the delay (latency) between stimulus onset and first action potential encodes information.

Typical examples of latency coding involve small (<50 ms) latency differences across cells. A notable exception is the olfactory bulb, where odors evoke distinct spatiotemporal activity patterns (including long-latency spiking) that persist for many seconds (Chen et al., 2009; Luo and Katz, 2001; Junek et al., 2010). In this circuit, sensory neuron axons converge onto functionally segregated spheres of neuropil called glomeruli (Mombaerts et al., 1996), where they synapse onto dendrites of mitral and tufted cells. Each mitral and tufted cell receives input from a single glomerulus, and forms reciprocal synapses with inhibitory granule cells before projecting to higher-order cortical areas (Shepherd, 2004).

Multiple cell types contribute to long timescale activity in the olfactory bulb including peripheral sensory inputs from olfactory receptor neurons (Spors and Grinvald, 2002; Spors et

al., 2006; Lin et al., 2006) as well as local circuits. In slices of olfactory bulb, calcium imaging has been used to characterize the response latencies of inhibitory granule cells following brief stimulation of individual glomeruli. Surprisingly, individual granule cells respond with first spike latencies spanning extremely long time periods, ranging from 0 to 1000 milliseconds (Kapoor and Urban, 2006). What is perhaps even more surprising is the temporal precision of these responses across trials. Individual granule cells respond with stimulus-specific latencies, even though the probability of a spiking response on any given trial is low. Long-latency inhibition is mechanistically and functionally intriguing because long timescales (Friedrich and Laurent, 2001; Uchida and Mainen, 2003; Abraham et al., 2004; Abraham et al., 2010; Rinberg et al., 2006) and inhibitory circuits (Stopfer et al., 1997; Nusser et al., 2001; Abraham et al., 2010) are behaviorally important for olfaction. Further, the impact of long-latency inhibitory inputs has not been investigated.

How does long-latency inhibition arise and contribute to olfactory coding? Our results indicate that tufted cells play a pivotal role in controlling granule cell latency. Tufted cells demonstrate the ability to fire at highly variable latencies, owing to intrinsic membrane properties. This flexibility enables them to drive granule cell activity in a temporally precise, stimulus-specific manner. We show that the resultant distributed-latency inhibition decorrelates mitral cell firing patterns across stimuli. These results describe a straightforward mechanism that can generate long timescale activity and improve encoding, suggesting that long-latency inhibition may provide a computational advantage to olfactory physiology.

3.3 LONG-LATENCY SPIKING IN GRANULE CELLS

Olfactory bulb inhibition is characterized by long-lasting barrages of $GABA_A$ receptor-mediated inhibitory postsynaptic currents (Isaacson and Strowbridge, 1998; Schoppa et al., 1998; Urban and Sakmann, 2002). Previously, our lab showed that the long duration of olfactory bulb inhibition is caused by widely distributed first spike latencies across the granule cell population (Kapoor and Urban, 2006). However, the mechanisms controlling these long response latencies remained unclear. To elucidate these mechanisms, we began by characterizing granule cell spiking activity and membrane potential preceding spiking activity (**Figure 3.1 A**). To activate granule cells, we applied a brief current pulse to stimulate single glomeruli (coiled wire in schematic). We selected this method because it allowed us to transiently stimulate the olfactory bulb in a focally precise manner. This method is conceptually akin to a brief "sniff" that activates a single glomerulus. Electrical stimulation of a single glomerulus activates the resident mitral and tufted cells, which in turn depolarize granule cells. We monitored the membrane potential responses of nearby granule cells using patch clamp techniques.

Activated granule cells responded to glomerular stimulation with membrane potential depolarization, and in some cases, spiking. All activated granule cells responded with an initial depolarization that occurred immediately and decayed slowly (**Figure 3.1 B**; stimulation time denoted by arrowhead; τ_{rise} = 48 ± 39 ms, $\Delta V_{m,peak}$ = 19.2 ± 7.4 mV, τ_{decay} = 2,130 ± 163 ms; n = 11 cells). In a subset of cells, spiking activity was observed atop this depolarization. While the amplitude and time course of the subthreshold depolarization were similar across cells, granule cell first spike latencies were widely variable across cells, ranging from 18 ms to 681 ms.

Consistent with previous reports (Kapoor and Urban, 2006), despite the wide range of observed spike latencies, granule cell spiking was temporally reliable from trial-to-trial (average standard deviation across trials was 118.6 ± 88 ms). Eight trials from an example granule cell are shown in **Figure 3.1 C**. This example exhibits two typical features of our granule cell recordings: a large yet subthreshold depolarization occurs immediately following glomerular stimulation, and temporally precise spiking occurred tens to hundreds of milliseconds later. Importantly, this long-lasting subthreshold depolarization is distinct from the stimulation artifact (such as the vertical line under the triangle in Figure 3.1B.) While the stimulation artifact is seen in all granule cell recordings, depolarization and spiking are only observed in the subset of granule cells that are connected to stimulated mitral and tufted cells.

The data we report here were collected from slices bathed in higher concentrations of magnesium than the previous study (1.0 mM vs. 0.2 mM). This manipulation might be expected to eliminate some of the long-latency spikes observed in low magnesium by blocking NMDA receptors. However, the range of granule cell spike latencies observed here was similar to previous reports (Kapoor and Urban, 2006), despite methodological differences. Spiking probability varied widely across activated granule cells, ranging from 3-88% (mean probability = 48%; n = 18 cells). Latency to first spike was reliable across trials and mean spike latencies ranged from 0-1000 ms (**Figure 3.1 D**; mean first spike latency = 252 ± 171 ms, n=18 cells). Thus, granule cell recruitment following glomerular stimulation was characterized by a short latency, subthreshold depolarization, followed by temporally precise long-latency spiking.

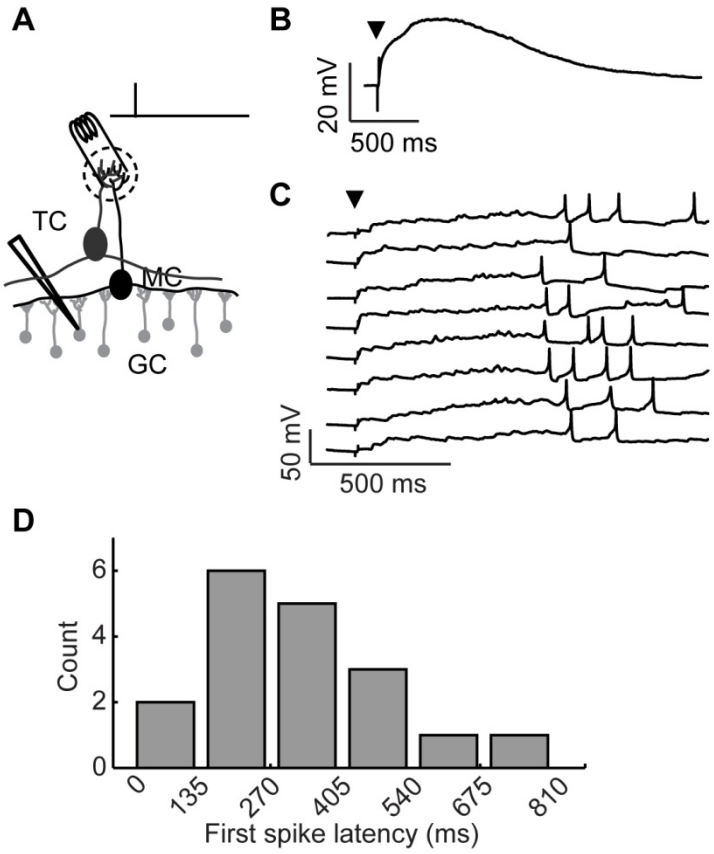

Figure 3.1: Long-latency granule cell activity. (**A)** Experimental setup: A brief, 300 μs stimulation pulse was applied via an extracellular stimulation electrode impaled into a glomerulus. Responses of inhibitory granule cells were recorded using patch clamp. **(B)** Average depolarization following glomerular stimulation. Arrowhead denotes stimulation time. **(C)** Example voltage traces from a granule cell following glomerular stimulation (arrowhead), 8 trials shown. **(D)** Distribution of mean first spike latencies across granule cell population (n = 18 granule cells).

3.4 LONG-LATENCY EXCITATION OF GRANULE CELLS

Thus far we have observed brief glomerular stimulation and granule cell spikes occurring much later in time (shown schematically in **Figure 3.2 A**). We wanted to understand what was happening during this delay that determined granule cell spike timing. What mechanism(s) could account for granule cell responses that were very short under certain conditions and very long under others?

We considered two possible mechanisms that could mediate the distributed-latency spiking that we observed in granule cells. First, the timing of excitatory inputs could determine granule cell latency (**Figure 3.2 B**). That is, short-latency excitation could drive short-latency spiking and long-latency excitation could drive long-latency spiking. Variable-latency excitation could explain the temporal precision and stimulus-specificity of granule cell responses. However, no such source of long-latency excitation is known. Alternatively, different stimuli might elicit excitation that varies in magnitude rather than latency (**Figure 3.2 C**). In this case, granule cell latency could be determined by an interaction between synaptic input and intrinsic cellular properties (such as voltage-gated ion channels). This could account for widely-distributed latencies by allowing granule cells to integrate weak inputs very slowly (thus causing long-latency spiking), while integrating strong inputs rapidly (and causing short-latency spiking) (Molineux et al., 2005; Storm, 1988).

To distinguish between these two possibilities, we recorded in current clamp during glomerular stimulation to characterize spiking activity (**Figure 3.2 D**). We then recorded from these same cells in voltage clamp (using the same stimulation conditions) to characterize

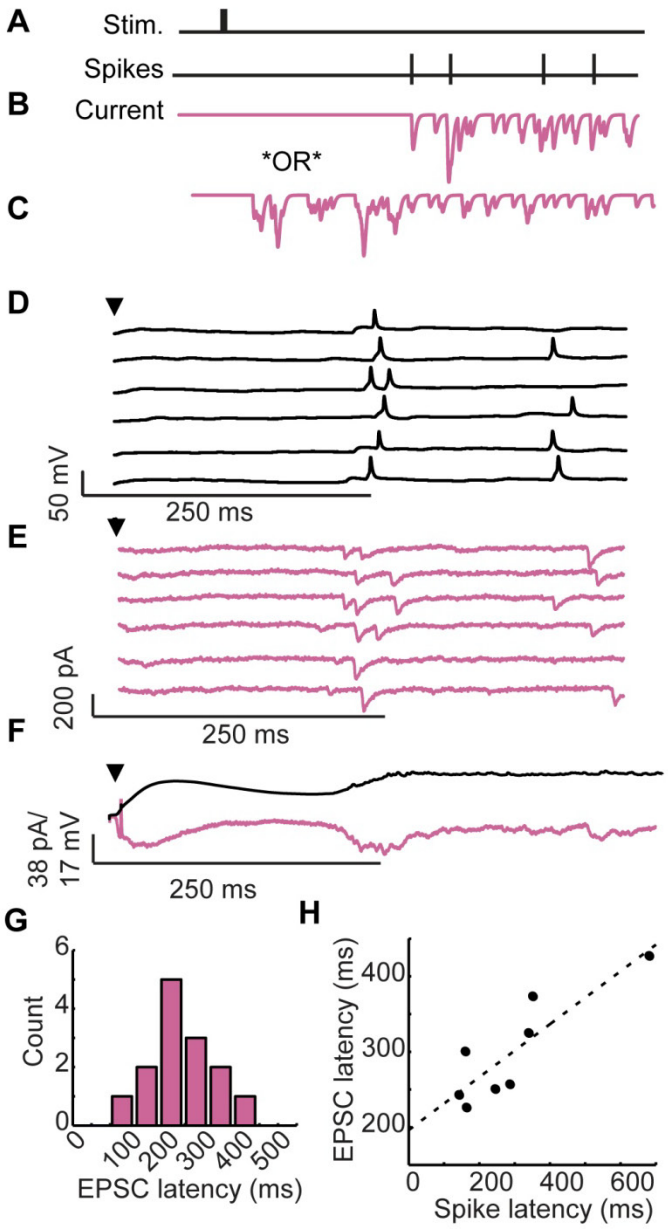

Figure 3.2: Long-latency granule cell activity is driven by late onset excitatory inputs. **(A)** Two mechanisms could account for brief stimulation followed by long-latency spiking: **(B)** temporally precise late onset excitatory inputs, or **(C)** short-latency inputs that are integrated slowly over time. **(D)** Membrane voltage and **(E)** membrane currents of a single granule cell following brief glomerular stimulation (arrowhead). 6 trials shown. **(F)** Membrane potential (upper) and somatic currents (lower) averaged across trials. **(G)** Distribution of EPSC onset across cells. **(H)** Correlation between first spike latency and EPSC latency across cells.

synaptic currents following stimulation (**Figure 3.2 E**). As is shown for a single cell in Figure 3.2 D-E, we observed a remarkable correspondence between granule cell first spike latency (spiking onset = 287 ± 89 ms) and the onset of fast excitatory post-synaptic currents (EPSCs; onset = 254 ± 88 ms).

In our voltage clamp recordings such as those shown in Figure 3.2 E, we typically did not observe obvious fast EPSCs in the 0-200 ms time window, raising questions about the source of the early depolarization characteristic of granule cell recordings. However, when the voltage clamp traces are averaged (**Figure 3.2 F**; lower), clear inward currents were observed immediately following glomerular stimulation in a pattern that closely matches the average time course of membrane potential depolarization (**Figure 3.2 F;** upper). This suggests that the initial slow depolarization may be due to a large pool of asynchronous and relatively weak excitatory inputs, making individual EPSCs difficult to identify.

Across cells, EPSC onsets were widely distributed (mean EPSC onset = 282 ± 90 ms, n = 14 granule cells with identifiable EPSCs; **Figure 3.2 G**) and correlated to first spike latency (r= 0.81, Spearman-rho test, n = 8 cells with identifiable EPSCs and spikes; **Figure 3.2 H**). These findings indicate that short-latency granule cells receive short-latency excitatory inputs whereas long-latency granule cells receive long-latency inputs. This supports the mechanistic hypothesis (depicted in **Figure 3.2 B**) that EPSCs with reliable, input-specific latencies cause precisely-timed spikes in granule cells, including long-latency spiking. These results also suggest that there is a concurrent source of excitation providing immediate excitatory input to granule cells following glomerular stimulation.

3.5 LONG-LATENCY TUFTED CELL ACTIVITY

We next wanted to characterize the activity of excitatory neurons providing inputs to granule cells. In particular, we were interested in understanding the source of early subthreshold depolarizations and late suprathreshold depolarizations observed in granule cells, as they could come from one or more populations. Two types of excitatory neurons have been described in the mouse olfactory bulb: mitral and tufted cells, with tufted cells coming in several subtypes (Shepherd, 2004). We began by recording from mitral cells that were activated by stimulation of a single glomerulus (**Figure 3.3 A**; black). Consistent with our previous work (Kapoor and Urban, 2006), mitral cell spikes were observed at short latency following glomerular stimulation. This timescale is consistent with the immediate subthreshold depolarizations observed in granule cells (mean first spike latency = 68 ± 53 ms, n = 14 cells; **Figure 3.3 B**; black). However, the lack of any long-latency responses make mitral cells an unlikely source of late-onset excitation to granule cells.

Next, we examined the spiking responses of tufted cells, focusing on middle tufted cells whose somata are located in the plexiform layer. In contrast to mitral cells, some tufted cells exhibited very long first spike latencies following brief glomerular stimulation (**Figure 3.3 A**; blue). The first spike latencies observed in the tufted cell population were widely distributed and ranged from 15 to 600 ms (**Figure 3.3 B;** blue n = 19 cells). The distribution of first spike latencies observed in tufted cells closely matched the observed distribution in granule cells (no significant difference; Kolmogorov-Smirnov test, p=0.15). Thus tufted (and not mitral) cells are poised to provide distributed-latency excitation to granule cells following brief glomerular stimulation.

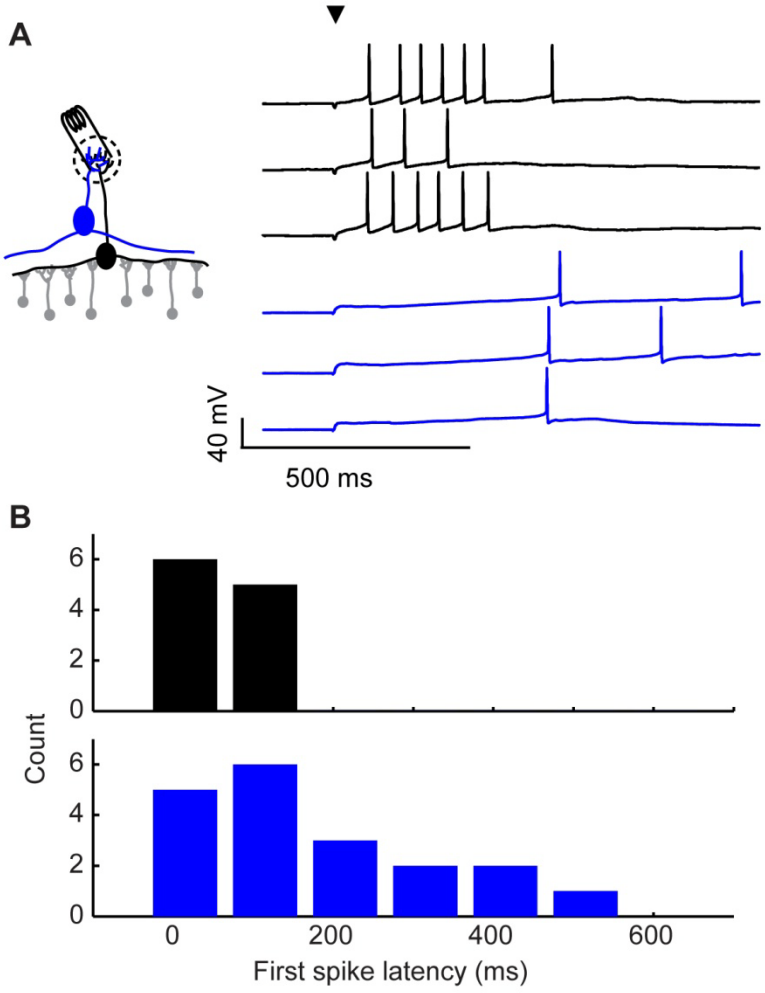

Figure 3.3: Long-latency excitation comes from tufted cells. (A) Example of a mitral cell (black) and tufted cell (blue) response to glomerular stimulation (arrowhead). Three trials shown for each example. **(B)** Distribution of first spike latencies following glomerular stimulation in mitral (black) and tufted cells (blue).

Given the closely matched latency distributions of tufted and granule cells, we hypothesized that activity in single tufted cells might be sufficient to drive spiking in granule cells. To test this possibility, we monitored the activity of many granule cells simultaneously using calcium imaging. In this experiment, the calcium indicator fura-2 AM was bulk loaded into slices of olfactory bulb. Once this dye is internalized, it emits light depending upon calcium concentration and can be used to reliably identify when cells begin firing action potentials. We monitored granule cell fluorescence while stimulating a single tufted cell via somatic current injection to understand how granule cells responded to stimulation from one tufted cell.

However, contrary to our hypothesis, we never observed granule cell activity following stimulation of single tufted cells (9 tufted cells, monitored 55 granule cells, 20-25 trials each). This might be expected from previous work suggesting that granule cells require multiple inputs to be depolarized to threshold (Schoppa et al., 1998; Isaacson and Strowbridge, 1998; Christie et al., 2001). Since activity in single tufted cells was insufficient to drive granule cell spiking, we hypothesized that granule cell activation may require convergent synaptic input from multiple sources. For example, one input that depolarizes granule cells to a subthreshold level (as seen in **Figure 3.1 B**) and a long-latency source of suprathreshold excitation which determines spike timing (as seen in tufted cells; **Figure 3.3 B**).

To test this possibility, we used calcium imaging to monitor granule cell recruitment following glomerular stimulation. We looked for granule cells whose spike latencies could be controlled by the activity of a single tufted cell (**Figure 3.4 A**). To accomplish this, we placed an extracellular stimulation electrode into a glomerulus, and patched a nearby tufted cell that did not receive input from the stimulated glomerulus. This allowed us to independently control excitation of the glomerulus and excitation of a single tufted cell. We positioned the microscope

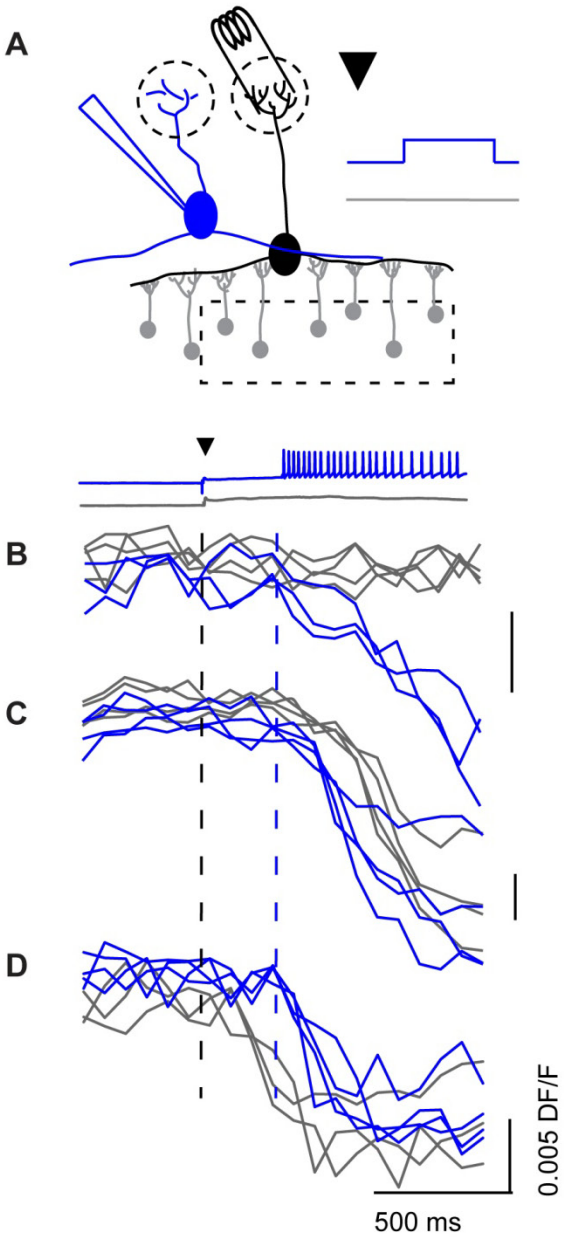

Figure 3.4: Activity from a single tufted cell can alter granule cell latency. (A) Optical imaging setup. A stimulation electrode was impaled into a glomerulus and a nearby (but not connected) tufted cell was patched. The glomerulus was stimulated on every trial, while the tufted cell was made to fire on every other trial (blue versus gray). Responses from three granule cells **(B-D)** to glomerular stimulation with (blue) and without (gray) additional tufted cell input were monitored optically. Black dash denotes timing of glomerular stimulation, blue dash denotes onset of tufted cell activity for tufted stimulation trials (blue).

over the granule cell layer and recorded fluorescence triggered to glomerular stimulation. On half of the trials, late onset action potentials were initiated in the tufted cell via strong somatic current injection, and on the other half of trials the tufted cell was kept at its resting potential, preventing firing. In this way, we were able to observe how the timing of granule cell activity depended on the activity of a single tufted cell.

For individual granule cells, we examined activity on trials with glomerular stimulation alone, and compared this to trials in which both the glomerulus and additional tufted cell were stimulated. Many cells show no difference in their responses, because they are not connected to both the stimulated glomerulus AND the patched tufted cell. However, we found several examples of granule cells whose activity was dynamically gated by activity in the single tufted cell. In some granule cells (such as the granule cell shown in **Figure 3.4 B**; gray traces), glomerular stimulation alone was insufficient to drive spiking, but reached threshold with the additional input from a single tufted cell (blue traces). In other cases, granule cells exhibited reliable long-latency firing in response to glomerular stimulation alone. In these cells (like the one plotted in **Figure 3.4 C**), adding tufted cell input *prior* to the glomerulus-specific latency shifted latency earlier to coincide with tufted cell stimulation. Lastly, in some granule cells, glomerular stimulation elicited short latency firing (like the granule cell shown in **Figure 3.4 D**; gray traces). Thus, with glomerular stimulation alone, the activity of these granule cells was characterized as either short latency firing, or failure to fire. In these cells, the addition of late onset tufted cell input converted some of the failure trials to long-latency trials (blue traces). These examples demonstrate that the activity of a single tufted cell can determine first spike latency in granule cells.

Our results support a model in which long-latency firing of granule cells is driven by two types of excitation. First, there is immediate excitation (from mitral cells or early active tufted cells) that leads to a prolonged, subthreshold depolarization of granule cells. Next, a secondary source of excitation (tufted cells), provides a "kick" of excitation that depolarizes granule cells to threshold and determines spike timing. The histograms of first spike latency in mitral and tufted cells (**Figure 3.3**) are consistent with this model. Further, single cells demonstrate evidence of receiving early and late excitation. **Figure 3.5 A** shows this effect at the single cell level by plotting the latency-triggered average; a calculation which aligns first spike latency across trials and averages the preceding membrane potential. Here, we observe two clear phases of depolarization: one which occurs hundreds of milliseconds prior to the first spike, and a second phase which occurs immediately preceding the first spike (**Figure 3.5 B**).

As a proof of concept, we wanted to test whether prolonged depolarization plus late excitation was necessary and sufficient to drive granule cell spiking. **Figure 3.5 C** shows example voltage traces from a cell that always responded to glomerular stimulation with a prolonged depolarization, but never emitted any action potentials in response to this stimulus (middle traces). In this cell, the prolonged depolarization alone was insufficient to cause spiking. Similarly, injecting a brief current pulse was always insufficient to initiate spiking (lower traces). However, when these two forces were combined (prolonged depolarization + late excitation), the granule cell always fired an action potential that coincided with the late input (upper). This simple example illustrates that our model of granule cell recruitment (which is based on observation of population activity in the olfactory bulb) is capable of driving temporally precise activity in single granule cells.

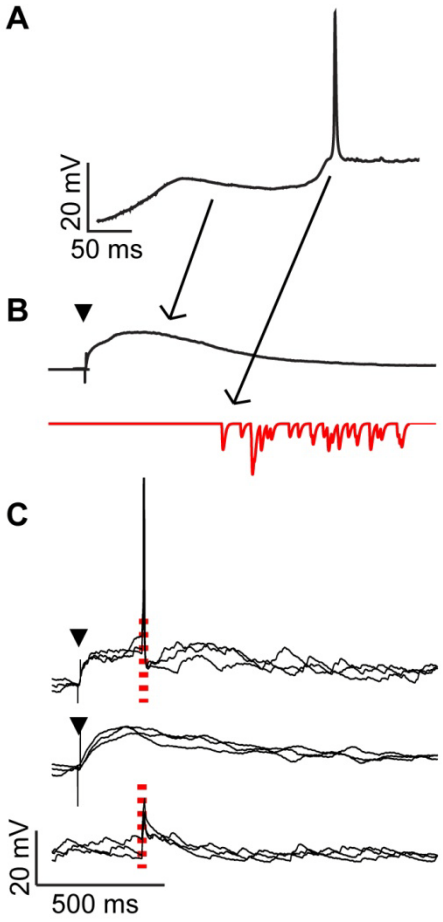

Figure 3.5: Model of granule cell recruitment. Granule cells are recruited for long-latency spiking by the combination of an initial subthreshold depolarization (from putative mitral cell inputs) and long-latency excitation (from tufted cell inputs). **(A)** Latency-triggered average reveals two phases of depolarization: **(B)** an early, prolonged source of depolarization (black) followed by variable-onset late excitation (red). **(C)** Voltage traces from a single granule cell show that late excitation alone (red dash; lower) and prolonged depolarization alone (glomerular stimulation denoted with arrowhead; middle) are both insufficient to elicit spiking. However, when prolonged depolarization is combined with late excitation (arrowhead + red dash; upper), together they generate temporally precise long-latency granule cell spiking.

3.6 INTRINSIC BIOPHYSICAL PROPERTIES OF MITRAL AND TUFTED CELLS

We wondered whether the observed differences between mitral and tufted cell latencies arose from cellular or circuit-level differences. One possibility is that mitral and tufted cells differ in their intrinsic properties that shape spike latency. If this were the case, latency differences would persist in the absence of synaptic stimulation and input. To test this possibility, we began by observing mitral cell responses to somatic step current injection rather than glomerular stimulation (**Figure 3.6 A**; black). In these recordings, spike latency varied as a function of firing rate, with longer latencies for low firing rates and shorter latencies for higher firing rates (**Figure 3.6 D**; black, n=10 cells).

We compared this relationship to the responses of tufted cells (**Figure 3.6 A, D** blue, n = 12 cells) and observed that tufted cells had significantly longer latencies for matched firing rates ($p<0.05$, K-S test). Mitral cell latencies were on average 36.7 ± 15% shorter than tufted cell latencies ($p<0.05$ for firing rates between 1 and 18 Hz, t-test). Mitral and tufted cell subthreshold responses differed as well, with tufted cells exhibiting a stronger "ramping up" of membrane potential across the stimulation epoch than did mitral cells (**Figure 3.6 B**; blue vs. black). Since latency differences between mitral and tufted cells persist without synaptic input, these results suggest that mitral and tufted cells differ in their intrinsic cellular properties. These differences may promote long-latency firing in tufted but not mitral cells.

Numerous studies have implicated inactivation of voltage-gated potassium channels in regulating first spike latency using the potassium channel blocker 4-aminopyridine (4-AP) (Storm, 1988; Balu et al., 2004; Schoppa and Westbrook, 1999). We wondered whether the

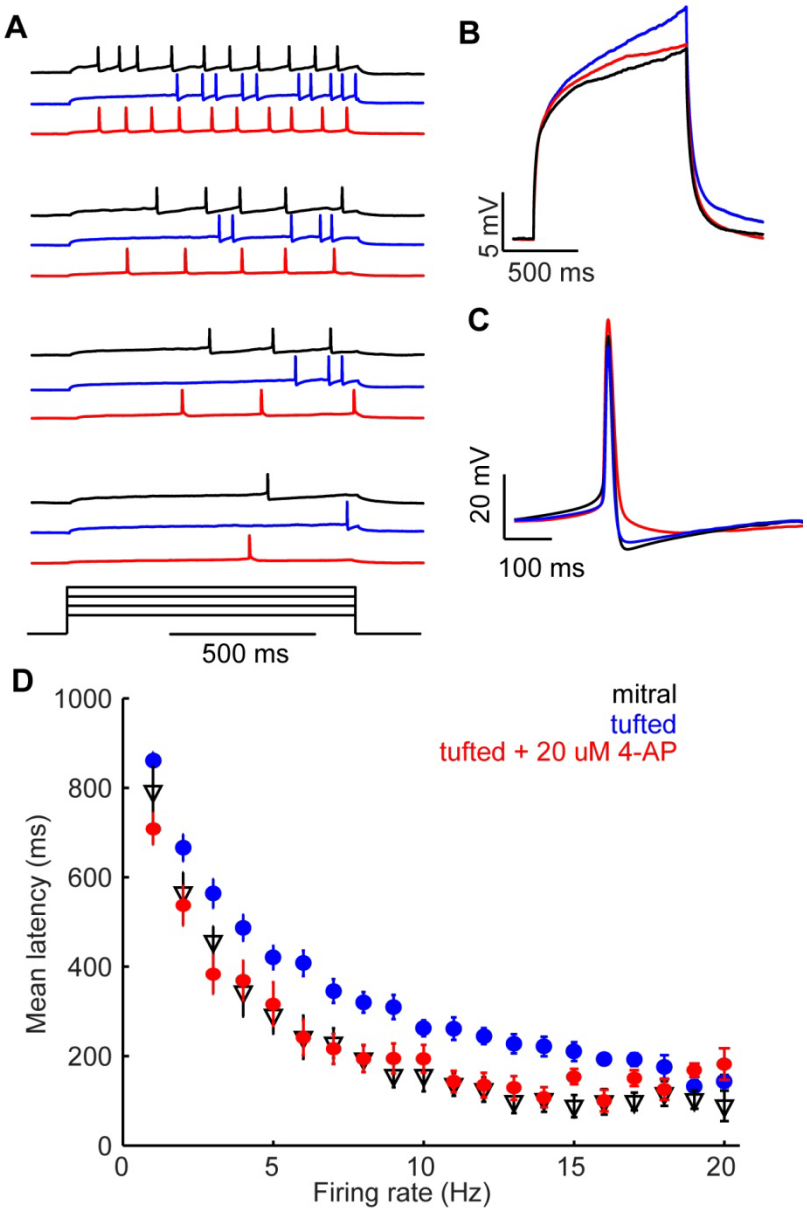

Figure 3.6: Long-latency activation is an intrinsic property specific to tufted cells. (A) Example mitral (black), tufted (blue) and tufted cell + 4-AP (red) responses to four amplitudes of injected current. Same color key is used throughout. **(B)** Average membrane potential for subthreshold responses to 1000 ms long direct current injection. **(C)** Average spike shape. **(D)** Firing rate/latency relationship in response to somatic current injection across the population of mitral cells, tufted cells, and tufted + 20 μM 4-AP. Bars indicate s.e.m.

latency differences between mitral and tufted cells could be altered with this drug, which blocks a number of potassium channels, mostly of the K_v1 family, at concentrations <100 μM. When we repeated our tufted cell recordings in the presence of 20 μM 4-AP (**Figure 3.6 A, D**; red), tufted cell latencies were reduced back to mitral cell levels ($p = 0.5$; K-S test). First spike latency reduction was frequency dependent, with maximum 4-AP-induced latency reductions occurring between 5 and 10 Hz (43 ± 3% reduction in latency, $p<0.05$, t-test, n=12 cells). 4-AP decreased the subthreshold ramping observed in tufted cells and also reduced the afterhyperpolarization characteristic of voltage gated potassium activation (**Figure 3.6 C**). These findings suggest that long-latency activation is an intrinsic property of tufted cells that relies on a 4-AP-sensitive current. Intrinsic long-latency responses distinguish tufted cells from mitral cells and provide a mechanistic substrate for latency coding in the olfactory bulb.

3.7 DISTRIBUTED-LATENCY INHIBITION IMPROVES STIMULUS DISCRIMINATION

Thus far in this chapter, we have described how distributed-latency inhibition is generated in the olfactory bulb network. However, we also wondered about the consequences of distributed-latency inhibition. This activity pattern is very unique and operates on an extremely long timescale—why does the olfactory bulb have it? With this question in mind, we sought to understand how distributed-latency inhibition might confer advantages to ethologically relevant behaviors like olfactory discrimination. We built a computational model that allowed us to investigate how population coding is affected by altering the distribution of interneuron latency. Our model consisted of 100 leaky integrate-and-fire neurons (LIFs; simulated mitral cells) and

50 inhibitory interneurons. Each model mitral cell received inputs from a randomly selected 10% of the inhibitory neurons.

We wished to use this population to model responses to a variety of different stimuli. Our method for generating different stimuli was inspired by olfactory bulb physiology. There, stimulation at different locations evokes different granule cell latency patterns (Kapoor and Urban, 2006). Thus, a given granule cell responds with one stereotyped latency for stimulus A, and a *different* latency for stimulus B, etc. We replicated this stimulus-evoked phenomenon in our model by assigning each interneuron a random, stimulus-specific response latency for each of 200 stimuli. In this way, we have modeled stimuli by their specific activation sequences of granule cells.

For each stimulus, we generated a "template" of inhibition by creating a peri-stimulus time histogram of the granule cell population (**Figure 3.7 A**; black trace above spike rasters). From each of these stimulus templates, we generated narrowly (**Figure 3.7 A**; black spike raster) and widely distributed (**Figure 3.7 A**; red spike raster) latency variants. We accomplished this by keeping the total amount of inhibition constant while varying the range of inhibitory first spike latencies across the population. In this way, each stimulus generated a pattern of inhibition that was equal in magnitude, but unique in the temporal patterning of interneuron latency. The model with the narrowest distribution restricted interneuron latencies to between 0 and 100 ms (top) while in the most widely distributed model (based on granule cell physiology) latencies ranged from 0 to 1000 ms (bottom). This setup allowed us to investigate very specifically how the distribution of interneuron latency affects mitral cell firing while keeping the total amount of inhibition and connectivity identical.

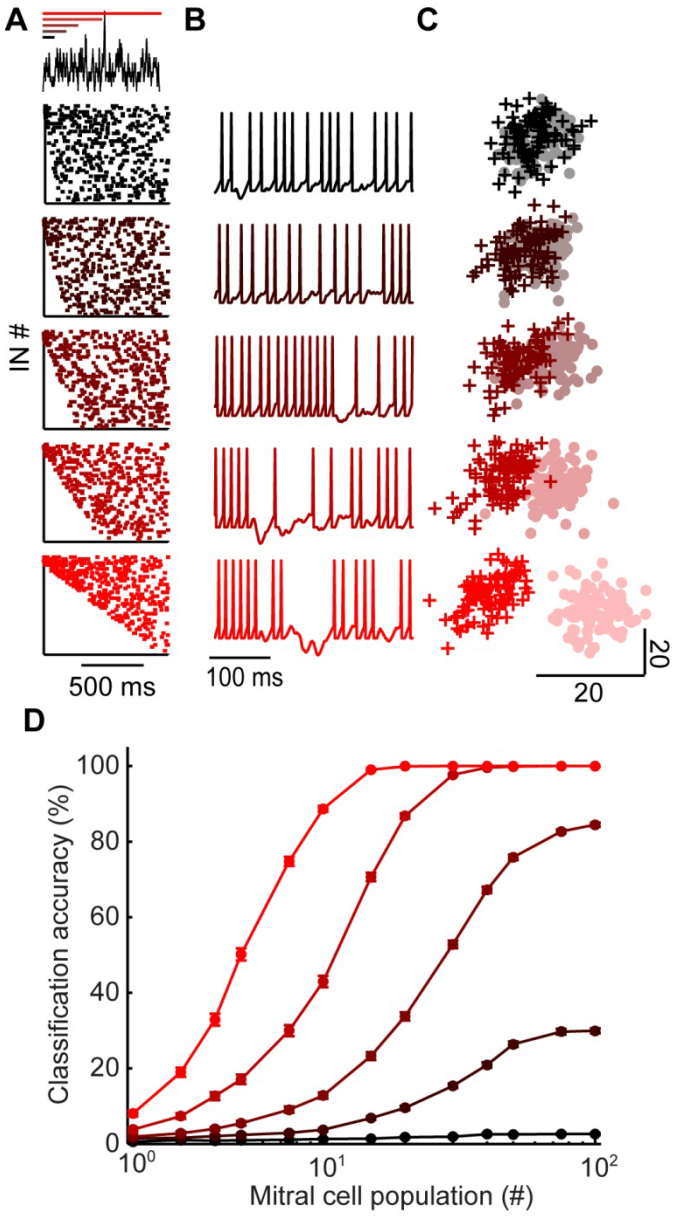

Figure 3.7: Widely-distributed latency inhibition improves stimulus discrimination. (A) Spike raster plots of the interneuron population for five model variants. First spike latencies ranged between 0 and (from top to bottom) 100, 200, 300, 500, or 1000 ms. Total spiking is equal in all cases (peri-stimulus time histogram shown above in black, latency ranges denoted with bars). **(B)** Example of mitral cell spike trains receiving inhibition from each model variant shown in A. **(C)** First two principal components of mitral cell population firing for one pair of stimuli. Stimulus 1 = +; stimulus 2 =●. For each model variant, 100 trials are plotted per stimulus. **(D)** Stimulus classification accuracy as a function of population size. Colors correspond to model variants plotted in A-C. Bars denote s.e.m.

Mitral cells receiving narrowly distributed inhibition tended to fire more regularly (**Figure 3.7 B**; upper), while widely distributed inhibition caused gaps in firing at various points throughout stimulus presentation (lower). Notably, this type of firing—with epochs of high and low firing—is typical of odor-evoked responses (Wilson and Laurent, 2005; Margrie et al., 2001). In our widely distributed models, temporal variability in spiking arose because some mitral cells received inhibition primarily during one portion of a trial. For example, mitral cells that (by chance) received mostly short-latency inhibitory inputs tended to have firing gaps at the beginning of the trial. Despite these differences in temporal variability, each mitral cell received the same total amount of inhibition in each model and mean mitral cell firing rates were equal in all model variants.

To investigate population-level encoding, we visualized stimulus-evoked activity patterns using principal component analysis of model mitral cell firing. This gave us a low-dimensional representation of population responses (example of two stimuli shown in **Figure 3.7 C**; 47% of variance captured by the first two principal components shown). In these plots, each point denotes the population response to stimulus 1 (+) or stimulus 2 (•) on a single trial. Since there is some variability in population responses from trial-to-trial, each stimulus occupies a "cloud" of space. When two clouds are overlapping (as can be seen in the most narrowly distributed network, upper), the population responses are ambiguous and discrimination is difficult. As the range of interneuron latencies was increased to olfactory bulb levels (lower), the same pair of stimuli became readily separable.

How well can an observer of our model's output distinguish between each of the applied stimuli? We used a linear discriminant analysis on the unprocessed data (spike count vectors without reducing dimensionality) to quantify the encoding performance. We examined the

classification accuracy as a function of mitral cell population size for each model (**Figure 3.7 D**). While the classifier reached near perfect accuracy with as few as 10 cells in the most widely distributed latency condition (red), it performed at chance levels in the narrowest latency network, even when all of the mitral cell data was available.

We wanted to verify that the advantage of latency coding does not depend critically on the specific parameters of our model (namely the timescales of inhibition and behavior that we selected). Stated differently, is latency coding still helpful if a network must make a discrimination decision after 100 ms, 200 ms, or some other time period? To test this, we measured classification accuracy of our model's output over a range of decision times (rather than the fixed, 500 ms time window used in Figure 3.7 D; **Figure 3.8 A**). While classification accuracy varies as a function of behavioral timescale, accuracy improves when longer latencies are available (lighter colors toward top of plot).

Our model was designed to mimic the stimulus-specific interneuron latency patterns observed in olfactory bulb slices (Kapoor and Urban, 2006). That is, each stimulus evokes a distinct temporal sequence on interneuron recruitment. We selected this method of stimulus generation because it allowed us to directly probe the influence of latency distribution on stimulus discrimination. However, olfactory stimuli evoke stimulus-specific subsets of interneurons in addition to stimulus-specific latency patterns. To verify that our results were robust to different methods of stimulus generation, we modified our model to contain 70 interneurons, 50 of which were active for each stimulus. As before, each interneuron was assigned a stimulus-specific latency for each stimulus, and we tested latency ranges from 0 to 100, 200, 300, 500, and 1000 ms. Additionally, a stimulus-specific subset of 20 interneurons was

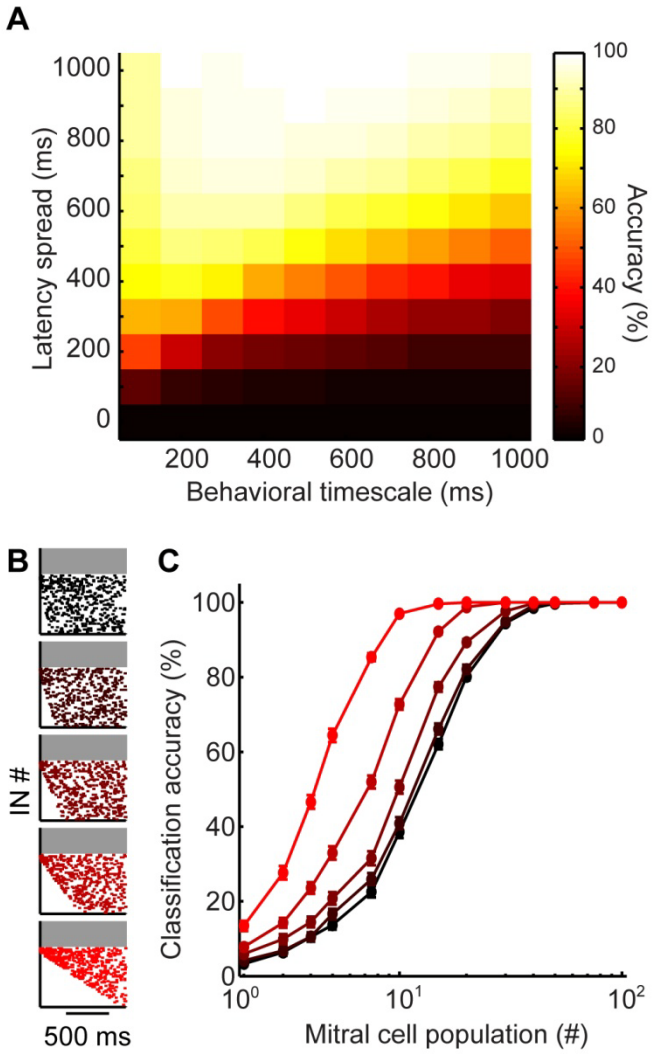

Figure 3.8: Latency-induced improvements are robust to parameter changes. (A) Heatmap of classification accuracy for varying ranges of latency spread at different behavioral decision time points. **(B)** Alternate stimulus generation: spike raster plots of the inhibitory interneuron population for 5 ranges of interneuron latency. From top to bottom, latencies range from zero to 100, 200, 300, 500, and 1000 ms. Each stimulus has a stimulus specific latency pattern, as well as a stimulus-specific subset of active interneurons (color vs. gray). **(C)** Classification accuracy as a function of mitral cell population size. Color corresponds to latency ranges in B.

designated to be silent for each stimulus (**Figure 3.8 B**; gray). In this way, we were able to mimic both stimulus-specific latency and stimulus-specific subsets of active interneurons.

All of the models showed better classification accuracy when both latency and the activated subset of interneurons were stimulus-specific (**Figure 3.8 C**, compared to **Figure 3.7 D**). However, the advantage of widely distributed inhibition is still clear—while all latency ranges reach near perfect accuracy when the full population is available, accuracy still varies as a function of latency range for smaller population sizes. These results suggest that stimulus-specificity of interneuron recruitment and latency both act to improve encoding.

3.8 DISCUSSION

Long-latency inhibition in the olfactory bulb arises from a simple circuit mechanism whereby glomerular stimulation drives two types of output: short-latency spiking in mitral cells, and variable-latency spiking from tufted cells. These two types of excitation provide a mechanistic substrate for variable-latency spiking in granule cells, which is driven by early onset subthreshold depolarization followed by later onset excitatory inputs that drive precise spiking. Interestingly, the mechanism driving long-latency activity is intrinsic for tufted cells, and synaptic for granule cells. This mechanism accounts for the distribution of first spike latencies observed in granule cells, as well as their striking glomerular specificity (Kapoor and Urban, 2006). Here, we focus on the impact of widely distributed interneuron latencies from the perspective of mitral cells receiving this type of inhibition. However, tufted cells also project to

cortex (Ekstrand et al., 2001; Shin Nagayama et al., 2010), adding additional complexity to the temporal properties of odor-evoked activity.

While our results indicate that granule cell recruitment often involves a combination of mitral and tufted cell-mediated inputs, they do not exclude the possibility that other combinations of inputs could drive granule cell activity. For example, given sufficient mitral cell inputs and a low firing threshold, a granule cell's latency could in principle be determined by mitral cell firing alone. Conversely, one could envision a scenario in which tufted cells could provide both early, subthreshold excitation, as well as late, suprathreshold excitation. In order to estimate the prevalence of these alternate mechanisms, we would need to know more about the connectivity between granule cells and mitral cells as well as between granule cells and tufted cells. It is possible that the connection probabilities and relative synaptic strengths of these two types of connections are different between mitral and tufted cells. Further, there could be diversity amongst granule cells in the makeup of their excitatory inputs.

Our pharmacological experiments demonstrate that tufted cell latency can be controlled dynamically by altering the activity of voltage-gated potassium channels. While this result is robust and consistent with previous reports of 4-AP shifting first spike latency, it still leaves many questions unanswered regarding the mechanism of intrinsic long-latency action potential generation. Voltage gated potassium channels are traditionally known for their involvement in action potential repolarization—an effect that takes place immediately after spiking. Here, we show that blocking voltage gated potassium channels exerts an effect on spiking behavior that occurs *before* any action potentials have been initiated. This effect could involve a compensatory change in the activity of calcium channels, or potentially other leaky currents that

contribute to the "ramping" of subthreshold membrane potential before spiking (as seen in Figure 3.6).

The observed differences in mitral and tufted cell membrane properties suggest that differences in voltage-gated potassium signaling can, in part, explain observed differences in latency patterns following glomerular excitation. However, there are most likely additional synaptic contributions that amplify these differences further. Given the curves plotted in Figure 3.6D, we would still expect to observe some mitral cells firing at long latencies when they receive weak inputs from a glomerulus. The fact that none of these long latencies were observed suggests that there may be additional mechanisms acting within a glomerulus that act to reduce the impact of such weak inputs. A recent paper lends insight into this issue. Gire et al. report that mitral cells terminating within the same glomerulus are very strongly coupled via gap junctions (Gire et al., 2012). They observed that this coupling acted to shunt weak inputs thus reducing mitral cell responsiveness to weak inputs. This suggests that glomerular circuitry might act to promote all-or-nothing activation of homotypic mitral cells, thus eliminating responses to weak inputs (as is seen in the 0-10 Hz range of Figure 3.6D) and facilitating strong responses among many mitral cells.

The differences in first spike latency that we observe between mitral and tufted cells are somewhat surprising, given the fact that tufted cell activity has been observed to precede mitral cell activity in a number of studies (De Saint Jan et al., 2009). Several factors could account for these differences. Importantly, most studies reporting tufted cell activity refer to the activity of external tufted cells, whereas we recorded from middle tufted cells. There are also diverse stimulation protocols by which mitral and tufted cell activity can be elicited—glomerular stimulation (as we used here), but olfactory nerve stimulation or odor stimulation have also been

used to characterize latency responses. Given that latency structure is likely also conferred by olfactory receptor neurons (Spors et al., 2006), primary inputs may have an additional effect on shaping latency (in addition to the intrinsic circuit mechanisms that we investigated here).

Our examination of the intrinsic properties of middle tufted cells suggests that they can scale their latency more linearly with firing rate (Figure 3.6), independent of inputs. This raises the possibility that mitral and tufted cells may differ in the number or relative strength of their primary sensory inputs (Gire et al., 2012) that would allow them to integrate weak inputs slowly (whereas mitral cells receiving weak inputs may not spike at all). By this model, input to a single glomerulus would elicit all-or-none, short-latency spiking responses of mitral cells and would elicit variable latency spiking in tufted cells, based on the strength of primary sensory input.

In order to isolate changes that were truly specific to the distribution of granule cell first spike latencies, we designed our model to keep granule cell spiking statistics constant across model variants. With this motivation in mind, we kept the total population activity constant across variants (as seen in Figure 3.7A, black line), as well as keeping the total firing rate of individual model granule cells constant across variants. We also attempted to keep inter-spike intervals (ISIs) equivalent across variants, but the ability to ensure constant ISI distributions is limited. For example, in the most widely distributed model variant (Figure 3.7A; red spike raster), spiking must occur at the very beginning of the trial, but very few model granule cells are available to spike, because most cells have not yet passed their specified first spike latency time. For this reason, the model granule cells near the top of the raster must fire rapidly to match the number of spikes dictated by the stimulus-specific peri-stimulus time histogram. In these extreme cases, the mean ISI of some model granule cells is reduced (as evidenced by the

"clustering" of points near the top of the spike raster plot), meaning that these models include not only a distribution change, but also a change in inter-spike intervals. An alternate approach would be to hold the ISIs constant, but this would come at the cost of changing the stimulus-specific peri-stimulus time histogram. We have selected the method described here because it does not disrupt the stimulus-specific inhibition pattern. Importantly, this limitation is only a moderate concern for the most widely distributed latency ranges (as there are no significant differences in mean inter-spike intervals between the 0-100 and 0-200 ms variants) whereas improvements to classification accuracy are readily observed between model variants without this confound.

Our computational model demonstrates that latency coding in inhibitory interneurons can improve stimulus discriminability. Here, we have based simulations on a highly simplified representation of the olfactory circuit. While this model lacks detailed features of olfactory bulb physiology, it has the advantage of allowing us to evaluate the benefits of latency coding in isolation from other potential effects on inhibition. The observed improvements in stimulus encoding are a surprising consequence of long-latency inhibition. Inhibition is believed to improve olfactory encoding by a variety of mechanisms including tuning curve sharpening, lateral inhibition, and shaping pattern correlations (Laurent, 2002). One might anticipate that a network would benefit from enacting any of these mechanisms immediately following stimulus presentation. Our results suggest that inhibitory latency coding can work in concert with these known mechanisms to further decorrelate stimulus representations and that distributed latency inhibition actually increases the magnitude of decorrelation. Just as a symphony can play a more complex piece of music when different sections of the orchestra are cued at different times, the

olfactory bulb can encode more complex stimuli when granule cells vary in their first spike latency.

In our network models of olfactory bulb activity we have remained agnostic about whether specific temporal features are decoded by downstream neurons. We consider granule cell latency as a temporal coding scheme because it satisfies the definition of having temporally precise and stimulus specific first spike times. However, this activity pattern also fits nicely into a rate coding framework. Because the differences in first spike latency across cells are so long, this leads to large differences in mean spike count calculated at large bins even if, following the first action potential, all cells have equal firing rates and interspike intervals.

Importantly, the improvement in encoding reported in our model is likely an underestimate of the improvement *in vivo* because there, latency is subject to additional forms of modulation. For example, latency differences have been reported at the level of olfactory receptor neuron inputs to the olfactory bulb (Spors and Grinvald, 2002). These two forms of latency could work together to drive even more complex and dynamic activity patterns. Further, the activity-dependent recruitment of inhibitory circuits can likely magnify latency differences (Arevian et al., 2008). Together, these multiple stages of temporal patterning could work together to generate temporal patterning at a behaviorally relevant timescale.

4.0 TIMESCALE-DEPENDENT SHAPING OF CORRELATION BY OLFACTORY BULB LATERAL INHIBITION

4.1 ABSTRACT

Neurons respond to sensory stimuli by altering the rate and temporal pattern of action potentials. These spike trains both encode and propagate information that guides behavior. Local inhibitory networks can affect the information encoded and propagated by neurons by altering correlations between different spike trains. Correlations introduce redundancy that can reduce encoding but also facilitate propagation of activity to downstream targets. Given this trade-off, how can networks maximize both encoding and propagation efficacy? Here, we examine this problem by measuring the effects of olfactory bulb inhibition on the pairwise statistics of mitral cell spiking. We evoked spiking activity in the olfactory bulb *in vitro* and measured how lateral inhibition shapes correlations across timescales. We show that inhibitory circuits simultaneously increase fast correlation (i.e., synchrony increases) and decrease slow correlation (i.e., firing rates become less similar). Further, we use computational models to show the benefits of fast correlation/slow decorrelation in the context of odor coding. Olfactory bulb inhibition enhances population-level discrimination of similar inputs, while improving propagation of mitral cell activity to cortex. Our findings represent a targeted strategy by which a network can optimize the correlation structure of its output in a dynamic, activity-dependent

manner. The propagation/encoding trade-off is not specific to the olfactory system, but rather our work highlights mechanisms by which neurons can simultaneously accomplish multiple, and sometimes competing, aspects of sensory processing.

4.2 INTRODUCTION

Inhibitory circuits (like the granule cells described in the previous chapter) are believed to shape stimulus-evoked activity and facilitate sensory-guided behavior in the olfactory system (Stopfer et al., 1997; Abraham et al., 2010) as well as many other brain areas (Ferster and Miller, 2000; Pinto et al., 2003; Wehr and Zador, 2003; Doiron et al., 2003; Le Masson et al., 2002). Inhibitory inputs can alter the patterns and rates of postsynaptic action potentials. By investigating how inhibitory granule cells alter the spike train statistics of mitral cells, we can describe the transformations that occur in the olfactory bulb and how those changes affect the bulb's output to cortex.

Action potentials are the currency of information exchange between neurons. These action potentials are emitted by principal neurons in response to stimuli, and they are the sole means of both encoding information and propagating activity to downstream neurons. One statistic of spike trains that can be altered by inhibitory inputs is the correlation of spiking across neurons (Tiesinga et al., 2008). In some situations, lateral inhibition promotes competition between neurons (Srinivasan et al., 1982), resulting in decorrelation of spike trains (Arevian et

al., 2008) or stimulus-evoked patterns (Friedrich and Laurent, 2001; Wiechert et al., 2010). In other situations, inhibition correlates spiking across pairs of neurons by acting as a source of common, fast fluctuations (Galan et al., 2006; van Vreeswijk et al., 1994; MacLeod and Laurent, 1996; Wang and Buzsaki, 1996; Schoppa, 2006; Hasenstaub et al., 2005). Several studies have shown that inhibitory inputs can alter rates and correlations differentially, suggesting that these circuits may be capable of encoding stimulus information at multiple timescales (Tiesinga and Sejnowski, 2004; Panzeri et al., 2010; Fairhall et al., 2001; Kayser et al., 2009; Butts et al., 2007). Thus inhibition can influence population activity in a variety of ways according to the details of the circuitry and the patterns of population activity.

The relationship between changes in correlation and sensory processing remains controversial. Correlation may be helpful or harmful depending on stimulus statistics, noise statistics, population size and decoding mechanisms (Simoncelli and Olshausen, 2001; Series et al., 2004; Romo et al., 2003; Barlow, 2001; Schneidman et al., 2003; Kumar et al., 2010; Averbeck and Lee, 2006). Here we focus on how correlations influence two primary functions of spike trains: encoding information and propagating activity to downstream neurons. Imagine hearing a group of people talking simultaneously. A tradeoff arises between the quality and quantity of communicated messages; a single phrase chanted in unison is loud, but simple. Conversely, each person saying a different phrase is informative, but no single message is loud enough to be understood. Neurons face a conceptually similar problem. Correlated spiking has been shown to facilitate propagation (Salinas and Sejnowski, 2001; Kumar et al., 2010; Reyes, 2003; Wang et al., 2010). However, these correlations also reduce the available repertoire of population activity patterns (Zohary et al., 1994; Barlow, 1959; Averbeck and Lee, 2006) thereby potentially impairing sensory discriminations (Romo et al., 2003). Since correlations

can impact propagation and encoding in opposing ways, how do networks structure their correlations? And how should they? We investigate this problem here by considering the inhibitory circuits of the olfactory bulb.

The mouse olfactory bulb provides an excellent model system to study the effects of inhibitory circuits on pairwise properties of spike trains. Mitral (and the related tufted) cells receive direct input from sensory neurons and provide the only output projections from the olfactory bulb (Shepherd, 2004). Because they function as an obligatory processing stage, the ~100,000 mitral cells must effectively propagate activity to millions of neurons in areas such as cortex and amygdala. Moreover, mitral cell odor coding must minimize redundancy because these cells are few in number compared to the number of sensory neurons that provide their inputs (~10,000,000/mouse) (Shepherd, 2004). Mitral cells interact with each other primarily via disynaptic inhibition mediated by granule cells (Shepherd, 2004). Olfactory bulb inhibition is believed to improve the discriminability of structurally and psychophysically similar odors (Stopfer et al., 1997; Abraham et al., 2010). Therefore inhibition-evoked changes to mitral cell correlations are an attractive model for studying the effects of correlations on propagation and encoding. Further, these changes also represent a behaviorally relevant component of stimulus processing in this circuit.

Here we examine the effect of olfactory bulb inhibition on the correlation of mitral cell activity as well as on stimulus-evoked population activity patterns. We examined correlations measured at small and large time windows, and explored how these changes affected propagation and encoding. Using experimental and computational approaches, we measured correlations at timescales ranging from milliseconds to seconds and show that inhibitory circuits in the olfactory

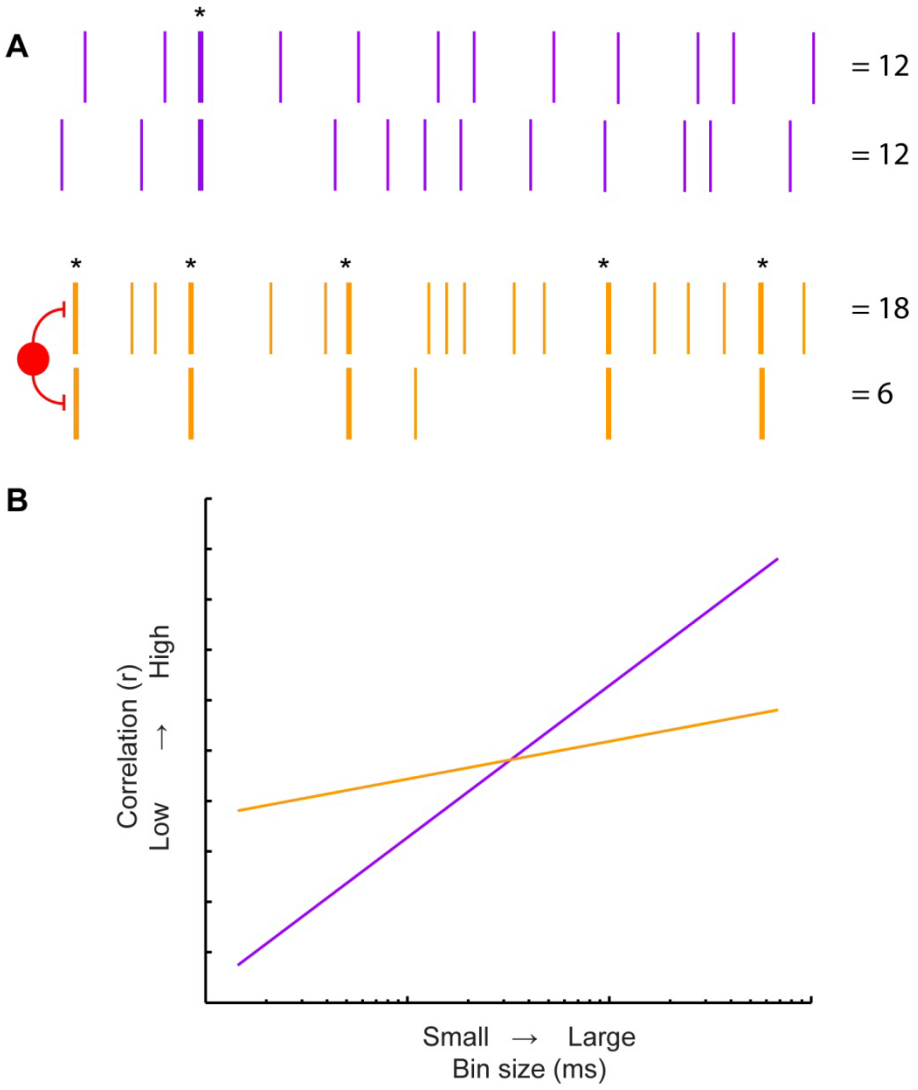

Figure 4.1: Schematic of timescale-dependent correlation changes. (A) Two spike train pairs are depicted here; purple and orange. In the purple pair, both cells emit the same total number of action potentials (12), but these action potentials rarely occur simultaneously (shown in bold and marked with asterisk). Conversely, the orange pair has many synchronous spikes, but dissimilar overall firing rates. **(B)** Such differences in correlation patterns can be captured by measuring pairwise correlation across timescales. In this example, the orange pair has high fast timescale correlation and low slow timescale correlation while the opposite is true of the purple pair. The work in this chapter focuses on these types of correlation changes that are mediated by interneuron recruitment (red cell in A).

bulb mediate simultaneous fast correlation (i.e. synchrony increases) and slow decorrelation (i.e. firing rates become less similar). This idea is illustrated schematically in **Figure 4.1 A-B**). We argue that the combination of fast correlation and slow decorrelation enhances population level discrimination of similar inputs, while promoting propagation of mitral cell activity to cortex. Thus, inhibition in olfactory circuits is structured to take advantage of the encoding and propagation benefits that correlation can confer, while mitigating the deleterious aspects of the propagation/encoding tradeoff.

4.3 TIMESCALE-DEPENDENT CORRELATION CHANGES IN MITRAL CELL PAIRS

We first directly measured how the inhibition recruited by two active mitral cells changed correlations between the two mitral cell spike trains. We performed simultaneous whole-cell voltage recordings from pairs of nearby mitral cells in slices of mouse olfactory bulb. Firing was evoked via somatic direct current injection. The amplitude of injected current was selected to evoke physiologically realistic firing rates (~30 Hz (Cang and Isaacson, 2003)). We first examined pairs of spike trains that were recorded simultaneously (**Figure 4.2 A-B**; orange box). We hypothesized that in this situation, activity in the pair of mitral cells would recruit interneuron activity, and that the evoked inhibition would feed back onto either one or both cells in the pair, altering pairwise correlations. Notably, we expect these interactions to be nearly exclusively inhibitory as mitral cells are disynaptically coupled via interneurons and lack direct

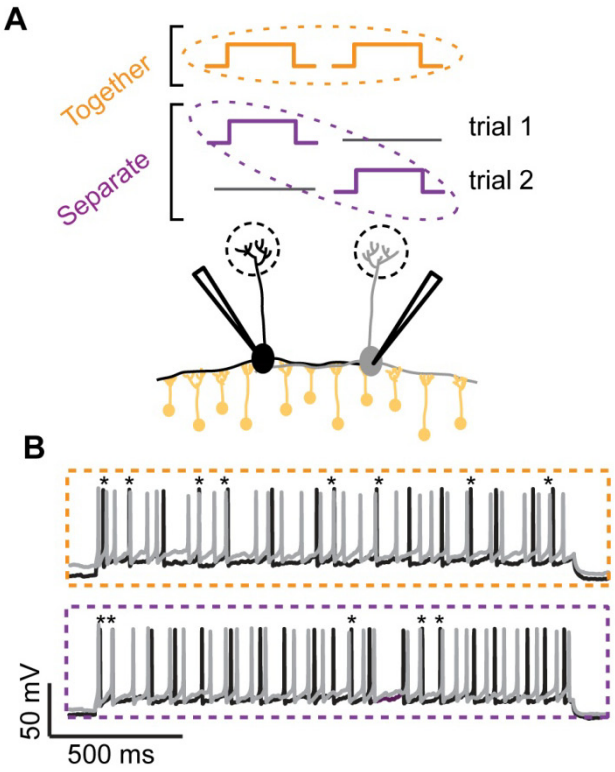

Figure 4.2: Experimental setup. (A) Pairs of mitral cells were depolarized via DC current injection. Pairwise correlation was measured in the presence (recorded together; orange) and absence (recorded on separate trials; purple) of shared inhibition. **(B)** Example voltage traces for the shared inhibition (orange) and no shared inhibition (purple) conditions. Synchronous spikes denoted with asterisks.

excitatory connections (although excitatory coupling has been observed in homotypic mitral cells terminating in the same glomerulus (Isaacson, 1999; Schoppa and Westbrook, 2001; Schoppa and Westbrook, 2002; Urban and Sakmann, 2002)). Since we recorded mitral cells terminating in different glomeruli, we did not observe excitatory coupling in any of our pairs.

Simultaneously recorded spike trains have correlations from several sources. We wanted to isolate changes in correlation that arise due to trial-to-trial shared synaptic input and ignore correlations from other sources. To eliminate other sources of correlation (e.g. those that arise from the transient induced by somatic current injection or repeated input patterns) we compared the simultaneously recorded spike trains described above to pairs of spike trains recorded on interleaved trials (i.e. cell 1, sweep 1 is compared to cell 2, sweep 2; **Figure 4.2 A-B**, purple box). As before, stimulated mitral cells can still recruit activity in inhibitory interneurons. But unlike the simultaneous recordings, the evoked inhibition can only act on one cell in the pair, since the second spike train is recorded much later in time. This comparison provides a useful internal control because all traces include the same sources of spurious correlations (transients and repeated input patterns) while only the cells recorded together receive the shared inputs that are of interest to us.

To quantify spike train correlation (ρ) across timescales, we constructed histograms of each cell's activity for bin sizes ranging from 1–1000 ms (**Figure 4.3 A**). From these spike count vectors, we calculated Pearson's correlation coefficient for each bin size (**Figure 4.3 B**). Thus, for each bin size we calculate spike count correlation with (orange) and without (purple) shared inhibition, allowing us to measure the effects of the simplest lateral inhibitory circuit at a variety of timescales. We observed modest but significant timescale-dependent changes in

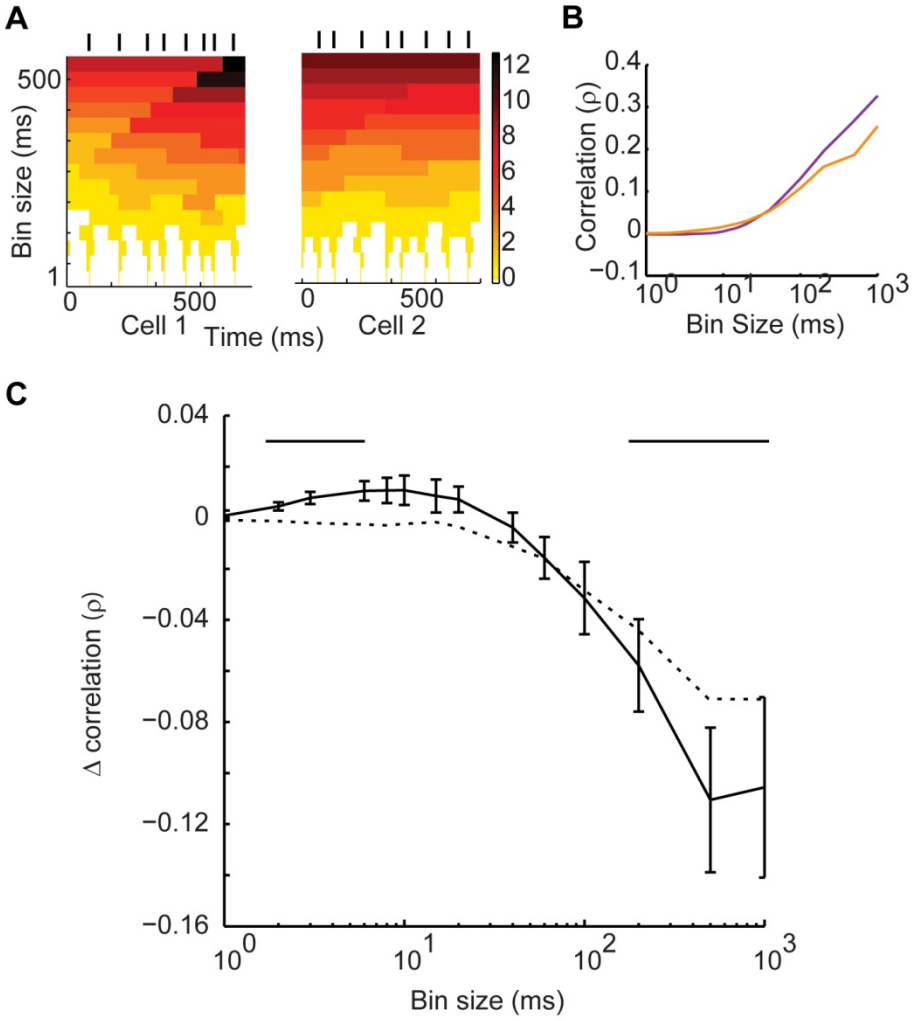

Figure 4.3: Mitral cell correlations across timescales. (A) Spiking data was binned by counting the number of spikes occurring across bins of different sizes. The heatmap shows how two spike trains (tick marks; above) are binned across timescales (rows). Heatmap denotes number of spikes in each bin. **(B)** The Pearson correlation coefficient was calculated across fast and slow timescales (bin sizes 1–1000 ms; rows of spike counts shown in A) for pairs recorded in the separate (purple) and together (orange) conditions. **(C)** Taking the difference between the orange and purple lines in B reveals that shared inhibition induces correlation changes across timescales (solid black). Bars, above, mark bins with significant correlation change. Shuffled data shown by dotted black line.

correlation in the simultaneously recorded spike trains (**Figure 4.3 C**; $p<0.05$ in bins marked with bars, n=12 mitral cell pairs, 9 animals).

When the trials were shuffled (**Figure 4.3** C; dotted line), fast correlation was abolished ($p<0.05$ bins<100 ms) while slow decorrelation was largely preserved ($\Delta\rho_{slow}$=-0.07±0.005, $p<0.05$ all bins≥100 ms). Thus the specific timing of correlating inhibition was variable from trial to trial, whereas decorrelation was replicable across trials. Mechanistically, this suggests that slow timescale decorrelation relies on a competitive mechanism. Consistent with this, the difference in firing rate between the pair increased in the together condition (**Figure 4.4 A**). To investigate whether firing rate reduction is consistently larger for one cell in pair, we analyzed the average change in firing rate in each cell across trials. We found that each pair had one cell whose firing rate was less affected by inhibition than the other cell (**Figure 4.4 B**; $p<0.05$), suggesting that there is a "winner" and "loser" with respect to firing rate. The fact that the identity of the winner is conserved across trials suggests that slow competition relies on features of the circuit that are conserved across trials (for example, differences in connectivity that determine a cell's ability to recruit lateral inhibition). While the observed slow decorrelation is significant, average firing rate changes were quite small (3.1%).

Given the remarkable temporal precision of long-lasting granule cell activation (see Chapter 3 and Kapoor, 2006) one might expect that fast correlations would also be preserved across trials. However, this is unlikely given the low response probabilities of individual granule cells, which only respond on ~10% of trials during glomerular stimulation (Kapoor and Urban, 2006). Given this low response probability following glomerular stimulation, it is likely that individual granule cells respond even less frequently in response to stimulation of single mitral cells. The timescale of maximum correlation changes vary across pairs, since each pair is

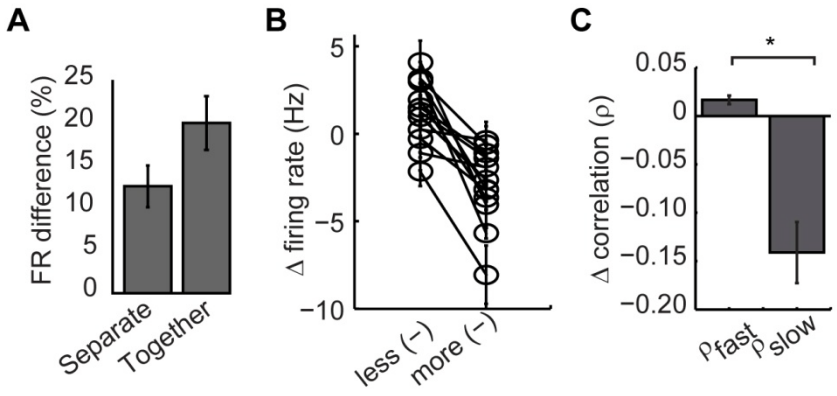

Figure 4.4: Competition in timescale-dependent correlation changes (A) Firing rate difference between the mitral cell pair in the two recording conditions. **(B)** Inhibition-induced rate change for less reduced and more reduced cell for each recorded pair. **(C)** Average peak fast correlation and peak slow decorrelation.

influenced by a unique inhibitory network. Given this variability, averaging inhibition-induced changes across pairs (as shown in **Figure 4.3 C**) shows smaller peak changes than are achieved by individual pairs. For this reason, peak correlation changes were identified in each pair for small (bin size<30 ms, average $\Delta\rho_{fast}$=0.016±0.005; $p<0.05$) and large bin sizes (bin size>100 ms, average $\Delta\rho_{slow}$=-0.14±0.03, $p<0.05$; **Figure 4.4 C**).

4.4 FAST, SHARED, ACTIVITY-DEPENDENT INHIBITION

Given our experimental results, we sought a mechanistic understanding of timescale-dependent correlation changes. Which features of inhibition were responsible for fast and slow timescale changes, respectively? First, we hypothesized that fast correlation arose from shared inhibition with rapid kinetics (Galan et al., 2006; van Vreeswijk et al., 1994). Such inputs have been observed from GABAergic granule cells (Schoppa, 2006) and may synchronize mitral cell firing via a mechanism dubbed "stochastic synchronization" (Galan et al., 2006). Secondly, we hypothesized that slow decorrelation arose from long latency, competitive recruitment of these same granule cells (Arevian et al., 2008; Friedrich and Laurent, 2001; Isaacson and Strowbridge, 1998; Kapoor and Urban, 2006), giving rise to lateral inhibition whereby more active cells suppress firing of less active cells (Arevian et al., 2008). We predicted that our experimental results might be explained by these known features of olfactory bulb inhibition.

To understand the requisite features of inhibition, we constructed a highly simplified model consisting of two leaky integrate and fire neurons (simulated mitral cells) that received inhibitory inputs (**Figure 4.5 A_2**). Each cell received both shared inhibition and inhibition

independent to each cell. Inhibitory firing was generated using an inhomogeneous Poisson process driven by excitatory firing. We selected this simplified representation of the olfactory circuit because it allowed us to isolate the features of inhibition that are necessary and sufficient to mediate cross-timescale correlation changes between a single pair of neurons. We generated pairs of model spike trains and calculated correlation across timescales as described above. For comparison, we generated spike trains with inhibition removed from the model (**Figure 4.5 A_1**). Shared, activity-dependent inhibition reduced firing rate (Δ_{FR}=-27.8±0.03%, $p<0.05$; **Figure 4.5 B**). Further, synchrony increased ($\Delta\rho_{\text{bin size=10 ms}}$=0.07±0.01) while slow timescale correlation decreased ($\Delta\rho_{\text{bin size=1000 ms}}$=-0.04±0.015; **Figure 4.5 C**; $p<0.05$ for all points). Thus, this simple circuit is sufficient to generate the simultaneous fast correlation and slow decorrelation observed in slice experiments.

We next manipulated the kinetics, correlation, and activity-dependence of evoked inhibition in our model to observe the contribution of each in timescale-dependent changes. We first altered the kinetics of inhibition by varying the parameter τ_α (which controls the rise and decay times of individual IPSCs). For very fast inhibition (τ_α=1), the zero-crossing point (timescale at which inhibition shifts from being correlating to decorrelating, shown by arrowheads in **Figure 4.5 D**, inset) occurred at small bin sizes (**Figure 4.5 D**). As inhibition becomes slower (τ_α=6), the zero-crossing point shifted to larger bin sizes, suggesting that IPSC kinetics determine the upper range of correlating timescales.

Next, we varied the fraction of shared inhibition (c) to alter the portion of shared inhibitory inputs while keeping the total amount of inhibition constant. As c increases, fast

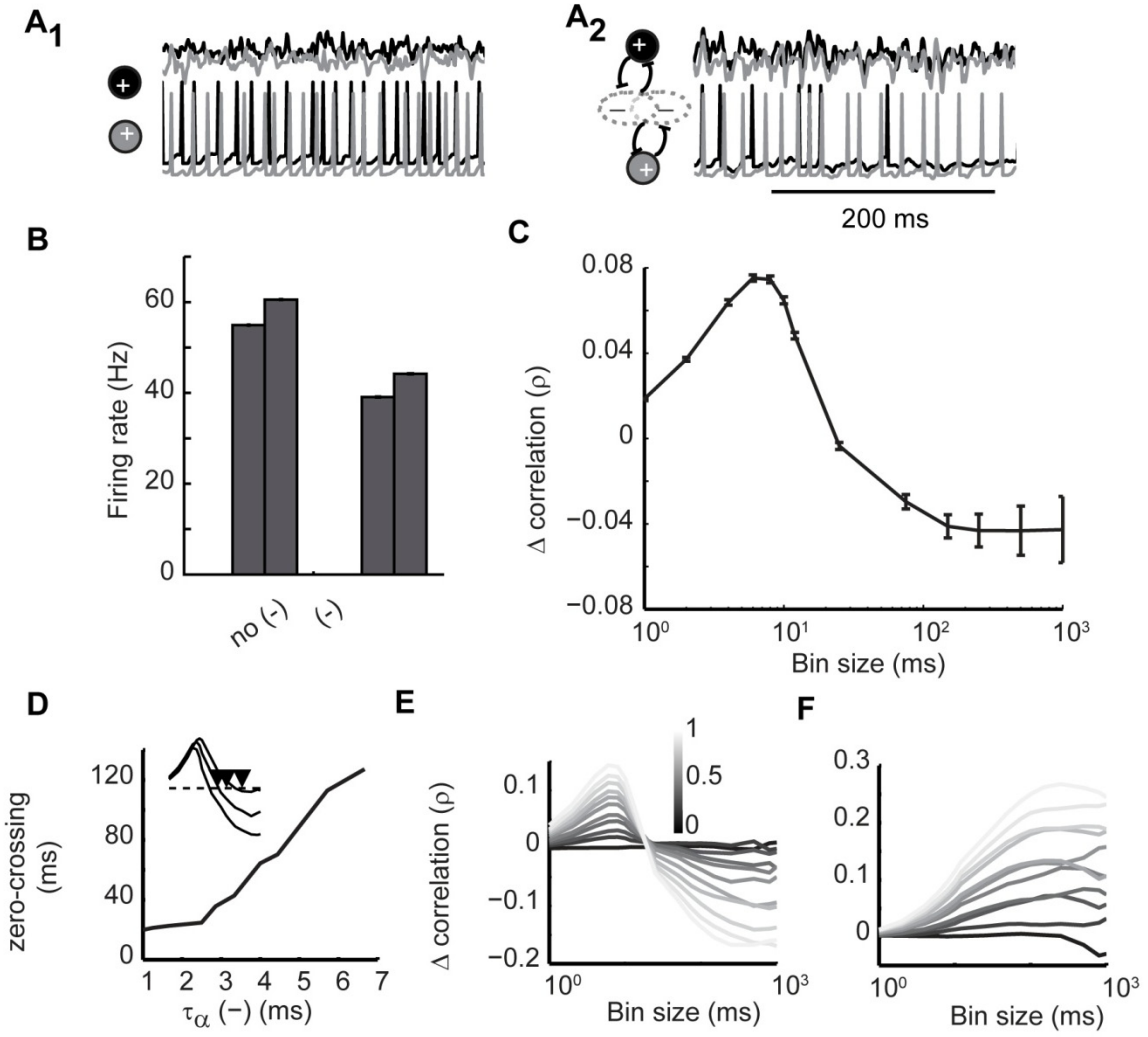

Figure 4.5: Timescale-dependent correlation changes in simple 2-cell model. (A) Model schematic and raw traces. Model contains 2 excitatory LIF neurons coupled by activity-dependent Poisson inhibition **(A_2)**. A portion of the inhibition is shared by the pair (constant, c; gray overlap) and a portion is independent to each cell (constant, 1-c; non-overlapping gray). Firing in this model is compared to firing with inhibitory coupling removed **(A_1)**. Top: currents received by each cell. Bottom: membrane voltages of the pair. **(B)** Firing rate for each cell with and without inhibitory coupling. **(C)** Inhibition-evoked change in correlation across timescales. Error bars indicate standard error. **(D)** IPSC kinetics shift zero-crossing point of cross-timescale changes. Inset: example correlation changes for 3 values of τ_α, zero-crossing points marked with arrowheads. **(E)** Varying c (portion of shared inhibition) alters the magnitude of timescale-dependent correlation changes. Color bar denotes value of c. **(F)** Removing activity dependence of inhibition preserves inhibition-induced correlation increases (with changes in C) but removes slow timescale decorrelation. Error bars indicate standard error.

correlation increases ($p<0.05$) and slow correlation decreases (**Figure 4.5 E**; $p<0.05$ for $c>0.3$). Notably, timescale-dependent correlation changes were observed when 100% of inhibition was shared, indicating that a single inhibitory population is capable of mediating correlation changes at both timescales.

Lastly, we eliminated the activity-dependence of recruited inhibition and instead generated IPSCs with a fixed Poisson rate (rather than as an inhomogeneous Poisson process). Increasing c in this condition increased correlation (due to increased coincident inputs; **Figure 4.5 F**). However, this increase extended into long timescales, with no slow decorrelation as observed in the activity-dependent case. Thus, when inhibition was evoked by an external source rather than the local circuit, common inputs were correlating at all timescales because there is no asymmetry of one cell recruiting inhibition more effectively. Taken together, these results indicate that rapid, shared, activity-dependent inhibition provides a simple and biologically plausible mechanism of timescale-dependent correlation changes.

4.5 IMPROVEMENTS TO BOTH PROPAGATION AND ENCODING

Two kinds of correlations are often considered in analyzing sensory processing (Wiechert et al., 2010): channel correlations (within-trial correlations between pairs of neurons), and pattern correlations (across trial correlations between population activity evoked by *different* stimuli). Above, we have considered channel correlations between pairs of mitral cell spike trains. Since changes to channel correlations may contribute to pattern decorrelation in the olfactory system, we developed an expanded model to investigate these changes at the network level. We constructed an olfactory bulb model with 100 excitatory cells reciprocally connected

to 800 inhibitory interneurons (see section 2.4.3 for methodological details). This model allowed us to ask two important questions related to our experimental results. First, do inhibitory circuits enact timescale-dependent correlation changes in this network model? And secondly, how do changes in correlation influence the propagation/encoding tradeoff during a simulated detection/discrimination task?

To answer the first question, we activated inputs to all excitatory cells in the network and recorded their spike trains. For comparison, we removed all synaptic coupling and again recorded spike trains from the excitatory cells. We measured cross-timescale correlation for all pairwise combinations of excitatory cells in both conditions. This model olfactory bulb network replicates the timescale-dependent correlation changes observed experimentally (**Figure 4.6 A**; orange versus purple; $\Delta\rho_{fast}$=0.10±0.01, $\Delta\rho_{slow}$=-0.10±0.02, $p<0.05$).

Olfactory bulb inhibition is important for behavioral discriminations, particularly between highly similar stimuli that elicit overlapping patterns of activity (Stopfer et al., 1997; Friedrich and Laurent, 2001; Abraham et al., 2004; Abraham et al., 2010). For example, mixtures containing the same odorants at slightly different ratios can be perceptually very similar. A mixture containing 55% odor A and 45% odor B might activate one glomerulus at a higher intensity and a second glomerulus at a lower intensity whereas a 45/55% mixture would do the opposite (Abraham et al., 2004). To implement this olfaction-inspired scenario in our model, excitatory cells were randomly divided into two groups shown schematically in **Figure 4.6 B**: group A (stimulated at a particular intensity; top, light grey) and group B (stimulated at an intensity ~10% less than group A; top, dark gray). To generate a second, highly similar stimulus, we simply reversed the stimulation intensities applied to groups A and B (**Figure 4.6 B**; lower).

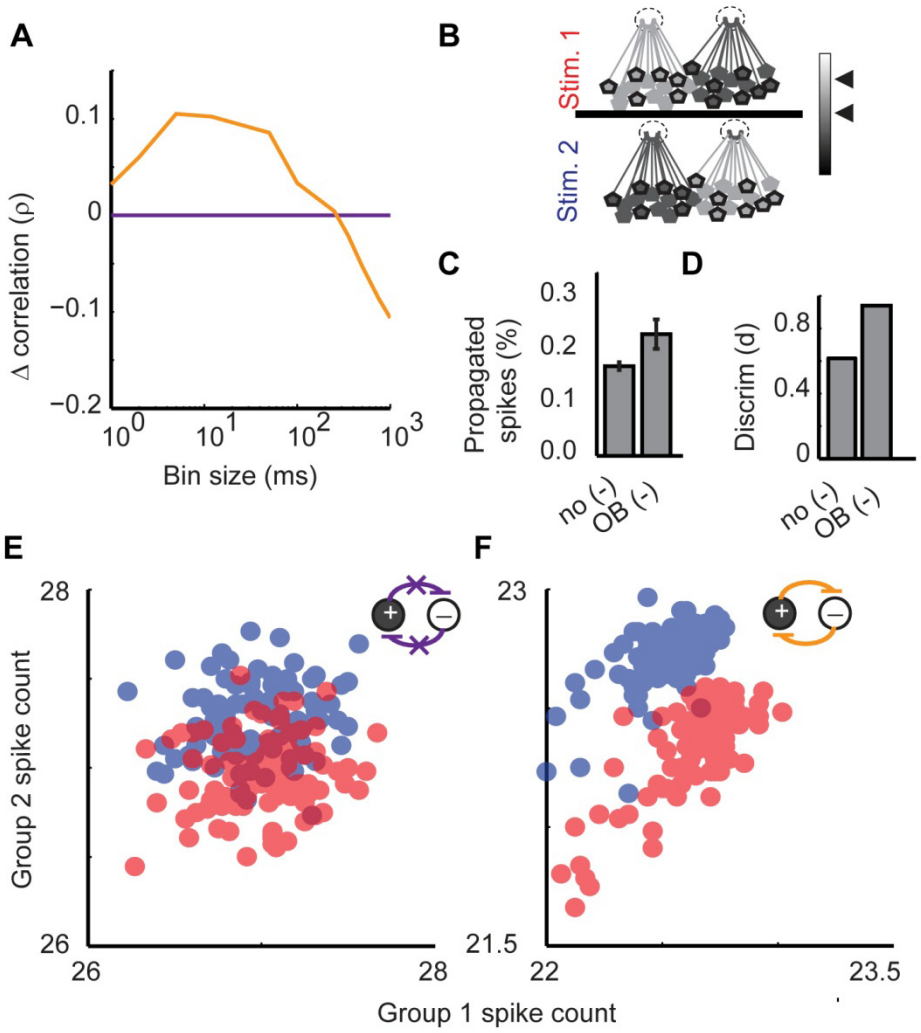

Figure 4.6: Model of timescale-dependent correlation, propagation, and encoding. (A) Cross-timescale correlation changes for olfactory bulb model (orange) and model with no inhibitory coupling (purple). **(B)** Stimulus generation: for stimulus 1 (top) one subpopulation received higher magnitude stimulation (left; filled with light gray) while the other subpopulation received lower magnitude stimulation (right; dark gray). Stimulus 2 (lower) reversed which subpopulation received the higher and lower magnitude stimulation, respectively. The mean activity of two randomly selected groups--group 1 (black outlines) and group 2 (no outlines)--was monitored. **(C)** Percent propagated spikes and **(D)** stimulus discriminability for both model variants. **(E-F)** Average firing rate in group 1 (x-axis) and group 2 (y-axis) during stimulus 1 (red) and stimulus 2 (blue). Each point represents mean firing rates over 500 ms in groups 1 and 2 for a single trial in the no coupling model (E) and olfactory bulb model (F).

Thus a particular cell stimulated at higher intensity for stimulus 1 received lower intensity stimulation for stimulus 2. This provides a simple model of responses to stimuli that evoke activity in overlapping sets of glomeruli.

We evaluated our model's propagation efficacy and stimulus discriminability, with and without inhibitory coupling. To test propagation efficacy, we created a second layer of decoding neurons, each of which received input from 20 layer 1 mitral cells. Thresholds were set so that activation of layer 2 cells required roughly 12 coincident inputs. We selected this setup based on properties of neurons in piriform cortex, which receive convergent inputs and have high firing thresholds (Apicella et al., 2010; Luna and Schoppa, 2008), We calculated the portion of layer 1 spikes that elicited a postsynaptic spike in layer 2. In the network with coupling absent, 0.17±0.01% of layer 1 spikes are successfully propagated to layer 2 (**Figure 4.6 C**, $p<0.05$). In the olfactory bulb-like model, propagation is increased to 0.23±0.03% ($p<0.05$). These results suggest that timescale-dependent correlation changes can maintain propagation even when average firing rate is reduced (see **Figure 4.7 B**; Δ_{FR}=-19±3%, $p<0.05$).

Next, we measured stimulus discriminability in layer 1 by measuring the correlation between the two stimulus-evoked patterns. To obtain a simple quantification of the network's output patterns, we randomly divided excitatory cells into two observation groups (**Figure 4.6 B**; group 1—black outlines, group 2—no outlines). For each stimulus, we compared the average firing rate in groups 1 and 2, giving a readout of whether an unbiased observer of firing rate can discriminate between stimuli. We applied stimulus 1 to the no coupling network 150 times, giving us an estimate of the mean and variance of the stimulus 1-evoked pattern (**Figure 4.6 E**; center and spread of red representation). Next, we again monitored the evoked mean and distribution of the pattern evoked by stimulus 2 (shown in blue). For non-overlapping stimulus-

evoked distributions, it is clear which stimulus was presented for any single observation of evoked firing patterns. However, when two distributions overlap (as in **Figure 4.6 E**), there is a range of observed patterns for which the presented stimulus is ambiguous to a downstream decoder.

Encoding performance was quantified using a two-dimensional linear discriminant analysis using a receiver operator characteristic. Without interneuron-mediated coupling, pattern overlap is sizable (d=0.6 where d is proportional to area under the ROC; **Figure 4.6 D**). The two stimuli were next applied to the olfactory bulb model, which greatly reduced pattern overlap (**Figure 4.6 F**; d=0.97). Excitatory cells cooperatively recruit inhibitory interneurons, resulting in competitive interactions between the two excitatory neurons of the pair. Like the electrophysiological results shown in **Figure 4.4 A**, this competition causes a separation of the firing rates between subpopulations. At the population level, competition alters average firing rates such that that overlap in the stimulus-evoked patterns is reduced. Thus inhibition-mediated timescale-dependent changes in channel correlation persist at the network level, and these changes improve both the propagation efficacy and discriminability of applied stimuli.

4.6 SYNERGISTIC AVOIDANCE OF PROPAGATION/ENCODING TRADEOFF

Thus far, we have seen that interneuron coupling can achieve simultaneous fast correlation and slow decorrelation, which can benefit both propagation and encoding. We wondered whether the observed improvements to propagation and encoding were truly specific to a timescale-dependent correlation strategy (as observed in the olfactory bulb), or whether they could be achieved via correlation changes at a single timescale. Our two-cell model shown in

Figure 4.5 suggests that shared, competitively recruited input is required for fast correlation/slow decorrelation. Since these mechanistic components can be isolated in our network model, we manipulated properties governing inhibitory synapses to investigate how fast correlation and slow decorrelation independently affect encoding and propagation.

To isolate fast correlation changes, we modified interneuron polarity so that for each interneuron spike, output had equal probability of being excitatory or inhibitory ($sync_{(\pm)}$ model). Although not biologically realistic, this simple manipulation preserved shared fast fluctuations while eliminating slower inhibitory influences on firing rate (**Figure 4.7 A**; black). The opposing model variant isolated slow decorrelation by disrupting the timing of GABAergic inhibition ($async_{(-)}$; gray). In this model, a random lag (0–50 ms) was imposed after interneuron spiking so that each postsynaptic target received inhibitory current at a different point in time. This kept the total amount of inhibition constant and activity-dependent, while eliminating shared fast fluctuations. These manipulations effectively isolated correlation changes at the timescales of interest (**Figure 4.7 A**; $sync_{(\pm)}$ $\Delta\rho$=0.12±0.02, $async_{(-)}$ $\Delta\rho$=-0.15±0.01, $p<0.05$) while matching firing rates to the no coupling and olfactory bulb variants (**Figure 4.7 B**).

In the $sync_{(\pm)}$ variant, propagation is increased to 0.34±0.05% (propagation changes across models summarized in **Figure 4.8**). However, discriminability is severely hindered in this case because increased spike covariance stretches response patterns along the diagonal axis (**Figure 4.7 C, E-F**; d=0.2). Conversely, in the $async_{(-)}$ variant, pattern overlap is reduced because the more active group suppresses firing rate in the less active group, stretching the two distributions along the antidiagonal (**Figure 4.7 D-F**; d=0.82). However, the decrease in firing rate reduces propagation to 0.03±0.004%. Notably, even though the olfactory-like model

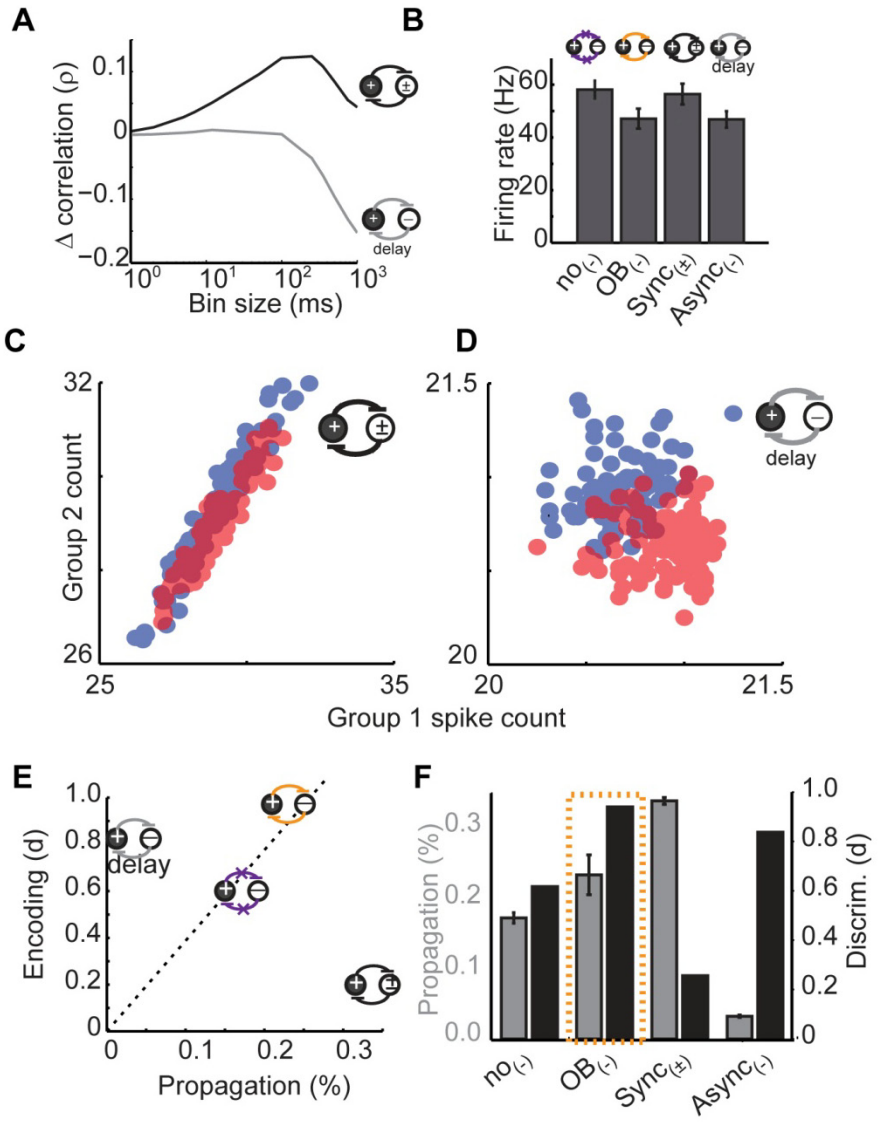

Figure 4.7: Benefits of timescale-dependent correlation changes. **(A)** Cross-timescale interneuron-induced change in correlation for $async_{(-)}$ (gray) and $sync_{(\pm)}$ (black) variants. **(B)** Mean firing rates for all four model variants. Evoked responses to stimuli 1 and 2 in $sync_{(\pm)}$ **(C)** and $async_{(-)}$ models **(D).** **(E)** Propagation/encoding tradeoff: $async_{(-)}$ facilitates encoding at the expense of propagation (gray, left), while $sync_{(\pm)}$ facilitates propagation at the expense of encoding (black, right). Timescale-dependent correlation changes simultaneously improve both propagation and encoding (orange, top). **(F)** Propagation efficacy and discriminability for each model variant. Error bars denote standard error.

combines the timescale-specific correlation changes represented in the $sync_{(\pm)}$ and $async_{(-)}$ variants, it outperforms the propagation and encoding predicted by the mean of these models. These models further highlight the benefits of the olfactory bulb-like inhibition with respect to the propagation/encoding tradeoff. Without any interneuron-mediated coupling, the model performs poorly with respect to both propagation and encoding (**Figure 4.7 E**, purple). While the $sync_{(\pm)}$ (black) and $async_{(-)}$ (gray) variants improve one aspect of processing, they do so at the expense of the other function. Only the olfactory-like timescale-dependent correlation model (orange) improves both propagation and encoding simultaneously (**Figure 4.7 F**, orange box).

4.7 DISCUSSION

Our results show that interneuron-mediated coupling between principal neurons can modulate pairwise spike train correlations in a timescale-dependent manner. Simultaneous fast and slow correlation changes depend on two features of granule recruitment. First, granule cells provide $GABA_A$ inhibition to subsets of mitral cells. This fast, shared input acts to synchronize spike timing (Galan et al., 2006; van Vreeswijk et al., 1994; Schoppa, 2006; MacLeod and Laurent, 1996; Tiesinga and Sejnowski, 2004). Secondly, inhibition is recruited competitively, resulting in slow decorrelation between mitral cells (Arevian et al., 2008; Friedrich and Laurent, 2001; Tiesinga, 2005). That is, more active mitral cells are more effective at recruiting lateral inhibition that suppresses the firing rate of less-active mitral cells. Like the recently described "synchrony by competition (Tiesinga and Sejnowski, 2004)" mechanism, timescale-dependent

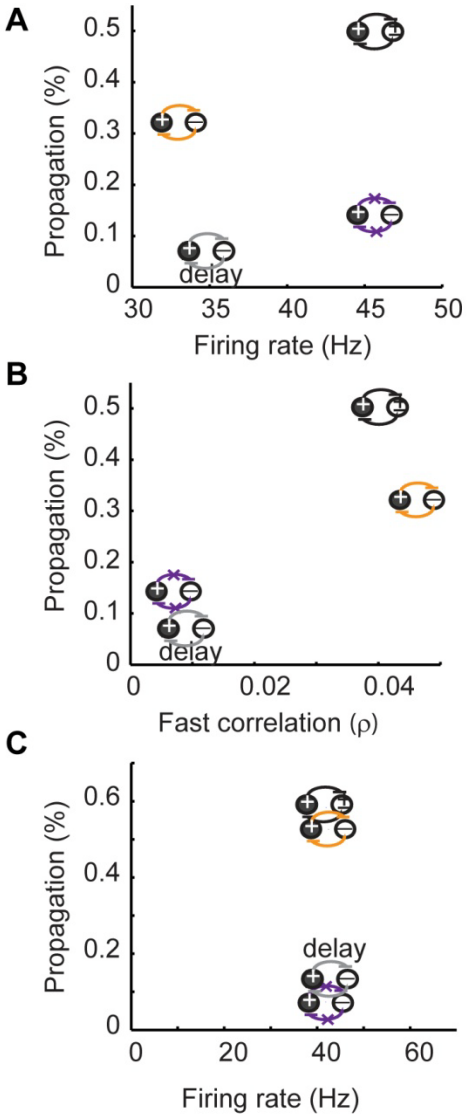

Figure 4.8: Comparison of propagation between network model variants. (A) Differences in propagation between model variants that are paired for firing rate (olfactory bulb, async$_{(-)}$, no coupling, sync$_{(\pm)}$) are attributable to differences in fast-timescale correlation. **(B)** Likewise, in model variants that are paired for fast correlation differences in propagation are attributable to firing rate differences. (C) When firing rate is equal for all model variants (by increasing amplitude of current stimulation), async$_{(-)}$ and no coupling have low propagation whereas olfactory bulb and sync(±) have high propagation.

correlation changes rely on competitively recruited synchronizing inhibition. Our study provides a novel perspective on correlation by considering multiple timescales and their impact on propagation and encoding. While the impact of correlation changes on sensory coding has been extensively discussed (Abbott and Dayan, 1999; Zohary et al., 1994; Schoppa, 2006; Salinas and Sejnowski, 2001; Sompolinsky et al., 2001; Romo et al., 2003; Reyes, 2003; van der Togt et al., 2006; Wang et al., 2010), measuring correlation changes at different timescales is not typically quantified in physiological data. Our report of timescale-dependent correlation changes in a real biological circuit demonstrates not only that this effect arises naturally from recruitment of local inhibitory circuits, but that it can be accomplished in a minimal circuit to study pairwise correlation. Downstream neurons may be sensitive to coincident inputs due to short membrane time constants, high firing thresholds or feedback inhibition. For these neurons (like pyramidal cells in olfactory cortex (Bathellier et al., 2009; Luna and Schoppa, 2008)) increased correlation of input spike trains increases propagation efficacy. Timescale-dependent changes can take advantage of the benefits of spike synchrony while simultaneously decorrelating response patterns to improve discriminability. Like other recently discussed mechanisms (Wiechert et al., 2010), timescale-dependent correlation changes have the advantage of biological simplicity, and they decorrelate overlapping patterns without requiring learning or prior knowledge of stimulus sets.

While the increase in fast timescale correlation is highly significant, the magnitude of this change observed between mitral cell pairs in slice is small due both to physiological and analytic causes. Physiologically, we expect this change to be small because it is induced by the inhibitory circuits recruited by a single pair of mitral cells. Since odor stimuli recruit tens to hundreds of neurons *in vivo*, this observed change likely represents a small fraction of the changes that would

be seen in vivo. Analytically, spike count correlation will always approach zero as bin size is reduced (Kass and Ventura, 2006). Given these limitations, we found it quite striking that significant changes in correlation were observed in these experiments.

Numerous studies have investigated the role of olfactory bulb inhibition in shaping behavior. In honeybees, selective disruption of inhibition-induced synchrony impairs behavioral performance only for difficult olfactory discriminations (Stopfer et al., 1997). This has also been observed in mice whose GABAergic signaling has been reduced genetically (Abraham et al., 2010). Conversely, genetic enhancement of GABAergic transmission improves performance on difficult olfactory discrimination tasks (Abraham et al., 2010; Nusser et al., 2001). Despite the clear behavioral improvements conferred by olfactory inhibition, their relationship to correlating (van Vreeswijk et al., 1994; Schoppa, 2006; Galan et al., 2006) or decorrelating (Friedrich and Laurent, 2001; Wiechert et al., 2010; Arevian et al., 2008; Urban, 2002) inhibition has remained unclear. Our results suggest that a single mechanism can account for increases and decreases in correlation, and that these changes result in improvements in signal propagation and encoding.

Given that several features of inhibition discussed here are unique to the olfactory bulb, inhibition-mediated timescale-dependent correlation changes may be particularly well suited for this system. Unlike purely center-surround lateral inhibitory circuits (such as the retina (Kuffler, 1953)), olfactory bulb lateral inhibition is less topographically confined (Arevian et al., 2008; Fantana et al., 2008; Cleland and Sethupathy, 2006) and mitral cells can laterally influence distant cells via their unusually long dendrites (Debarbieux et al., 2003; Margrie et al., 2001; Xiong and Chen, 2002; Shepherd, 2004). Further, the reciprocal nature of dendrodendritic synapses in the olfactory bulb may facilitate the generation and activation of shared inputs. However, inhibition-mediated cross-timescale correlation changes can in principle be

accomplished without these specific anatomical features (Smith and Kohn, 2008). As discussed in Figure 4.5, timescale-dependent correlation changes require inhibition that is fast, shared, and activity dependent; features that are quite general to neural circuits. Further, timescale-dependent correlation changes were observed over a broad range of parameter changes as long as these requisite features remained intact. Many neural networks represent information by patterns of population activity. Further, propagation is rarely 100% as downstream neurons often generate a sparsened representation of presynaptic activity. Given these generalities, we believe that our described mechanism could be efficacious for a wide variety of networks and tasks.

We present a novel perspective of lateral inhibition within the context of sensory coding. Examining correlations across different timescales reveals that inhibition shapes spike train correlations between principal cells in a highly specialized fashion. This mechanism integrates the traditional view of lateral inhibition (pattern decorrelation (Kuffler, 1953; Hartline and Ratliff, 1957)) with more recent studies detailing fast-timescale correlation changes (Stopfer et al., 1997; van Vreeswijk et al., 1994; Schoppa, 2006; Galan et al., 2006; Nusser et al., 2001). This perspective views spike timing and rate information not as opposing coding strategies, but rather as features that can be modulated semi-independently. This represents a targeted strategy by which a network can optimize the correlation structure of its output in a dynamic, activity-dependent manner. For example, networks may have an optimal correlation structure, given their inputs and processing demands (Yu et al., 2004). Thus timescales of increased and decreased correlation may be shaped by biological features such as time constants of downstream neurons, kinetics of neurotransmitter release, or particular stimulus statistics.

The propagation/encoding tradeoff is not specific to the olfactory system, but rather highlights that neurons must simultaneously accomplish multiple, and sometimes competing

aspects of sensory processing. This tradeoff provides a framework within which failures of neural processing (such as detection or discrimination) can be understood in diverse neural systems. Modulation of mitral cell activity by olfactory bulb inhibition generates timescale-dependent correlation changes that offer benefits for both propagation and encoding, circumventing the common correlation-induced tradeoff between propagation and encoding.

5.0 GENERAL DISCUSSION

5.1 SUMMARY OF FINDINGS

Over the past few decades, new techniques have drastically increased the ability of scientists to record neural activity. However, understanding brain function relies not only on the technology to record from neurons, but also on the ability to identify which features of spiking activity are relevant. Scientists and mathematicians have developed a broad array of metrics to quantify neural activity. These metrics have greatly improved our knowledge of neural coding, yet our understanding of how the brain represents sensory stimuli remains incomplete. Here, I have described a body of research that places particular emphasis on examining neural activity across different timescales. While this approach employs many standard metrics that have been used ubiquitously to describe neural activity, through emphasis on timescales, I have identified patterns of neural activity emerge that would otherwise go undetected. This timescales framework has revealed unusual and interesting properties of inhibitory circuits within the olfactory bulb.

5.1.1 Mechanisms of granule cell recruitment

In chapter 3, I described a series of experiments that investigated how olfactory bulb granule cells are recruited at exceptionally long timescales. Before this set of experiments, it was widely assumed that granule cells received only short-latency inputs and were able to integrate those inputs very slowly due to intrinsic membrane properties (Kapoor and Urban, 2006; Egger, 2008). However, I found that spike latency—whether short or long—was strongly correlated to the onset of excitatory synaptic currents received by granule cells. I interpreted this as evidence that the timing of granule cell recruitment is largely driven by the timing of distributed-latency excitatory inputs, representing a significant change in our model of inputs to granule cells.

I next characterized the spiking patterns of mitral and tufted cells to understand the temporal patterning excitation to granule cells. Whereas the latency patterns of mitral and tufted cells were assumed to be short and homogeneous, I observed that tufted cells (much like granule cells) responded to glomerular stimulation with a wide range of first spike latencies. Given the similarity of the first spike latency distributions of tufted and granule cells, I predicted that spike timing of single tufted cells might be sufficient to determine first spike latency in granule cells. I used calcium imaging to test this hypothesis by characterizing the latency patterns of granule cells with and without long-latency input from a single tufted cell. Indeed, first spike latency in connected granule cells could be dynamically changed by the timing of tufted cell activity. These results indicate that tufted cells play a specialized role in recruiting long-latency inhibition.

To investigate the possibility that intrinsic differences between mitral and tufted cells contribute to latency differences, I recorded frequency-intensity curves in mitral and tufted cells. Even in the absence of any synaptic inputs, tufted cells exhibited significantly longer first spike latencies in response to current injection and exhibited a slow ramping up of subthreshold membrane potential. This difference was abolished in the presence of the voltage-gated potassium channel blocker, 4-AP. I interpreted this data as evidence that potassium buffering in tufted cells contributes to the generation of long first spike latencies.

I constructed a simple model of the olfactory bulb to investigate the effects of distributed-latency inhibition on excitatory neurons. I compared the spiking outputs of model populations whose interneuron latencies were either restricted to short ranges, or were widely distributed (as seen in olfactory bulb granule cells). I found that mitral cell activity patterns were more effectively decorrelated from one another in the widely distributed latency case, suggesting that distributed-latency inhibition can be a useful circuit motif for disambiguating similar patterns. Distributed-latency inhibition represents a novel form of excitatory-inhibitory interactions because it acts as a source of decorrelation across long timescales while providing precise temporal patterning at short timescales. As such, distributed-latency inhibition could be an informative strategy for local processing in many different contexts.

5.1.2 Structure of olfactory bulb correlations

Olfactory bulb inhibition shapes stimulus-evoked patterns by altering the firing of mitral and tufted cells. These interactions had been observed to change the spiking statistics of

individual neurons as well as spiking relationships across neurons (Friedrich and Laurent, 2001; Wiechert et al., 2010; Arevian et al., 2008). However, it was unclear whether olfactory bulb inhibition acted to make mitral cell firing patterns more or less similar to one another. To understand the impact of olfactory bulb inhibition on pairwise spike train correlations, I performed an experiment in which I recorded from pairs of mitral cells and examined correlations in the absence and presence of shared inhibition. Importantly, I measured these correlations across a wide range of timescales ranging from milliseconds to seconds. I found that the inhibition recruited by a pair of mitral cells simultaneously shaped correlations in two opposing ways. At short timescales (~10 ms) inhibition increased correlation and promoted synchronous spiking. At long timescales (~100-1000 ms) inhibition decreased correlation and promoted divergence of firing rates. This experiment provides evidence that granule cells can modulate olfactory bulb correlations in a precise and timescale-dependent manner. In a more general context, these data demonstrate a concrete example of local inhibitory circuits simultaneously modulating correlations in opposing directions across timescales.

I hypothesized that mechanistically, timescale-dependent correlation changes could be mediated by a combination of competitive recruitment (which operates at a long timescale), and shared fast fluctuations (operating at a short timescale). I used a variety of computational models to demonstrate that shared, fast, competitively recruited inhibition is sufficient to mediate timescale-dependent correlations changes between model neurons. I also constructed more complex population models demonstrateingthat these timescale-dependent correlation changes between pairs can persist in large populations and can be helpful for maximizing propagation and encoding simultaneously. The consequences of correlated activity have been a source of intense debate in neuroscience communities because they can vary significantly based on the structure

and magnitude of neural correlations (Simoncelli and Olshausen, 2001; Series et al., 2004; Romo et al., 2003; Barlow, 2001; Schneidman et al., 2003; Kumar et al., 2010; Averbeck and Lee, 2006; Salinas and Sejnowski, 2001). The work presented here can work towards resolving some of this conflict by emphasizing that correlations cannot be fully described by a single value. Instead, a full description of neural correlations requires quantifying correlation across different bin sizes. Thus while previously published arguments about the helpfulness or harmfulness of correlations still hold true, these functional implications may be restricted to particular timescales, allowing cells to use other bandwidths to optimize their outputs.

5.2 PHYSIOLOGICAL RELEVANCE OF SHORT AND LONG TIMESCALES IN OLFACTION

In this thesis, I describe neural activity collected in slices of olfactory bulb and characterize activity across a wide range of timescales. We show that granule cells can be activated over a wide range of timescales, ranging from 1 to 1000 milliseconds. We show that granule cell activation increases mitral cell correlations at bin sizes smaller than 50 milliseconds, and reduces them at bin sizes greater than 100 milliseconds. This brings up important questions about the physiological relevance of the different timescales discussed here. What do these bin sizes—1, 50, 100, and 1000 milliseconds—mean for an intact mouse? To put these timescales in context, the following sections discuss and compare these timescales to those documented in *in vivo* preparations, focusing on the oscillations and behavioral literature.

5.2.1 Relationship to oscillations literature

One useful reference point for understanding the short, medium, and long timescales discussed in this thesis is the extensive body of literature concerning oscillatory correlations in the olfactory bulb/antennal lobe. However before comparing the timescales of oscillations with our data on olfactory bulb correlations, the relationship between oscillatory and non-oscillatory correlations is worth mentioning. Oscillatory correlations are related to, yet distinct from, the non-oscillatory correlations discussed in chapter 4. In contrast to measuring correlations at particular bin sizes, oscillatory power reflects correlated activity occurring at a predictable interval. This distinction is shown schematically in **Figure 5.1 A**. Two cross-correlograms are plotted here, one depicting oscillatory correlations (blue) and one depicting non-oscillatory correlations (black). Both examples exhibit zero-lag correlation—when a spike occurs in cell 1, there is an increased probability of a spike occurring in cell 2, as evidenced by the peak at time = 0. The width of this peak can vary in both cases, corresponding to the temporal precision of correlated spiking (precise synchrony versus spiking that is "jittered" across a wider time bin).

A key difference between measuring correlations at different bin sizes and measuring oscillations at different bin sizes is that correlations measure different widths of the zero-lag peak while oscillations measure the distance between peaks. For example, correlation at a 10 millisecond bin size refer to the peak between -5 and 5 milliseconds, while a 10 Hz oscillation reflects correlated activity every 100 milliseconds. Another important distinction is that oscillatory activity is often characterized from local field potential (LFP) recordings rather than pairwise spiking data. An example of this type of recording is shown in **Figure 5.1 B**. LFP

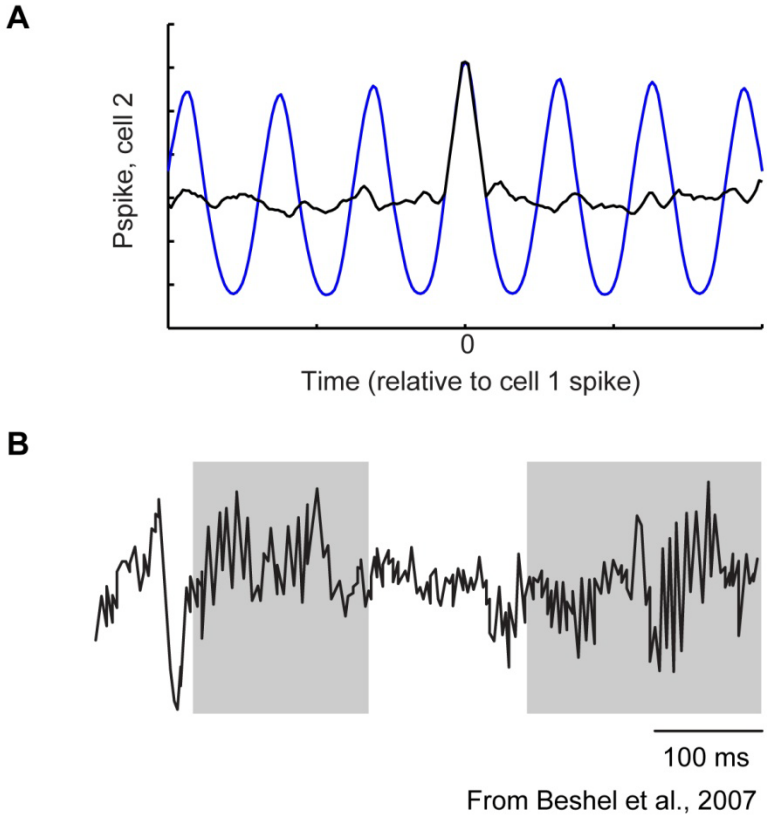

Figure 5.1: **Relationship between oscillations and correlation.** **(A)** Schematic cross-correlograms of spike train pairs with oscillatory (blue) and non-oscillatory (black) correlation. **(B)** Example olfactory bulb LFP recording during odor application, from Beshel, et al. 2007. Epochs of gamma-band oscillations highlighted in gray.

oscillations reflect periodic correlations in spiking and synaptic input (Van Hooser et al., 2000) across a population of neurons. Thus they reflect more global, periodic covariation across cells rather than the targeted pairwise changed discussed in chapter 4.

Studies of oscillatory activity in the olfactory bulb are a useful reference point in our discussion of timescales because these studies have the advantage of considering a wide range of timescales and studying olfactory rhythms *in vivo* during odor-evoked activity. Odor stimulation elicits robust oscillations in the olfactory bulb and antennal lobe (Adrian, 1942; Beshel et al., 2007; Bressler and Freeman, 1980; Freeman and Schneider, 1982; Chabaud et al., 2000; Laurent and Davidowitz, 1994). The magnitude and frequency content of these oscillations changes with odor stimulation, yet it is unclear how or whether these frequency transitions are related to stimulus features, as odor-evoked oscillations remain fairly stereotyped across a wide range of stimuli and concentrations (Ito et al., 2009; Stopfer et al., 2003). This invariance suggests that oscillatory correlations may be enacted by local circuits to facilitate processing(Lagier et al., 2004) rather than reflect particular stimulus features.

What can the dynamics of olfactory bulb oscillations tell us about the role of timing in olfactory coding? Fast oscillatory activity is particularly prominent during difficult olfactory discriminations (Stopfer et al., 1997; Nusser et al., 2001; Beshel et al., 2007; Kay and Beshel, 2010; Chapuis and Wilson, 2011). Oscillations in the beta and gamma range (corresponding to 10-100 ms periods of oscillation) have garnered particular attention due to their association with attention during cognitively demanding tasks. Increased correlation at these short timescales has been posited to improve processing within the olfactory bulb (Beshel et al., 2007; Kay et al., 2009; Neville and Haberly, 2003) as well as other brain areas (Saleh et al., 2010). These short timescale oscillations may confer the same benefits to propagation as nonoscillatory correlations,

as discussed in chapter 4. This may be particularly advantageous in promoting propagation across regions (Macrides et al., 1982). Fast oscillatory synchrony may also improve olfactory representations by binding together the activity of stimulus-specific subsets of neurons (Milner, 1974; Singer and Gray, 1995; Laurent and Davidowitz, 1994).

At longer timescales (100-100 ms periods of oscillation), oscillatory activity does not appear to be associated with sensory processing. In the olfactory bulb and other areas, long timescale oscillations are most commonly associated with sleep and quiet wakefulness (Nusser et al., 2001; Poulet and Petersen, 2008; Steriade and Timofeev, 2003) rather than active sensory processing. Together with the large body of evidence implicating fast timescale oscillations in active sensory processing, these results are conceptually very similar to our model of timescale-dependent correlations presented in chapter 4. There, we showed evidence that local interneuron recruitment acts to increase fast correlations in bin sizes less than 50 ms while decreasing correlation at bin sizes larger than 100 ms. The timescales of increased fast correlation loosely match up to the timescales of increased fast oscillations (beta and gamma range) while long timescale decorrelation may be related to a reduction in slow oscillations associated with active sensation.

However, the relationship between oscillations and coding timescales is not always clear. Several reasons contribute to this. For one, some correlation changes are better captured by non-oscillatory measures. This is true of the fast timescale correlation changes measured in chapter 4 (in which synchrony occurs frequently, but at unpredictable intervals), as well as non-oscillatory correlation changes captured *in vivo* (Aylwin et al., 2005; Gerkin et al., 2012). Non-oscillatory correlation changes may be particularly prevalent at long timescales. Take, for example, lateral inhibition-induced firing rate changes and pattern decorrelation. These correlation changes

typically occur over long timescales, yet they do not recur periodically over time and would not be captured with oscillatory measures. A second instance in which metrics of global oscillations (such as LFP recordings) can fail to capture correlation changes is when correlation changes are restricted to relatively few neurons. A correlation change (even an oscillatory one) between two neurons is unlikely to exert a dominant force on the LFP. Instead, this pattern will likely be drowned out by the noise of other uncorrelated neurons. Lastly the dynamics of oscillations appear to depend (at least partially) on anesthesia (Fontanini and Bower, 2005), suggesting that oscillations may in some cases be drug-related rather than processing-related. Correlations conferred from anesthesia or breathing rhythms (Aylwin et al., 2005; Phillips et al., 2012) may represent external influences on correlation structure that are not directly related to correlation changes associated with stimulus processing.

The small pairwise correlations discussed in chapter 4 may have advantages over more global oscillations because they can restrict correlations to a stimulus- or task-dependent subset of neurons and minimize the spread of that redundancy across the population. Whether the ubiquity of oscillatory behavior derives from its additional utility over non-oscillatory correlations or because it is a convenient vehicle for maintaining correlations remains debated (Kay et al., 2009). In either case, oscillatory activity in the bulb and antennal lobe can be extremely helpful for understanding timescales of neural activity and their relationship to behavior, particularly in highlighting the advantages of fast timescale correlations (Stopfer et al., 1997; Nusser et al., 2001; Beshel et al., 2007; Kay and Beshel, 2010). Combining this information with spiking data from single cells is an invaluable tool for obtaining a complete picture of the spiking structure of cells across a population.

5.2.2 Timescales of behavior

A second important temporal reference frame is the timescale of olfactory-guided behavior. Nearly all olfactory-guided behaviors occur somewhere within the 1-1000 millisecond time windows discussed in this thesis. Certain tasks, such as recognizing a novel odor, can be accomplished in as little as 140 ms (Wesson et al., 2008a). Other simple behavioral tasks can also be accomplished very rapidly (~200 ms) (Goldberg and Moulton, 1987; Abraham et al., 2004; Uchida and Mainen, 2003; Rinberg et al., 2006). Thus under certain conditions, perceptual decisions can be mediated at the timescale of a single sniff (Uchida et al., 2006; Kepecs et al., 2006). While granule cells are certainly recruited during this time period, there is no evidence that their inputs are required for these simple tasks.

However, more difficult perceptual decisions tend to rely more heavily on local inhibition and require more time to complete. Chemically and psychophysically different odors (for example, lemon versus coffee) elicit largely separate and non-overlapping activity patterns (Lin et al., 2006), and are discriminated between with relative ease. Conversely, discrimination of very similar stimuli (such as 40:60 vs. 60:40 mixtures of two odorants) is a much more difficult problem for animals to solve. The relevant timescales for difficult decisions remain debated. Some studies suggest that task difficulty determines the maximal accuracy that an animal can achieve, regardless of how long they are given to make their decision (Uchida and Mainen, 2003). This model suggests that olfactory bulb output is optimized to operate within the timescale of a single sniff (≤200 ms). Conversely, other data suggest that difficult tasks can be accomplished more accurately if animals are allowed increased time to make a perceptual decision (Rinberg et al., 2006; Abraham et al., 2004; Abraham et al., 2010). This phenomenon is

known as a speed-accuracy tradeoff and has been reported in the visual (Swensson, 1972; Pew, 1969) and auditory systems (Green and Luce, 1971) in addition to the olfactory bulb. Olfactory discriminations between psychophysically dissimilar odors can typically be accomplished in 200-300 ms, whereas difficult discrimination tasks can take anywhere between 230 (Uchida and Mainen, 2003) and 550 ms (Rinberg et al., 2006) (**Figure 5.2**).

While the particular details of response times vary across studies, all of these behavioral timescales (ranging from 250-550 ms) are of high interest within the context of this thesis. The observed delay in responses during difficult discriminations (as compared to easy tasks) suggests that some processing going on during this time window may be required for difficult tasks. Further, performance on these tasks is significantly impaired when olfactory bulb inhibitory circuits are disrupted (Stopfer et al., 1997; Abraham et al., 2010; Mwilaria et al., 2008; Gheusi et al., 2000), suggesting that granule cells may play a key role.

Our results offer several intriguing mechanisms that could facilitate discrimination tasks at the 250-550 ms timescale. Granule cells are poised to alter stimulus-evoked activity patterns during this time window by shaping the correlations between pairs and groups of cells. Inhibition-induced correlation changes are thought to be important for discrimination tasks because they can selectively correlate and decorrelate stimulus-specific subsets of neurons. Take the example of two neurons, A and B, which are both activated by two stimuli, lemon and lime. Discrimination of lemon versus lime requires that a downstream decoder can tell whether cell A is firing more rapidly (lemon) or whether cell B is firing more rapidly (lime). If both stimuli evoke similar firing rates in both cells (because of noise or low stimulus-specificity), this discrimination will not be possible. However, if competitively recruited inhibition acts between

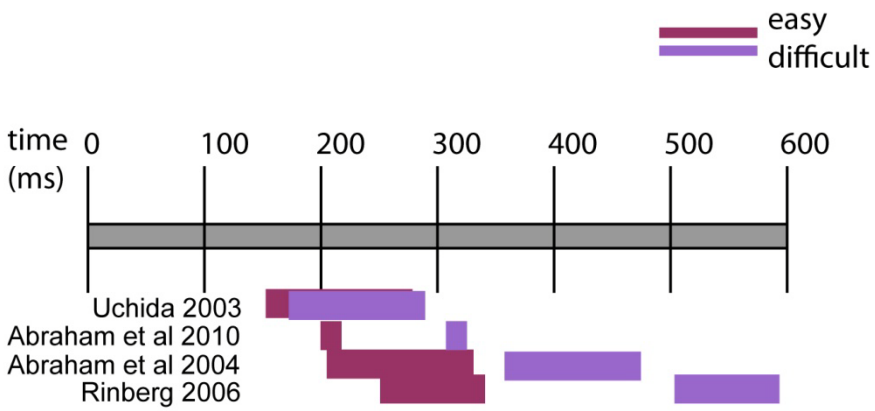

Figure 5.2: Timescales of behavior. Behavioral approaches to studying timescales and discrimination reveal that easy and difficult discriminations can be performed accurately, yet difficult discriminations take longer, (and rely more heavily on inhibitory circuits (Abraham et al., 2010)).

these two cells, it will magnify even small differences in firing rate, decorrelating them to enable discrimination. This same idea can be applied to groups of neurons. For example, faced with many A-like cells and many B-like cells, inhibition can decorrelate stimulus-evoked patterns to manipulate the firing of stimulus-specific subsets of neurons.

This example illustrates a simple motif whereby granule cell-mediated decorrelation could facilitate discrimination. Our results indicate that granule cells are capable of mediating this simple lateral inhibition motif, but are also capable of shaping correlations in a more targeted way. The timescale-dependent correlation changes discussed in chapter 4 show that granule cells can increase correlations at bin sizes less than 50 ms, while decreasing correlation at large (>100 ms) bin sizes. The granule cell-mediated decorrelation in 100-500 ms bins could facilitate difficult discriminations during the delay associated with processing of difficult stimuli. Our results indicate that during this time frame, the network may benefit not only from granule cell-mediated decorrelation, but also from increased synchrony to facilitate propagation.

Our results reported in chapter 3 suggest that granule cell latency may also play an important role during difficult tasks. Since granule cells are recruited at widely distributed latencies, additional granule cells are continually being recruited during the 250-550 ms time period. This may further facilitate decorrelation by preferentially recruiting additional granule cells that are connected to a strongly stimulated glomerulus. For example, initial odor stimulation may activate a large population of mitral, tufted, and granule cells within the first 200 ms following odor onset. If the decorrelation enacted by these early-recruited granule cells does not sufficiently decorrelate different stimulus-evoked patterns, the animal may have to wait until additional granule cells are recruited to tip the balance in favor of a particular stimulus.

These examples of the timescales of oscillations and behavior illustrate that the timescales of olfactory bulb activity discussed in this thesis are highly relevant to behavior. Our results provide several intriguing mechanisms that may facilitate odor processing during these important time windows. In the future, recordings of granule cell activity during difficult olfactory discriminations will be very helpful in translating the timescales of granule cell activity in slice to those operating during complex processing.

5.3 IMPLICATIONS FOR OLFACTORY BULB PROCESSING

5.3.1 Implications for mitral and tufted cell coding

Chapter 3 describes a series of experiments that aimed to understand the mechanisms controlling long-latency inhibition *in vitro*. These experiments were motivated by a previous study in the lab which demonstrated that olfactory bulb granule cells are recruited at long latencies (Kapoor and Urban, 2006). This study revealed a fascinating and previously unknown activity pattern in the olfactory bulb, but the cellular and synaptic mechanisms contributing to these latencies remained unknown. To elucidate these mechanisms, we used a combination of electrophysiological recordings, calcium imaging, and pharmacological approaches. Our results reported here have resolved the mechanistic ambiguity surrounding granule cell latency in slice by showing that granule cells are driven to fire at temporally precise latencies by a combination

of subthreshold depolarization from mitral cells and distributed-latency suprathreshold excitation provided by middle tufted cells.

While these results provide a mechanistic explanation of the latency phenomena observed in slice, the factors shaping latency patterns in vivo are undoubtedly more complicated. Several lines of physiological evidence support our interpretation of specialized roles for mitral and tufted cells, however the details of their physiology varies across studies. *In vivo* studies have shown that tufted cells have less respiration-coupled firing patterns and tend to respond to odors with larger changes in firing rate than do mitral cells (Phillips et al., 2012). *In vitro* studies have also shown that tufted cells are more reactive and prone to bursting than are mitral cells (Hayar et al., 2004). Thus tufted cells are generally believed to be more excitable than mitral cells, and have been observed to have *shorter* spike latencies than mitral cells (De Saint Jan et al., 2009).

At the surface, short first spike latencies in tufted cells seem at odds with our observation of long first-spike latencies in tufted cells. However, these patterns are not mutually exclusive. I interpreted the long and rate-dependent first spike latencies as evidence that tufted cells can scale their latency more linearly with input intensity. That is, given weak inputs, they will respond with long latencies whereas they will respond with short latencies given strong inputs. The disparate spike latency observations reported here and by De Saint Jan can be reconciled under this framework. Perhaps tufted cells *in vivo* tend to receive stronger sensory stimulation than mitral cells (causing them to have short spike latencies) while glomerular stimulation provides stronger input to mitral cells. Recent evidence suggests that tufted cells do indeed receive much stronger primary sensory input than do mitral cells (Gire et al., 2012). Further, these authors identify a multisynaptic pathway through which mitral cells are excited, providing further delays in mitral cell latencies *in vivo*.

Other methodological differences could also contribute to the differences in tufted cell latency patterns across preparations. For one, most studies of tufted cell latency focus on external tufted cells, whose somata are located adjacent to glomeruli. While the exact relationships between the physiological properties of external tufted, middle tufted, and mitral cells remain to be elucidated, it is possible that middle tufted cells differ significantly from external tufted cells in their evoked responses. Different methods of stimulation (for example, odor stimulation versus olfactory nerve stimulation, versus glomerular stimulation) may also affect olfactory bulb response properties by changing the dynamics of inputs to mitral and tufted cells. While the particular temporal patterns of mitral and tufted cell activity will vary based on the way they are stimulated, our results contribute to this literature by giving a mechanistic explanation of latency data observed in slice, and provide further support for the idea that mitral and tufted cells play specialized roles that lead to complex temporal patterning.

If mitral and tufted cells do indeed have specialized jobs in olfactory processing, what are they? Given that tufted cells exhibit higher excitability, stronger connections with olfactory receptor neurons (Gire et al., 2012), and ability to fire at flexible latencies, these cells may be ideally suited to amplify weak inputs or represent information related to intensity. In the olfactory system, odor concentration is the stimulus parameter most closely related to intensity. Within the olfactory bulb, increasing odorant concentration tends to recruit additional glomeruli (Johnson and Leon, 2000; Stewart et al., 1979). Tufted cells might be well-suited to mediate this activation of additional glomeruli because of their sensitivity to weak inputs while mitral cells could process other information about stimulus identity.

5.3.2 Implications for olfactory bulb inhibition

5.3.2.1. Latency coding

Latency patterns have been characterized in a variety of brain areas, yet the involvement and role of inhibitory circuits in these patterns has not been thoroughly investigated. While interneurons certainly participate in latency patterns in other brain areas, they may be activated multiple times within a single cascade, thus eliminating the long-lasting sequential activation observed in the olfactory bulb. It is possible that long-lasting cascades of interneuron recruitment are most likely to be observed in areas (like the olfactory bulb) where there is a very large population of interneurons or where the ratio of inhibitory to excitatory cells is high.

A general problem that can limit the utility and feasibility of latency codes is identifying the proper reference frame. By definition, latency is a delay in spiking with respect to some external event. Thus latency codes require a "clock" against which latency can be measured. In the olfactory bulb, this clock has been presumed to rely on global oscillations conferred by the respiratory cycle (Shusterman et al., 2011; Margrie and Schaefer, 2003). However, here we show an example of latency tiling which persists in the absence of these rhythms, suggesting that the olfactory bulb circuitry may be able to generate complex temporal patterns with respect to stimulus onset. Of course *in vivo*, we expect these patterns to be changed and additionally shaped by additional influences, such as the respiratory cycle, olfactory receptor neuron latency and cortical feedback. The latency patterns observed in slice are not predicted to be a replica of the latency patterns observed during olfactory behavior. However, they demonstrate that the olfactory bulb has its own local mechanisms that contribute to this patterning.

A recent report documented long-lasting olfactory bulb latency patterns *in vivo* during active sniffing (Shusterman et al., 2011), yet the mechanism(s) controlling this patterning remains unclear. Our demonstration of long-latency activity in olfactory bulb slices provides several useful hypotheses. Our results suggest that specifically disrupting tufted cell activation would disrupt these tiled patterns. This is predicted both because tufted cells participate in stimulus-evoked latency patterns, and also because they recruit inhibition in a manner that can further refine temporal patterns. Our results suggest that the stimulus-evoked latency patterns could be disrupted by blocking voltage-gated potassium channels in tufted cells. Disrupting granule cell latency patterns (while leaving tufted cell latency patterns in tact) might be accomplished by reducing their prolonged depolarizations (perhaps by blocking NMDA, I_{CAN} or T-type voltage-dependent Ca^{2+} (Egger, 2008; Egger et al., 2005)).

Under what physiological conditions is distributed latency inhibition likely to be most advantageous? In chapter 3, I used a simple model of the olfactory bulb to demonstrate the advantage of distributed latency inhibition on pattern decorrelation using a simple rate-based decoder. Thus, the short timescale temporal coding discussed here can be useful even in the face of a decoder that ignores temporal information. While some of the advantages of distributed latency inhibition do not require decoding of temporal patterns in cortex, its efficacy would most certainly be higher if this were the case. Indeed, recordings from piriform cortex (Apicella et al., 2010; Poo and Isaacson, 2009) and the insect mushroom body (Perez-Orive et al., 2002; Szyszka et al., 2005; Turner et al., 2008) suggest that downstream neurons are indeed sensitive to particular temporal patterns of mitral cells inputs. Given the temporal selectivity of these downstream neurons, latency coding might be particularly well-suited to encode complex,

multidimensional stimuli with a limited number of cells. A variety of different decoders and classifiers might be considered with this temporal specificity in mind.

5.3.2.2. Inhibition and cross-timescale correlations

The correlation changes described in chapter 4 are especially intriguing because the inhibition-induced changes to correlation vary across timescales not only in magnitude, but also in sign: correlations are enhanced at short timescales and reduced at long timescales. While we are (to our knowledge) the first to report such an effect, it is quite possibly an overlooked statistic in other neural circuits. The mechanistic model shown in Figure 4.5 demonstrates that simultaneous fast correlation and slow decorrelation can be accomplished in circuits in which inhibition is 1) fast, 2) shared, and 3) competitively recruited. These simple requirements could be met by many (if not most) networks containing a balance of excitatory and inhibitory neurons given enormous variety of cells that receive GABAergic inhibition via fast-acting $GABA_A$ receptors, the fact that most interneurons deliver inhibition onto more than one postsynaptic cell, and the fact that interneurons are often recruited competitively based on their drive from excitatory neurons in the network.

While timescale-dependent correlation changes may be a natural consequence of fast, shared, and competitively recruited inhibition, it is important to consider in which brain areas or during which functional tasks such correlations may be helpful. We have described the benefits of timescale-dependent correlation changes within the context of propagation/encoding tradeoffs which are potentially important in the bulb because stimulus representations are overlapping and

there is a high degree of divergence in the subsequent layer of processing. Similar constraints might apply in other areas that use population codes and must disambiguate complex information. For example, timescale-dependent correlation changes might be particularly well-suited for processing in areas like subregions of the hippocampus important for pattern separation (Leutgeb et al., 2007).

One intriguing and unanswered question about granule cell activation is how granule cell-mediated inhibition affects homotypic (same glomerulus) versus heterotypic (different glomeruli) pairs of mitral cells. Each glomerulus in the olfactory bulb contains the apical dendrites of approximately 60 mitral cells, often dubbed "sister mitral cells" (Ressler et al., 1994; Mombaerts et al., 1996). Sister mitral cells receive highly correlated sensory inputs in drosophila (Kazama and Wilson, 2009) and the same is presumed to be true in mammalian systems. In addition to input correlation, these cells are also correlated by glutamate spillover within a glomerulus and gap junction coupling between cells. If all cells within a single glomerulus are receiving highly similar information, then why does the bulb need so many cells to process a single signal?

One possibility is that inhibitory inputs act to alter the correlation structure of sister mitral cells to make their rate output more heterogeneous. In our model of timescale-dependent correlations discussed in 4.5, we focused our discussion on the impact of evoked patterns across glomeruli. However, the same circuit motif could potentially be useful in increasing the complexity of output from a single glomerulus. Rather than sending out 60 copies of the same signal, the rate output of sister mitral cells could be decorrelated. Even in the absence of inhibitory inputs, individual mitral cells respond differently to identical inputs (Padmanabhan and Urban, 2010), suggesting that mitral cells may also possess intrinsic properties that act to

diversify their outputs. Such processing could be useful for multiplexed coding of different stimulus features, or for driving downstream neurons with diverse tuning properties.

5.4 ALTERNATE INTERPRETATIONS

5.4.1 Involvement of other interneuron types

In the work presented here I have emphasized the importance of granule cell recruitment on mitral and tufted cell activity both in the context of latency coding and with cross-timescale correlations. We infer that most of the timescale-dependent correlation changes in mitral cells are due to granule cell firing given the large size of this population. However, we cannot exclude the possibility that other inhibitory interneurons such as periglomerular cells are playing a role in these changes. Periglomerular cells can also possess the requisite properties of being shared, fast, and competitively recruited. However, periglomerular-mediated changes would require that pairs of mitral cells have apical dendrites in neighboring glomeruli (or alternatively, have more complex long-range interaction via short axon cells). Further, we observed timescale-dependent correlation changes even in pairs in which one or more mitral cells had a severed apical dendrite. Because of these limitations of periglomerular cells in mediating timescale-

dependent correlation changes, we consider granule cell mediated inhibition to be a more likely substrate in the majority of situations.

Periglomerular cells may also be involved in the timing of mitral and tufted cell recruitment during latency cascades. Here we have focused on intrinsic differences between mitral and tufted cells rather than potential differences in arborization or synaptic connectivity within the glomerular layer. However, it is possible that the interactions with periglomerular cells also facilitate these temporal patterns. For example, periglomerular cells could provide inhibition that tracks mitral cell firing and subsides across hundreds of milliseconds. Such a mechanism could potentially contribute to long-latency firing in tufted cells via disinhibition. While we certainly observed activation of periglomerular cells following glomerular stimulation, we do not have any direct evidence of their role in shaping spike timing. Characterizing these interactions would add valuable insight into our understanding of how the glomerular microcircuit shapes mitral and tufted cell output.

5.4.2 Mitral and tufted cell differences

I have also argued that my results suggest that mitral and tufted cells may have distinct roles in how they recruit inhibitory circuits, and perhaps in how they more generally encode information. An alternate possibility is that specialized roles for mitral versus tufted cells may be restricted to a subset of possible olfactory bulb computations. For example, we report here differences in mitral and tufted cells that arise in response to weak and spatially focal glomerular stimulation. While it is reasonable to assume that this corresponds to some physiological

situations (such as detecting low concentrations of odorant or detecting small differences between similar stimuli) there are a wide range of environments in which evoked activity would be much stronger and spatially distributed. Thus it is clear that mitral and tufted cells differ in their responses characterized here, but that situation may only come up intermittently, and thus functional segregation of mitral and tufted cell activity may represent a specialized case.

Another interesting issue for future study is the response of cortical neurons to mitral versus tufted cell activity. While it is known that mitral and tufted cells differ in their axonal projections (Shin Nagayama et al., 2010; Haberly and Price, 1977; Schoenfeld and Macrides, 1984), the specific rules governing these synapses are not known. In this thesis, we have focused on the difference between mitral and tufted cells as a potential substrate for encoding complimentary stimulus information simultaneously. However, such differences may also be relevant for decoding in piriform cortext, as these cells are sensitive to the temporal structure of inputs (Luna and Schoppa, 2008). Responses of neurons in piriform cortex (and mushroom body) exhibit both mixture suppression—reduced activation in the presence of an odorant with additional components, as well as mixture facilitation—responses that are supralinear to responses of individual components (Yoshida and Mori, 2007; Zou and Buck, 2006; Stettler and Axel, 2009). Thus the complement of mitral and tufted cell inputs may also be useful for providing the temporal specificity to evoke activity in highly selective cortical neurons.

Lastly, while we have focused on the role of intrinsic membrane properties (such as voltage gated potassium channels) in shaping the timescales of neural activity, we cannot discount the contribution of receptor-mediated signaling. In particular, $GABA_B$, NMDA, and muscarinic glutamate receptors have long decay constants that may be involved in building long timescale activity in the olfactory bulb. Our computational results indicate that these features

may not be necessary to build these long timescale activity patterns, and yet their abundance in the olfactory bulb (Shepherd, 2004) suggests that they may be involved.

5.5 BEHAVIORAL PREDICTIONS

5.5.1 Latency structure

Recent *in vivo* data suggests that the distributed latency responses shown in this thesis do indeed persist in the intact mouse (Shusterman et al., 2011). However, targeted manipulation or disruption of these latency patterns have not yet been performed. What would be the expected outcome of eliminating, truncating, or otherwise disrupting olfactory bulb latency patterns?

We predict that disrupting olfactory bulb latency patterns may interfere with olfactory behaviors in two ways: by manipulating tufted cell firing patterns, and by disrupting granule cell-mediated inhibition. Our results suggest that latency patterns arise when tufted cells receive weak inputs and then integrate them over long timescales. We posited that such responses may be helpful in "deciding" whether or not a glomerulus participates in a stimulus evoked pattern because tufted cells can slowly integrate weak inputs that would otherwise not elicit spiking in mitral cells. Disrupting this gating may alter the number of glomeruli excited by a stimulus, and could perhaps disrupt the concentration-dependence of evoked glomerular activity patterns

(Johnson and Leon, 2000; Stewart et al., 1979). Further, disrupting tufted cell latency may be sufficient to disrupt olfactory representations (independent of glomerular gating) because the temporal patterns of tufted cell excitation may provide stimulus-specific information to piriform cortex and olfactory tubercle.

A second way in which disrupting olfactory bulb latency patterns may interfere with olfactory-guided behaviors is by interfering with granule cell-mediated inhibition. Odor stimulation evokes activity in mitral, tufted, and granule cells (Cang and Isaacson, 2003), and granule cell feedback is thought to dynamically shape odor representations (Abraham et al., 2010). As discussed previously, such inhibition is thought to be particularly important during difficult olfactory discriminations. It is possible that part of the utility of granule cell-mediated inhibition during these difficult tasks arises from granule cell latency patterns (as described in 5.2.2). If so, we would predict that disrupting granule cell latency patterns might increase discrimination thresholds between similar odors.

Identifying an optimal range of latencies remains a key question about latency codes. The model presented in chapter 3 employed a simple, rate-based decoder of excitatory output. In a situation like this, the optimal range of interneuron latencies would likely depend both on the timescales of behavior as well as the shape of the latency distribution. Assuming a uniform distribution (as we did in our models) the optimal latency spread is likely to be approximately twice the duration of behavioral decisions. At this point in time, half of interneurons are turned on, and the other half have yet to be activated. In a simple framework (making no assumptions about non-random connectivity, feedback, or reward structure), this is the time point at which the difference in inhibition delivered to different neurons is maximized (i.e. some cells have already received all of their inhibition, while others have received none). In a more complex and

physiologically realistic scenario, latency spread may be dynamically controlled based on these other considerations. In vivo evidence suggests the olfactory bulb may optimize its latency structure to coincide with the timescales of respiration (Shusterman et al., 2011), as single sniffs may be the most behaviorally relevant "unit" of odor processing (Kepecs et al., 2006; Uchida and Mainen, 2003).

5.5.2 Timescale-dependent firing changes

Chapter 4 discussed the advantages of timescale-dependent correlation changes for facilitating both propagation and encoding simultaneously. If this is the case, why haven't olfactory bulb networks come to organize themselves to make these correlation changes even stronger? If we could selectively alter olfactory bulb activity in a timescale-specific manner, what behaviors might this enhance or degrade? A number of previous studies lend insight that might apply to these questions.

Fast timescales correlations have been manipulated in the awake behaving animal by using pharmacological (Stopfer et al., 1997) or genetic (Nusser et al., 2001) approaches to enhance or degrade oscillatory correlations. The common finding in these studies was that enhancing fast correlations improves performance on difficult, but not simple, discrimination tasks. This phenomenon held true even though these studies used dramatically different methods of enhancing fast correlation as well as using different species. However, the gain of function from enhanced fast correlation comes at a cost. For example in the Nusser et al study, the animals with increased fast correlations initially performed better at discriminating between

different mixtures, yet had problems retaining this ability over trials. In other studies that enhanced inhibitory circuits, the cost of changing inhibition is unclear (Abraham et al., 2010) (although extensive behavioral testing across many odor-guided behaviors falls outside of the scope of these studies.)

Another prediction of correlation-enhanced propagation is that even low firing rates can be effectively propagated to cortex. In uncorrelated low-rate spike trains, the number of coincident spikes is low because spikes occur infrequently. As firing rate increases, coincidence and correlation (Doiron et al., 2003) increase. Adding fast timescale correlations means that even at low firing rates, synchronous spikes are more numerous. Mitral and tufted cells may fire at low rates during application of a non-preferred stimulus, or perhaps during application of low concentrations of a preferred odorant. Increased propagation in these examples might relate to increased detection of low concentrations, or perhaps increased sensitivity to detecting mixtures. Indeed, disrupting inhibition-mediated synchrony has been observed to increase detection thresholds in moths (Mwilaria et al., 2008). Synchronous firing is also associated with enhanced stimulus detection in the primate visual cortex, (yet decorrelation is associated with more accurate discriminations (van der Togt et al., 2006)). Thus the perceptual correlates of synchrony-facilitated propagation appear to vary in different situations.

As discussed above, long timescale decorrelations have been posited to facilitate accurate discriminations of stimuli with overlapping representations. The obvious disadvantage of relying on decorrelation at large time windows may be self-evident: these computations take a long time. Thus if short response time are a high priority, the increase acuity conferred by this strategy could be disadvantageous for quick decision-making. Behaving animals must cope with many of these competing demands simultaneously. While the timescale-dependent correlation

changes described here may be helpful for avoiding part of the propagation/encoding tradeoff, it is likely that the olfactory bulb circuit has already optimized the magnitude of timescale-dependent correlation in the face of additional competing demands.

5.5.3 Other behavioral considerations

Another important consideration is that the results described here are based on data collected from olfactory bulb slices. This preparation is extremely useful in that the activity of single cells can be closely controlled and monitored, yielding useful insight into the physiological properties governing olfactory bulb responses. However, the limitations of this preparation are worth noting, as slicing olfactory bulb tissue alters and omits several aspects of olfactory processing.

Slicing brain tissue alters cell morphology by severing neuronal processes. Severing of dendrites might be particularly common in the olfactory bulb preparation because the lateral dendrites of mitral and tufted cells can span very long distances (up to 1000 μm) from the cell body. Given the 300-400 μm thickness of slices, it is likely that many of the long-reaching dendrites are severed. Such changes might be expected to alter mitral cell excitability by reducing the number of functioning contacts with granule cells and perhaps changing passive membrane properties. Chapter 4 documents timescale-dependent correlation changes observed between pairs of mitral cells following slicing. Importantly, significant granule cell-mediated correlation changes were observed *despite* the fact that slicing reduces the number of synapses that could mediate these changes. Therefore we predict that granule cell-mediated changes to correlation *in vivo* would be even higher in the absence of this limitation, not only because the

full length of lateral dendrites are left intact, but also because granule cells are more excitable and might be recruited to enact these changes more readily.

Another aspect of olfactory physiology that is not addressed in our studies is the role of active sniffing as a means of odor sampling. Olfaction is an active sense, meaning that animals alter their behavior during stimulus sampling, presumably to gain better access to relevant stimulus features. Just as we evaluate visual scenes by scanning our eyes to different points in the visual field, or find a quarter in our pockets by moving the fingertips around, animals deliberately increase their respiration rate during odor sampling (Kepecs et al., 2007). This does not occur in anesthetized animals and reflects cortical control of odor sampling.

Several models of olfactory processing suggest that sniffing provides a series of "snapshots" of the olfactory periphery. Within the olfactory bulb, these snapshots involve the recruitment of excitatory and inhibitory circuits. Activity in the olfactory bulb is then transmitted to olfactory cortex, which is believed to integrate or compare patterns across time to enable identification and discrimination (Uchida et al., 2006; Gold and Shadlen, 2007; Haberly, 2001; Mainland and Sobel, 2006; Kepecs et al., 2006). A quintessential example of this type of comparison is thought to be scent tracking by blood hounds. They are thought to compare samples from a scent trail to a template (of a missing person, for example), and compare whether trail samples are more or less like the template as it moves around an environment.

Our data presented in chapter 3 were collected in response to isolated, rather than rhythmic stimulation of the olfactory bulb. Our results suggest that tufted cell latency varies as a function of input intensity and prior membrane potential. This raises the possibility that additional forms of modulation in evoked patterns could be elicited from sniffing. Since many

cells in the olfactory bulb remain depolarized for extended periods of time following brief stimulation, it is possible that the population baseline activity is significantly different across sniffs. For example, consider a population in which all cells are equally polarized prior to stimulation (**Figure 5.3 A**). In this situation, the first stimulus evokes activity in these neurons. The blue cell fires short-latency action potentials, the light blue cell fires long-latency action potentials, and the green cell becomes depolarized, but fires no action potentials. Our results indicate cells in the olfactory bulb participating in such patterns remain depolarized over hundreds to thousands of milliseconds following brief stimulation, which might facilitate the generation of temporally rich responses following limited sampling of odors (Karpov, 1980; Laing, 1986; Uchida and Mainen, 2003; Abraham et al., 2004). Therefore we predict that if a second stimulus is delivered much later in time (after all cells have become repolarized to their baseline levels), it will evoke the same pattern as the first stimulus presentation (**Figure 5.3 B**; box 1 versus box 2).

Conversely, if the second sampling period occurs while cells are still depolarized from the first stimulation epoch, the population latency patterns will likely be different because they are initiated atop a different baseline depolarization (**Figure 5.3 C**; because blue cells are already depolarized, their latencies shorten and the green cell receives sufficient additional depolarization to initiate spikes).

The timescales of depolarization in mitral, tufted, and granule cells are quite long, taking many hundreds to thousands of milliseconds to return to baseline. This timescale is significantly longer than the sampling periods dictated by the respiratory cycle, even during passive breathing (Wesson et al., 2008b). Thus it is possible that the scenario depicted in Figure 5.3 C is fairly common in the olfactory bulb. The potential utility of this phenomenon is that each sniff may

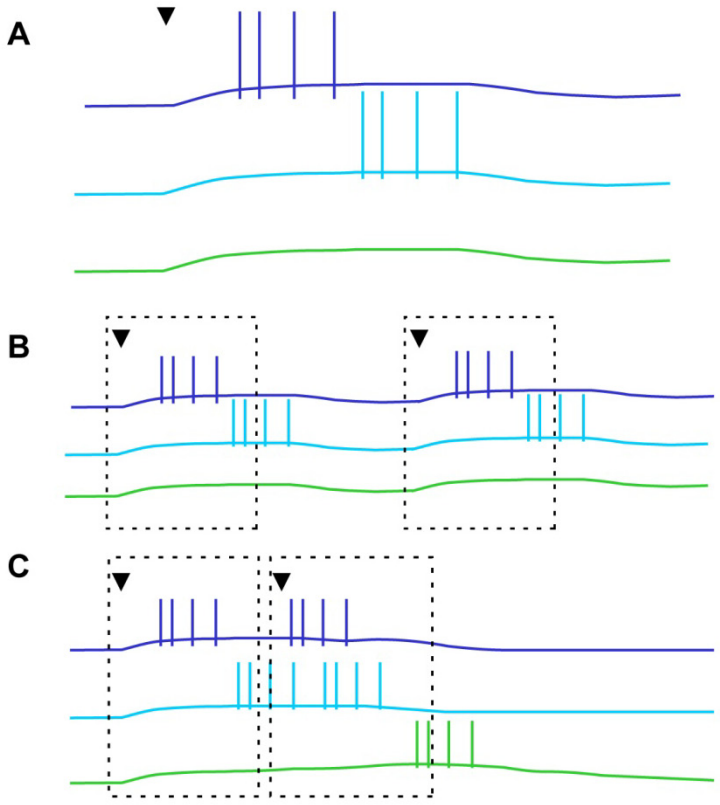

Figure 5.3: **Consequences of prolonged depolarizations on subsequent sampling. (A)** Schematic response of 3 neurons to a brief stimulus. Timing of stimulus application denoted by arrowhead. **(B-C)** Responses of same population to multiple applications of stimulus. In (B), the interval between stimulus samples is longer than the duration of depolarization, whereas the second stimulus is applied before repolarization in (C). In this way, resampling before prior stimulus-evoked activity has decayed could generate new latency patterns across consecutive samples.

not be a repeat of the previous sniff, but rather a relatively new sample. This argument is akin to the phenomenon of "never stepping in the same river twice" because the state of the river differs from moment to moment. Data from the antennal lobe suggest that insects may have mechanisms to ensure that stimulus-evoked patterns remain constant across different inter-stimulus intervals (Brown et al., 2005), but further studies will be required to determine whether latency patterns in the olfactory bulb follow this same principle.

Active sniffing raises an interesting question about the relationship between the timescales of active sniffing (5-12 Hz) and the timescales of neural activity in the bulb. If the olfactory bulb can generate long-lasting and potentially informative latency patterns, why would animals truncate these patterns to sniff rapidly? Some evidence suggests that rapid sniffing functions to simply bring odorants into contact with olfactory receptor neurons quickly (Wesson et al., 2009) (as opposed to influencing olfactory bulb representations). Interestingly, the changes in respiration during active sniffing are robust in rodents, but do not hold true in primates. For example, consider how humans smell wine, or sniff food to try to guess its elements. Rather than increasing our respiration rate by a factor of ~5, we instead *decrease* respiration rate to breathe in more deeply and slowly (Sobel et al., 2000). While the reasons for this remain unclear, they support the idea that active sampling strategies are selected based on inputs that most effectively facilitate perceptual goals.

5.6 GENERAL CONCLUSIONS

Our ability to sense and interact with the world depends critically on the ability of our nervous system to represent environmental information. My emphasis on timescales applies not only to correlation metrics, but to analysis of neural data in general. At the very least, this approach helps researchers to better understand and compare data collected and reported in different settings. Even better, analyzing data in this manner considers the utility of multiple timescales in coding, which may be a general and important feature of sensory encoding.

6.0 BIBLIOGRAPHY

Abbott LF, Dayan P (1999) The effect of correlated variability on the accuracy of a population code. Neural Computation 11:91-101.

Abraham NM, Egger V, Shimshek DR, Renden R, Fukunaga I, Sprengel R, Seeburg PH, Klugmann M, Margrie TW, Schaefer AT, Kuner T (2010) Synaptic Inhibition in the Olfactory Bulb Accelerates Odor Discrimination in Mice. Neuron 65:399-411.

Abraham NM, Spors H, Carleton A, Margrie TW, Kuner T, Schaefer AT (2004) Maintaining accuracy at the expense of speed: Stimulus similarity defines odor discrimination time in mice. Neuron 44:865-876.

Adrian ED (1928) The basis of sensation.

Adrian ED (1942) Olfactory reactions in the brain of the hedgehog. The journal of physiology 100:459.

Amoore JE (1969) A plan to identify most of the primary odors. Olfaction and Taste III158-171.

Apicella A, Yuan Q, Scanziani M, Isaacson JS (2010) Pyramidal cells in piriform cortex receive convergent input from distinct olfactory bulb glomeruli. The Journal of Neuroscience 30:14255-14260.

Araneda RC, Kini AD, Firestein S (2000) The molecular receptive range of an odorant receptor. Nature neuroscience 3:1248-1255.

Arevian AC, Kapoor V, Urban NN (2008) Activity-dependent gating of lateral inhibition in the mouse olfactory bulb. Nature Neuroscience 11:80-87.

Asahina K, Pavlenkovich V, Vosshall LB (2008) The survival advantage of olfaction in a competitive environment. Current Biology 18:1153-1155.

Averbeck BB, Latham PE, Pouget A (2006) Neural correlations, population coding and computation. Nature Reviews Neuroscience 7:358-366.

Averbeck BB, Lee D (2006) Effects of noise correlations on information encoding and decoding. Journal of Neurophysiology 95:3633-3644.

Aylwin ML, Diaz E, Maldonado PE (2005) Simultaneous single unit recording in the mitral cell layer of the rat olfactory bulb under nasal and tracheal breathing. Biol Res 38:13-26.

Bair W, Koch C (1996) Temporal precision of spike trains in extrastriate cortex of the behaving macaque monkey. Neural computation 8:1185-1202.

Balu R, Larimer P, Strowbridge BW (2004) Phasic stimuli evoke precisely timed spikes in intermittently discharging mitral cells. Journal of neurophysiology 92:743.

Barlow H (2001) Redundancy reduction revisited. Network-Computation in Neural Systems 12:241-253.

Barlow HB (1959) Sensory mechanisms, the reduction of redundancy, and intelligence. pp 535-539.

Bathellier B, Buhl DL, Accolla R, Carleton A (2008) Dynamic ensemble odor coding in the mammalian olfactory bulb: sensory information at different timescales. Neuron 57:586-598.

Bathellier B, Margrie TW, Larkum ME (2009) Properties of piriform cortex pyramidal cell dendrites: implications for olfactory circuit design. Journal of Neuroscience 29:12641.

Belitski A, Gretton A, Magri C, Murayama Y, Montemurro MA, Logothetis NK, Panzeri S (2008) Low-frequency local field potentials and spikes in primary visual cortex convey independent visual information. The Journal of Neuroscience 28:5696.

Belluscio L, Katz LC (2001) Symmetry, stereotypy, and topography of odorant representations in mouse olfactory bulbs. The Journal of Neuroscience 21:2113-2122.

Beshel J, Kopell N, Kay LM (2007) Olfactory bulb gamma oscillations are enhanced with task demands. The Journal of Neuroscience 27:8358-8365.

Blumstein DT, Mari M, Daniel JC, Ardron JG, Griffin AS, Evans CS (2002) Olfactory predator recognition: wallabies may have to learn to be wary. Animal Conservation 5:87-93.

Bressler SL, Freeman WJ (1980) Frequency analysis of olfactory system EEG in cat, rabbit, and rat. Electroencephalography and clinical neurophysiology 50:19-24.

Brody CD, Hopfield JJ (2003) Simple networks for spike-timing-based computation, with application to olfactory processing. Neuron 37:843-852.

Brown SL, Joseph J, Stopfer M (2005) Encoding a temporally structured stimulus with a temporally structured neural representation. Nature neuroscience 8:1568-1576.

Buck L, Axel R (1991) A Novel Multigene Family May Encode Odorant Receptors - A Molecular-Basis for Odor Recognition. Cell 65:175-187.

Buiakova OI, Baker H, Scott JW, Farbman A, Kream R, Grillo M, Franzen L, Richman M, Davis LM, Abbondanzo S (1996) Olfactory marker protein (OMP) gene deletion causes altered

physiological activity of olfactory sensory neurons. Proceedings of the National Academy of Sciences 93:9858.

Buonomano DV (2000) Decoding temporal information: a model based on short-term synaptic plasticity. The Journal of Neuroscience 20:1129.

Butts DA, Weng C, Jin J, Yeh CI, Lesica NA, Alonso JM, Stanley GB (2007) Temporal precision in the neural code and the timescales of natural vision. Nature 449:92-95.

Cajal S (1911) Ramon y: Histologie du Systeme nerveux. II.

Cang J, Isaacson JS (2003) In vivo whole-cell recording of odor-evoked synaptic transmission in the rat olfactory bulb. The Journal of Neuroscience 23:4108.

Castro JB, Hovis KR, Urban NN (2007) Recurrent dendrodendritic inhibition of accessory olfactory bulb mitral cells requires activation of group I metabotropic glutamate receptors. Journal of Neuroscience 27:5664-5671.

Chabaud P, Ravel N, Wilson DA, Mouly AM, Vigouroux M, Farget V, Gervais R (2000) Exposure to behaviourally relevant odour reveals differential characteristics in rat central olfactory pathways as studied through oscillatory activities. Chemical senses 25:561.

Chapuis J, Wilson DA (2011) Bidirectional plasticity of cortical pattern recognition and behavioral sensory acuity. Nature neuroscience.

Chase SM, Young ED (2007) First-spike latency information in single neurons increases when referenced to population onset. Proceedings of the National Academy of Sciences 104:5175.

Chechik G, Anderson MJ, Bar-Yosef O, Young ED, Tishby N, Nelken I (2006) Reduction of information redundancy in the ascending auditory pathway. Neuron 51:359-368.

Chen TW, Lin BJ, Schild D (2009) Odor coding by modules of coherent mitral/tufted cells in the vertebrate olfactory bulb. Proceedings of the National Academy of Sciences 106:2401.

Christensen TA, Lei H, Hildebrand JG (2003) Coordination of central odor representations through transient, non-oscillatory synchronization of glomerular output neurons. Proceedings of the National Academy of Sciences of the United States of America 100:11076.

Christie JM, Schoppa NE, Westbrook GL (2001) Tufted cell dendrodendritic inhibition in the olfactory bulb is dependent on NMDA receptor activity. Journal of neurophysiology 85:169.

Cinelli AR, Hamilton KA, Kauer JS (1995) Salamander olfactory bulb neuronal activity observed by video rate, voltage-sensitive dye imaging. III. Spatial and temporal properties of responses evoked by odorant stimulation. Journal of neurophysiology 73:2053-2071.

Cleland TA, Sethupathy P (2006) Non-topographical contrast enhancement in the olfactory bulb. BMC neuroscience 7:7.

Da Yu Lin SZZ, Block E, Katz LC (2005) Encoding social signals in the mouse main olfactory bulb. Nature 434:470-477.

Davison IG, Katz LC (2007) Sparse and selective odor coding by mitral/tufted neurons in the main olfactory bulb. The Journal of Neuroscience 27:2091-2101.

de la Rocha J, Doiron B, Shea-Brown E, Josic K, Reyes A (2007) Correlation between neural spike trains increases with firing rate. Nature 448:802-8U6.

De Saint Jan D, Hirnet D, Westbrook GL, Charpak S (2009) External tufted cells drive the output of olfactory bulb glomeruli. The Journal of Neuroscience 29:2043-2052.

Debarbieux F, Audinat E, Charpak S (2003) Action potential propagation in Dendrites of rat mitral cells in vivo. Journal of Neuroscience 23:5553-5560.

Doiron B, Chacron MJ, Maler L, Longtin A, Bastian J (2003) Inhibitory feedback required for network oscillatory responses to communication but not prey stimuli. Nature 421:539-543.

Dong HW, Hayar A, Ennis M (2007) Activation of group I metabotropic glutamate receptors on main olfactory bulb granule cells and periglomerular cells enhances synaptic inhibition of mitral cells. Journal of Neuroscience 27:5654-5663.

Egger V (2008) Synaptic sodium spikes trigger long lasting depolarizations and slow calcium entry in rat olfactory bulb granule cells. European Journal of Neuroscience 27:2066-2075.

Egger V, Stroh O (2009) Calcium buffering in rodent olfactory bulb granule cells and mitral cells. The journal of physiology 587:4467-4479.

Egger V, Svoboda K, Mainen ZF (2005) Dendrodendritic synaptic signals in olfactory bulb granule cells: local spine boost and global low-threshold spike. The Journal of Neuroscience 25:3521-3530.

Ekstrand JJ, Domroese ME, Johnson DMG, Feig SL, Knodel SM, Behan M, Haberly LB (2001) A new subdivision of anterior piriform cortex and associated deep nucleus with novel features of interest for olfaction and epilepsy. The Journal of Comparative Neurology 434:289-307.

Ezeh PI, Wellis DP, Scott JW (1993) Organization of inhibition in the rat olfactory bulb external plexiform layer. Journal of neurophysiology 70:263-274.

Fairhall AL, Lewen GD, Bialek W, van Steveninck RRR (2001) Efficiency and ambiguity in an adaptive neural code. Nature 412:787-792.

Fantana AL, Soucy ER, Meister M (2008) Rat olfactory bulb mitral cells receive sparse glomerular inputs. Neuron 59:802-814.

Ferster D, Miller KD (2000) Neural mechanisms of orientation selectivity in the visual cortex. Annual Review of Neuroscience 23:441-471.

Fleming AS, Rosenblatt JS (1974a) Olfactory regulation of maternal behavior in rats: I. Effects of olfactory bulb removal in experienced and inexperienced lactating and cycling females. Journal of Comparative and Physiological Psychology 86:221.

Fleming AS, Rosenblatt JS (1974b) Olfactory regulation of maternal behavior in rats: II. Effects of peripherally induced anosmia and lesions of the lateral olfactory tract in pup-induced virgins. Journal of Comparative and Physiological Psychology 86:233.

Fontanini A, Bower JM (2005) Variable coupling between olfactory system activity and respiration in ketamine/xylazine anesthetized rats. Journal of neurophysiology 93:3573-3581.

Freeman WJ, Schneider W (1982) Changes in spatial patterns of rabbit olfactory EEG with conditioning to odors. Psychophysiology 19:44-56.

Friedrich RW, Habermann CJ, Laurent G (2004) Multiplexing using synchrony in the zebrafish olfactory bulb. Nature neuroscience 7:862-871.

Friedrich RW, Korsching SI (1997) Combinatorial and chemotopic odorant coding in the zebrafish olfactory bulb visualized by optical imaging. Neuron 18:737-752.

Friedrich RW, Korsching SI (1998) Chemotopic, combinatorial, and noncombinatorial odorant representations in the olfactory bulb revealed using a voltage-sensitive axon tracer. The Journal of Neuroscience 18:9977-9988.

Friedrich RW, Laurent G (2001) Dynamic optimization of odor representations by slow temporal patterning of mitral cell activity. Science 291:889-894.

Furukawa S, Middlebrooks JC (2002) Cortical representation of auditory space: information-bearing features of spike patterns. Journal of neurophysiology 87:1749.

Galan RF, Fourcaud-Trocme N, Ermentrout GB, Urban NN (2006) Correlation-induced synchronization of oscillations in olfactory bulb neurons. Journal of Neuroscience 26:3646-3655.

Gawne TJ, Kjaer TW, Richmond BJ (1996) Latency: another potential code for feature binding in striate cortex. Journal of neurophysiology 76:1356.

Gawne TJ, Richmond BJ (1993) How independent are the messages carried by adjacent inferior temporal cortical neurons? The Journal of Neuroscience 13:2758-2771.

Gerkin RC, Tripathy SJ, Urban NN (2012) Origins of Correlation in the Mammalian Olfactory Bulb. pp In preparation.

Gheusi G, Cremer H, McLean H, Chazal G, Vincent JD, Lledo PM (2000) Importance of newly generated neurons in the adult olfactory bulb for odor discrimination. Proceedings of the National Academy of Sciences 97:1823.

Gire DH, Franks KM, Zak JD, Tanaka KF, Whitesell JD, Mulligan AA, Hen R, Schoppa NE (2012) Mitral Cells in the Olfactory Bulb Are Mainly Excited through a Multistep Signaling Path. The Journal of Neuroscience 32:2964-2975.

Gold JI, Shadlen MN (2007) The neural basis of decision making. Annu Rev Neurosci 30:535-574.

Goldberg SJ, Moulton DG (1987) Olfactory bulb responses telemetered during an odor discrimination task in rats. Experimental neurology 96:430-442.

Gollisch T, Meister M (2008) Rapid neural coding in the retina with relative spike latencies. Science 319:1108.

Green DM, Luce RD (1971) Speed-accuracy tradeoff in auditory detection.

Gregory EH, Pfaff DW (1971) Development of olfactory-guided behavior in infant rats. Physiology & behavior 6:573-576.

Grossman KJ, Mallik AK, Ross J, Kay LM, Issa NP (2008) Glomerular activation patterns and the perception of odor mixtures. European Journal of Neuroscience 27:2676-2685.

Haberly LB (2001) Parallel-distributed processing in olfactory cortex: new insights from morphological and physiological analysis of neuronal circuitry. Chemical senses 26:551.

Haberly LB, Price JL (1977) The axonal projection patterns of the mitral and tufted cells of the olfactory bulb in the rat. Brain research 129:152.

Hartline HK, Ratliff F (1957) Inhibitory interaction of receptor units in the eye of Limulus. Journal of General Physiology 40:357.

Hasenstaub A, Shu Y, Haider B, Kraushaar U, Duque A, McCormick DA (2005) Inhibitory postsynaptic potentials carry synchronized frequency information in active cortical networks. Neuron 47:423.

Hayar A, Karnup S, Shipley MT, Ennis M (2004) Olfactory bulb glomeruli: external tufted cells intrinsically burst at theta frequency and are entrained by patterned olfactory input. The Journal of Neuroscience 24:1190-1199.

Hayar A, Shipley MT, Ennis M (2005) Olfactory bulb external tufted cells are synchronized by multiple intraglomerular mechanisms. The Journal of Neuroscience 25:8197.

Heil P, Irvine DRF (1996) On determinants of first-spike latency in auditory cortex. Neuroreport 7:3073.

Heil P, Irvine DRF (1997) First-spike timing of auditory-nerve fibers and comparison with auditory cortex. Journal of neurophysiology 78:2438.

Hill DL, Almli CR (1981) Olfactory bulbectomy in infant rats: survival, growth and ingestive behaviors. Physiology & behavior 27:811-817.

Hopfield JJ (1995) Pattern recognition computation using action potential timing for stimulus representation. Nature 376:33-36.

Hopfield JJ (1999) Odor space and olfactory processing: collective algorithms and neural implementation. Proceedings of the National Academy of Sciences 96:12506.

Hozumi S, Nakagawasai O, Tan-No K, Niijima F, Yamadera F, Murata A, Arai Y, Yasuhara H, Tadano T (2003) Characteristics of changes in cholinergic function and impairment of learning and memory-related behavior induced by olfactory bulbectomy. Behavioural brain research 138:9-15.

Isaacson JS (1999) Glutamate spillover mediates excitatory transmission in the rat olfactory bulb. Neuron 23:377-384.

Isaacson JS, Strowbridge BW (1998) Olfactory reciprocal synapses: dendritic signaling in the CNS. Neuron 20:749-761.

Ito I, Bazhenov M, Ong RC, Raman B, Stopfer M (2009) Frequency transitions in odor-evoked neural oscillations. Neuron 64:692-706.

Jahr CE, Nicoll RA (1980) Dendrodendritic inhibition: demonstration with intracellular recording. Science 207:1473.

Johansson RS, Birznieks I (2004) First spikes in ensembles of human tactile afferents code complex spatial fingertip events. Nature neuroscience 7:170-177.

Johnson BA, Leon M (2000) Modular representations of odorants in the glomerular layer of the rat olfactory bulb and the effects of stimulus concentration. The Journal of Comparative Neurology 422:496-509.

Johnson TK, Jorgensen CD (1981) Ability of desert rodents to find buried seeds. Journal of Range Management312-314.

Junek S, Kludt E, Wolf F, Schild D (2010) Olfactory coding with patterns of response latencies. Neuron 67:872-884.

Kapoor V, Urban NN (2006) Glomerulus-specific, long-latency activity in the olfactory bulb granule cell network. Journal of Neuroscience 26:11709-11719.

Karnup SV, Hayar A, Shipley MT, Kurnikova MG (2006) Spontaneous field potentials in the glomeruli of the olfactory bulb: the leading role of juxtaglomerular cells. Neuroscience 142:203-221.

Karpov AP (1980) Analysis of neuron activity in the rabbitÆs olfactory bulb during food-acquisition behavior. Neural Mechanisms of Goal-Directed Behavior Academic Press, New York273-282.

Kass RE, Ventura V (2006) Spike count correlation increases with length of time interval in the presence of trial-to-trial variation. Neural Computation 18:2583-2591.

Kay LM, Beshel J (2010) A beta oscillation network in the rat olfactory system during a 2-alternative choice odor discrimination task. Journal of neurophysiology 104:829-839.

Kay LM, Beshel J, Brea J, Martin C, Rojas-L+¡bano D, Kopell N (2009) Olfactory oscillations: the what, how and what for. TRENDS in Neurosciences 32:207-214.

Kayser C, Montemurro MA, Logothetis NK, Panzeri S (2009) Spike-phase coding boosts and stabilizes information carried by spatial and temporal spike patterns. Neuron 61:597-608.

Kazama H, Wilson RI (2009) Origins of correlated activity in an olfactory circuit. Nature neuroscience 12:1136-1144.

Keller A, Vosshall LB (2007) Influence of odorant receptor repertoire on odor perception in humans and fruit flies. Proceedings of the National Academy of Sciences 104:5614.

Keller A, Zhuang H, Chi Q, Vosshall LB, Matsunami H (2007) Genetic variation in a human odorant receptor alters odour perception. Nature 449:468-472.

Kepecs A, Uchida N, Mainen ZF (2006) The sniff as a unit of olfactory processing. Chemical senses 31:167.

Kepecs A, Uchida N, Mainen ZF (2007) Rapid and precise control of sniffing during olfactory discrimination in rats. Journal of neurophysiology 98:205-213.

Knudsen EI, Konishi M (1979) Mechanisms of sound localization in the barn owl (Tyto alba). Journal of Comparative Physiology A: Neuroethology, Sensory, Neural, and Behavioral Physiology 133:13-21.

Kuffler SW (1953) Discharge Patterns and Functional Organization of Mammalian Retina. Journal of Neurophysiology 16:37-68.

Kumar A, Rotter S, Aertsen A (2010) Spiking activity propagation in neuronal networks: reconciling different perspectives on neural coding. Nature Reviews Neuroscience 11:615-627.

Lagier S, Carleton A, Lledo PM (2004) Interplay between local GABAergic interneurons and relay neurons generates +¦ oscillations in the rat olfactory bulb. The Journal of Neuroscience 24:4382.

Lagier S, Panzanelli P, Russo RE, Nissant A, Bathellier B, Sasso+¿-Pognetto M, Fritschy JM, Lledo PM (2007) GABAergic inhibition at dendrodendritic synapses tunes +¦ oscillations in the olfactory bulb. Proceedings of the National Academy of Sciences 104:7259.

Laing DG (1986) Identification of single dissimilar odors is achieved by humans with a single sniff. Physiology & behavior 37:163-170.

Laurent G (2002) Olfactory network dynamics and the coding of multidimensional signals. Nature Reviews Neuroscience 3:884-895.

Laurent G, Davidowitz H (1994) Encoding of olfactory information with oscillating neural assemblies. Science 265:1872.

Le Masson G, Renaud-Le Masson S, Debay D, Bal T (2002) Feedback inhibition controls spike transfer in hybrid thalamic circuits. Nature 417:854-858.

Lee D, Port NL, Kruse W, Georgopoulos AP (1998) Variability and correlated noise in the discharge of neurons in motor and parietal areas of the primate cortex. The Journal of Neuroscience 18:1161-1170.

Leonard CM (1980) The Synaptic Organization of the Brain - Shepherd,Gm. Contemporary Psychology 25:619-620.

Leutgeb JK, Leutgeb S, Moser MB, Moser EI (2007) Pattern separation in the dentate gyrus and CA3 of the hippocampus. Science 315:961.

Lin DY, Shea SD, Katz LC (2006) Representation of natural stimuli in the rodent main olfactory bulb. Neuron 50:937-949.

Lin W, Arellano J, Slotnick B, Restrepo D (2004) Odors detected by mice deficient in cyclic nucleotide-gated channel subunit A2 stimulate the main olfactory system. The Journal of Neuroscience 24:3703-3710.

Linster C, Johnson BA, Yue E, Morse A, Xu Z, Hingco EE, Choi Y, Choi M, Messiha A, Leon M (2001) Perceptual correlates of neural representations evoked by odorant enantiomers. The Journal of Neuroscience 21:9837-9843.

Luna VM, Schoppa NE (2008) GABAergic circuits control input-spike coupling in the piriform cortex. Journal of Neuroscience 28:8851.

Luo M, Katz LC (2001) Response correlation maps of neurons in the mammalian olfactory bulb. Neuron 32:1165-1179.

Ma L, Qiu Q, Gradwohl S, Scott A, Elden QY, Alexander R, Wiegraebe W, Yu CR (2012) Distributed representation of chemical features and tunotopic organization of glomeruli in the mouse olfactory bulb. Proceedings of the National Academy of Sciences 109:5481-5486.

MacLeod K, Laurent G (1996) Distinct mechanisms for synchronization and temporal patterning of odor-encoding neural assemblies. Science 274:976-979.

Macrides F, Eichenbaum HB, Forbes WB (1982) Temporal relationship between sniffing and the limbic rhythm during odor discrimination reversal learning. J Neurosci 2:1705-1717.

Mainland J, Sobel N (2006) The sniff is part of the olfactory percept. Chemical senses 31:181.

Margrie TW, Sakmann B, Urban NN (2001) Action potential propagation in mitral cell lateral dendrites is decremental and controls recurrent and lateral inhibition in the mammalian olfactory bulb. Proceedings of the National Academy of Sciences of the United States of America 98:319.

Margrie TW, Schaefer AT (2003) Theta oscillation coupled spike latencies yield computational vigour in a mammalian sensory system. The journal of physiology 546:363.

Masuda N (2006) Simultaneous rate-synchrony codes in populations of spiking neurons. Neural computation 18:45-59.

Mazzoni A, Panzeri S, Logothetis NK, Brunel N (2008) Encoding of naturalistic stimuli by local field potential spectra in networks of excitatory and inhibitory neurons. PLoS computational biology 4:e1000239.

McClurkin JW, Optican LM, Richmond BJ, Gawne TJ (1991) Concurrent processing and complexity of temporally encoded neuronal messages in visual perception. Science 253:675.

Meinecke DL, Peters A (1987) GABA immunoreactive neurons in rat visual cortex. The Journal of Comparative Neurology 261:388-404.

Milner PM (1974) A model for visual shape recognition. Psychological Review 81:521.

Molineux ML, Fernandez FR, Mehaffey WH, Turner RW (2005) A-type and T-type currents interact to produce a novel spike latency-voltage relationship in cerebellar stellate cells. The Journal of Neuroscience 25:10863.

Mombaerts P, Wang F, Dulac C, Chao SK, Nemes A, Mendelsohn M, Edmondson J, Axel R (1996) Visualizing an olfactory sensory map. Cell 87:675-686.

Montemurro MA, Rasch MJ, Murayama Y, Logothetis NK, Panzeri S (2008) Phase-of-firing coding of natural visual stimuli in primary visual cortex. Current Biology 18:375-380.

Morest DK (1971) Dendrodendritic synapses of cells that have axons: the fine structure of the Golgi type II cell in the medial geniculate body of the cat. Anatomy and Embryology 133:216-246.

Mori K, Kishi K, Ojima H (1983) Distribution of dendrites of mitral, displaced mitral, tufted, and granule cells in the rabbit olfactory bulb. The Journal of Comparative Neurology 219:339-355.

Mori K, Mataga N, Imamura K (1992) Differential specificities of single mitral cells in rabbit olfactory bulb for a homologous series of fatty acid odor molecules. Journal of neurophysiology 67:786-789.

Mori K, Nagao H, Yoshihara Y (1999) The olfactory bulb: Coding and processing of odor molecule information. Science 286:711-715.

Mwilaria EK, Ghatak C, Daly KC (2008) Disruption of GABA(A) in the insect antennal lobe generally increases odor detection and discrimination thresholds. Chemical Senses 33:267-281.

Nagayama S, Takahashi YK, Yoshihara Y, Mori K (2004) Mitral and tufted cells differ in the decoding manner of odor maps in the rat olfactory bulb. Journal of neurophysiology 91:2532.

Neville KR, Haberly LB (2003) Beta and gamma oscillations in the olfactory system of the urethane-anesthetized rat. Journal of neurophysiology 90:3921.

Ngai J, Chess A, Dowling MM, Necles N, Macagno ER, Axel R (1993) Coding of olfactory information: topography of odorant receptor expression in the catfish olfactory epithelium. Cell 72:667-680.

Nicoll RA (1969) Inhibitory mechanisms in the rabbit olfactory bulb: dendrodendritic mechanisms. Brain research 14:157-172.

Nikonov AA, Finger TE, Caprio J (2005) Beyond the olfactory bulb: an odotopic map in the forebrain. Proceedings of the National Academy of Sciences of the United States of America 102:18688.

Nusser Z, Kay LM, Laurent G, Homanics GE, Mody I (2001) Disruption of GABA(A) receptors on GABAergic interneurons leads to increased oscillatory power in the olfactory bulb network. Journal of Neurophysiology 86:2823-2833.

Nyakas C, Endroczi E (1970) Olfaction guided approaching behaviour of infantile rats to the mother in maze box. Acta Physiologica Academiae Scientiarum Hungaricae 38:59.

Olsen SR, Wilson RI (2008) Lateral presynaptic inhibition mediates gain control in an olfactory circuit. Nature 452:956-960.

Orona E, Rainer EC, Scott JW (1984) Dendritic and axonal organization of mitral and tufted cells in the rat olfactory bulb. The Journal of Comparative Neurology 226:346-356.

Orona E, Scott JW, Rainer EC (1983) Different granule cell populations innervate superficial and deep regions of the external plexiform layer in rat olfactory bulb. The Journal of Comparative Neurology 217:227-237.

Padmanabhan K, Urban NN (2010) Intrinsic biophysical diversity decorrelates neuronal firing while increasing information content. Nature neuroscience 13:1276-1282.

Panzeri S, Brunel N, Logothetis NK, Kayser C (2010) Sensory neural codes using multiplexed temporal scales. Trends in Neurosciences 33:111-120.

Panzeri S, Petersen RS, Schultz SR, Lebedev M, Diamond ME (2001) The role of spike timing in the coding of stimulus location in rat somatosensory cortex. Neuron 29:769-777.

Perez-Orive J, Mazor O, Turner GC, Cassenaer S, Wilson RI, Laurent G (2002) Oscillations and sparsening of odor representations in the mushroom body. Science 297:359-365.

Petersen RS, Panzeri S, Diamond ME (2002) Population coding in somatosensory cortex. Current opinion in neurobiology 12:441-447.

Pew RW (1969) The speed-accuracy operating characteristic. Acta Psychologica 30:16-26.

Phillips CG, Powell TPS, Shepherd GM (1963) Responses of mitral cells to stimulation of the lateral olfactory tract in the rabbit. The journal of physiology 168:65.

Phillips ME, Sachdev RNS, Willhite DC, Shepherd GM (2012) Respiration Drives Network Activity and Modulates Synaptic and Circuit Processing of Lateral Inhibition in the Olfactory Bulb. The Journal of Neuroscience 32:85-98.

Pinault D, Smith Y, Deschenes M (1997) Dendrodendritic and axoaxonic synapses in the thalamic reticular nucleus of the adult rat. The Journal of Neuroscience 17:3215-3233.

Pinching AJ, Powell TPS (1971) The neuron types of the glomerular layer of the olfactory bulb. Journal of cell science 9:305.

Pinto DJ, Hartings JA, Simons DJ (2003) Cortical damping: Analysis of thalamocortical response transformations in rodent barrel cortex. Cerebral Cortex 13:33-44.

Poo C, Isaacson JS (2009) Odor Representations in Olfactory Cortex. Neuron 62:850-861.

Poulet JFA, Petersen CCH (2008) Internal brain state regulates membrane potential synchrony in barrel cortex of behaving mice. Nature 454:881-885.

Price JL, Powell TP (1970a) The synaptology of the granule cells of the olfactory bulb. Journal of cell science 7:125.

Price JL, Powell TPS (1970b) The morphology of the granule cells of the olfactory bulb. Journal of cell science 7:91.

Rall W, Shepherd GM, Reese TS, Brightman MW (1966) Dendrodendritic synaptic pathway for inhibition in the olfactory bulb. Experimental neurology 14:44-56.

Raman B, Joseph J, Tang J, Stopfer M (2010) Temporally diverse firing patterns in olfactory receptor neurons underlie spatiotemporal neural codes for odors. The Journal of Neuroscience 30:1994-2006.

Ressler KJ, Sullivan SL, Buck LB (1993) A zonal organization of odorant receptor gene expression in the olfactory epithelium. Cell 73:597-609.

Ressler KJ, Sullivan SL, Buck LB (1994) Information coding in the olfactory system: evidence for a stereotyped and highly organized epitope map in the olfactory bulb. Cell 79:1245-1255.

Reyes AD (2003) Synchrony-dependent propagation of firing rate in iteratively constructed networks in vitro. Nature Neuroscience 6:593-599.

Rinberg D, Koulakov A, Gelperin A (2006) Speed-accuracy tradeoff in olfaction. Neuron 51:351-358.

Romo R, Hernandez A, Zainos A, Salinas E (2003) Correlated neuronal discharges that increase coding efficiency during perceptual discrimination. Neuron 38:649-657.

Rubin BD, Katz LC (1999) Optical imaging of odorant representations in the mammalian olfactory bulb. Neuron 23:499-511.

Rubin BD, Katz LC (2001) Spatial coding of enantiomers in the rat olfactory bulb. Nature neuroscience 4:355-356.

Saleh M, Reimer J, Penn R, Ojakangas CL, Hatsopoulos NG (2010) Fast and slow oscillations in human primary motor cortex predict oncoming behaviorally relevant cues. Neuron 65:461-471.

Salinas E, Sejnowski TJ (2000) Impact of correlated synaptic input on output firing rate and variability in simple neuronal models. The Journal of Neuroscience 20:6193-6209.

Salinas E, Sejnowski TJ (2001) Correlated neuronal activity and the flow of neural information. Nature Reviews Neuroscience 2:539-550.

Schaefer AT, Margrie TW (2007) Spatiotemporal representations in the olfactory system. TRENDS in Neurosciences 30:92-100.

Schneidman E, Bialek W, Berry MJ (2003) Synergy, redundancy, and independence in population codes. Journal of Neuroscience 23:11539-11553.

Schoenfeld TA, Macrides F (1984) Topographic organization of connections between the main olfactory bulb and pars externa of the anterior olfactory nucleus in the hamster. The Journal of Comparative Neurology 227:121-135.

Schoppa NE (2006) Synchronization of olfactory bulb mitral cells by precisely timed inhibitory inputs. Neuron 49:271-283.

Schoppa NE, Kinzie JM, Sahara Y, Segerson TP, Westbrook GL (1998) Dendrodendritic inhibition in the olfactory bulb is driven by NMDA receptors. The Journal of Neuroscience 18:6790.

Schoppa NE, Westbrook GL (1999) Regulation of synaptic timing in the olfactory bulb by an A-type potassium current. Nature neuroscience 2:1106-1113.

Schoppa NE, Westbrook GL (2001) Glomerulus-specific synchronization of mitral cells in the olfactory bulb. Neuron 31:639-651.

Schoppa NE, Westbrook GL (2002) AMPA autoreceptors drive correlated spiking in olfactory bulb glomeruli. Nature Neuroscience 5:1194-1202.

Series P, Latham PE, Pouget A (2004) Tuning curve sharpening for orientation selectivity: coding efficiency and the impact of correlations. Nature Neuroscience 7:1129-1135.

Shadlen MN, Newsome WT (1998) The variable discharge of cortical neurons: implications for connectivity, computation, and information coding. The Journal of Neuroscience 18:3870-3896.

Sharp FR, Kauer JS, Shepherd GM (1975) Local sites of activity-related glucose metabolism in rat olfactory bulb during olfactory stimulation. Brain research.

Shepherd GM (2004) The synaptic organization of the brain. Oxford University Press, USA.

Shin Nagayama AE, Fletcher ML, Masurkar AV, Igarashi KM, Mori K, Chen WR (2010) Differential axonal projection of mitral and tufted cells in the mouse main olfactory system. Frontiers in neural circuits 4.

Shusterman R, Smear MC, Koulakov AA, Rinberg D (2011) Precise olfactory responses tile the sniff cycle. Nature neuroscience 14:1039-1044.

Simmons JA (1979) Perception of echo phase information in bat sonar. Science 204:1336.

Simoncelli EP, Olshausen BA (2001) Natural image statistics and neural representation. Annual Review of Neuroscience 24:1193-1216.

Singer W, Gray CM (1995) Visual feature integration and the temporal correlation hypothesis. Annual review of neuroscience 18:555-586.

Singh PJ, Tobach E (1975) Olfactory bulbectomy and nursing behavior in rat pups (Wistar DAB). Developmental psychobiology 8:151-164.

Smear M, Shusterman R, OΓÇÖConnor R, Bozza T, Rinberg D (2011) Perception of sniff phase in mouse olfaction. Nature.

Smith MA, Kohn A (2008) Spatial and Temporal Scales of Neuronal Correlation in Primary Visual Cortex. Journal of Neuroscience 28:12591-12603.

Sobel N, Khan RM, Hartley CA, Sullivan EV, Gabrieli JDE (2000) Sniffing longer rather than stronger to maintain olfactory detection threshold. Chemical senses 25:1-8.

Sompolinsky H, Yoon H, Kang KJ, Shamir M (2001) Population coding in neuronal systems with correlated noise. Physical Review e 6405.

Soucy ER, Albeanu DF, Fantana AL, Murthy VN, Meister M (2009) Precision and diversity in an odor map on the olfactory bulb. Nature neuroscience 12:210-220.

Spors H, Grinvald A (2002) Spatio-temporal dynamics of odor representations in the mammalian olfactory bulb. Neuron 34:301-315.

Spors H, Wachowiak M, Cohen LB, Friedrich RW (2006) Temporal dynamics and latency patterns of receptor neuron input to the olfactory bulb. The Journal of Neuroscience 26:1247.

Srinivasan MV, Laughlin SB, Dubs A (1982) Predictive Coding - A Fresh View of Inhibition in the Retina. Proceedings of the Royal Society of London Series B-Biological Sciences 216:427-459.

Steriade M, Timofeev I (2003) Neuronal plasticity in thalamocortical networks during sleep and waking oscillations. Neuron 37:563-576.

Stettler DD, Axel R (2009) Representations of odor in the piriform cortex. Neuron 63:854-864.

Stewart WB, Kauer JS, Shepherd GM (1979) Functional organization of rat olfactory bulb analysed by the 2ΓÇÉdeoxyglucose method. The Journal of Comparative Neurology 185:715-734.

Stopfer M, Bhagavan S, Smith BH, Laurent G (1997) Impaired odour discrimination on desynchronization of odour-encoding neural assemblies. Nature 390:70-74.

Stopfer M, Jayaraman V, Laurent G (2003) Intensity versus identity coding in an olfactory system. Neuron 39:991-1004.

Storm JF (1988) Temporal integration by a slowly inactivating K+ current in hippocampal neurons. Nature 336:379-381.

Swensson RG (1972) The elusive tradeoff: Speed vs accuracy in visual discrimination tasks. Attention, Perception, & Psychophysics 12:16-32.

Szyszka P, Ditzen M, Galkin A, Galizia CG, Menzel R (2005) Sparsening and temporal sharpening of olfactory representations in the honeybee mushroom bodies. Journal of neurophysiology 94:3303-3313.

Theunissen F, Miller JP (1995) Temporal encoding in nervous systems: a rigorous definition. Journal of Computational Neuroscience 2:149-162.

Thorpe SJ, Gautrais J (1997) Rapid visual processing using spike asynchrony. Advances in neural information processing systems901-907.

Tiesinga P, Fellous JM, Sejnowski TJ (2008) Regulation of spike timing in visual cortical circuits. Nature Reviews Neuroscience 9:97-107.

Tiesinga PHE (2005) Stimulus competition by inhibitory interference. Neural Computation 17:2421-2453.

Tiesinga PHE, Sejnowski TJ (2004) Rapid temporal modulation of synchrony by competition in cortical interneuron networks. Neural Computation 16:251-275.

Tobach E, Rouger Y, Schneirla TC (1967) Development of olfactory function in the rat pup. American Zoologist 7:792-793.

Turner GC, Bazhenov M, Laurent G (2008) Olfactory representations by Drosophila mushroom body neurons. Journal of neurophysiology 99:734-746.

Uchida N, Kepecs A, Mainen ZF (2006) Seeing at a glance, smelling in a whiff: rapid forms of perceptual decision making. Nature Reviews Neuroscience 7:485-491.

Uchida N, Mainen ZF (2003) Speed and accuracy of olfactory discrimination in the rat. Nature neuroscience 6:1224-1229.

Uchida N, Takahashi YK, Tanifuji M, Mori K (2000) Odor maps in the mammalian olfactory bulb: domain organization and odorant structural features. Nature neuroscience 3:1035-1043.

Urban NN (2002) Lateral inhibition in the olfactory bulb and in olfaction. Physiology & behavior 77:607-612.

Urban NN, Sakmann B (2002) Reciprocal intraglomerular excitation and intra-and interglomerular lateral inhibition between mouse olfactory bulb mitral cells. The Journal of Physiology 542:355.

van der Togt C, Kalitzin S, Spekreijse H, Lamme VAF, Super H (2006) Synchrony dynamics in monkey V1 predict success in visual detection. Cerebral Cortex 16:136-148.

Van Hooser SD, Hofmann UG, Kewley DT, Bower JM (2000) Relationship Between Field Potentials and Spike Activity in Rat S1: Multi-site Cortical Recordings and Analysis. Neurocomputing32-33.

Van Rullen R, Gautrais J, Delorme A, Thorpe S (1998) Face processing using one spike per neurone. Biosystems 48:229-239.

van Vreeswijk C, Abbott LF, Ermentrout GB (1994) When inhibition not excitation synchronizes neural firing. J Comput Neurosci 1:313-321.

Vander Wall SB (1998) Foraging success of granivorous rodents: effects of variation in seed and soil water on olfaction. Ecology 79:233-241.

Vassar R, Ngai J, Axel R (1993) Spatial segregation of odorant receptor expression in the mammalian olfactory epithelium. Cell 74:309-318.

Wang HP, Spencer D, Fellous JM, Sejnowski TJ (2010) Synchrony of Thalamocortical Inputs Maximizes Cortical Reliability. Science 328:106.

Wang XJ, Buzsaki G (1996) Gamma oscillation by synaptic inhibition in a hippocampal interneuronal network model. Journal of Neuroscience 16:6402-6413.

Wehr M, Zador AM (2003) Balanced inhibition underlies tuning and sharpens spike timing in auditory cortex. Nature 426:442-446.

Wesson DW, Carey RM, Verhagen JV, Wachowiak M (2008a) Rapid encoding and perception of novel odors in the rat. PLoS biology 6:e82.

Wesson DW, Donahou TN, Johnson MO, Wachowiak M (2008b) Sniffing behavior of mice during performance in odor-guided tasks. Chemical senses 33:581-596.

Wesson DW, Verhagen JV, Wachowiak M (2009) Why sniff fast? The relationship between sniff frequency, odor discrimination, and receptor neuron activation in the rat. Journal of neurophysiology 101:1089-1102.

Wiechert MT, Judkewitz B, Riecke H, Friedrich RW (2010) Mechanisms of pattern decorrelation by recurrent neuronal circuits. Nat Neurosci 13:1003-1010.

Wilson RI, Laurent G (2005) Role of GABAergic inhibition in shaping odor-evoked spatiotemporal patterns in the Drosophila antennal lobe. The Journal of Neuroscience 25:9069.

Wilson RI, Turner GC, Laurent G (2004) Transformation of olfactory representations in the Drosophila antennal lobe. Science's STKE 303:366.

Wise PM, Olsson MJ, Cain WS (2000) Quantification of odor quality. Chemical senses 25:429.

Wong ST, Trinh K, Hacker B, Chan GCK, Lowe G, Gaggar A, Xia Z, Gold GH, Storm DR (2000) Disruption of the type III adenylyl cyclase gene leads to peripheral and behavioral anosmia in transgenic mice. Neuron 27:487-497.

Xiong W, Chen WR (2002) Dynamic gating of spike propagation in the mitral cell lateral dendrites. Neuron 34:115-126.

Yoshida I, Mori K (2007) Odorant category profile selectivity of olfactory cortex neurons. The Journal of Neuroscience 27:9105-9114.

Young JM, Friedman C, Williams EM, Ross JA, Tonnes-Priddy L, Trask BJ (2002) Different evolutionary processes shaped the mouse and human olfactory receptor gene families. Human molecular genetics 11:535-546.

Youngentob SL, Johnson BA, Leon M, Sheehe PR, Kent PF (2006) Predicting odorant quality perceptions from multidimensional scaling of olfactory bulb glomerular activity patterns. Behavioral neuroscience 120:1337.

Youngentob SL, Margolis FL (1999) OMP gene deletion causes an elevation in behavioral threshold sensitivity. Neuroreport 10:15.

Youngentob SL, Margolis FL, Youngentob LM (2001) OMP gene deletion results in an alteration in odorant quality perception. Behavioral neuroscience 115:626.

Yu YG, Liu F, Wang W, Lee TS (2004) Optimal synchrony state for maximal information transmission. Neuroreport 15:1605-1610.

Zhang X, Firestein S (2002) The olfactory receptor gene superfamily of the mouse. Nature neuroscience 5:124-133.

Zhao H, Reed RR (2001) X Inactivation of the< i> OCNC1</i> Channel Gene Reveals a Role for Activity-Dependent Competition in the Olfactory System. Cell 104:651-660.

Zohary E, Shadlen MN, Newsome WT (1994) Correlated Neuronal Discharge Rate and Its Implications for Psychophysical Performance. Nature 370:140-143.

Zou Z, Buck LB (2006) Combinatorial effects of odorant mixes in olfactory cortex. Science's STKE 311:1477.

Zueger M, Urani A, Chourbaji S, Zacher C, Roche M, Harkin A, Gass P (2005) Olfactory bulbectomy in mice induces alterations in exploratory behavior. Neuroscience letters 374:142-146.